INTERNATIONAL ATOMIC ENERGY AGENCY
UNITED NATIONS EDUCATIONAL, SCIENTIFIC AND CULTURAL ORGANIZATION
INTERNATIONAL CENTRE FOR THEORETICAL PHYSICS
I.C.T.P., P.O. BOX 586, 34100 TRIESTE, ITALY, CABLE: CENTRATOM TRIESTE

UNITED NATIONS INDUSTRIAL DEVELOPMENT ORGANIZATION

INTERNATIONAL CENTRE FOR SCIENCE AND HIGH TECHNOLOGY

SMR.550 - 7

SPRING COLLEGE IN MATERIALS SCIENCE ON

"NUCLEATION, GROWTH AND SEGREGATION IN MATERIALS

SCIENCE AND ENGINEERING"

(6 May - 7 June 1991)

SEGREGATION PROCESSES AND EMBRITTLING PHENOMENA (INCLUDING RADIATION ENVIRONMENT AND TEMPER EMBRITTLEMENT)

R. BULLOUGH
AEA Technology, Harwell Laboratory
Building 329
Oxfordshire OX11 ORA
United Kingdom

Acta metall. Vol. 32, No. 9, pp 1381–1394, 1984
Printed in Great Britain.

0001-6160/84 $3.00 + 0.00

STRESS-DRIVEN SOLUTE ENRICHMENT OF CRACK-TIPS DURING LOW-DUCTILITY INTERGRANULAR FRACTURE OF LOW-ALLOY STEEL

C. A. HIPPSLEY†, H. RAUH‡ and R. BULLOUGH
Theoretical Physics Division, AERE Harwell, Didcot, Oxon OX11 0RA, England

(*Received* 20 *December* 1983; *in revised form* 9 *February* 1984)

Abstract—The local distribution of solute chemistry in the vicinity of crack-tips has been determined by scanning Auger spectroscopy in specimens of 2¼Cr1Mo steel subject to controlled crack growth by low-ductility intergranular fracture at elevated temperatures. A significant enrichment of sulphur in such regions is shown to be associated with this type of fracture occurring most commonly in low-alloy steels which suffer from stress-relief cracking during post-weld heat treatment. Theoretical analysis of the migration to a crack of dissolved solute atoms, under the influence of the crack-tip stress field, is presented and used to provide a quantitative explanation of the observed sulphur segregation near the crack-tip. The importance of sulphur to the embrittlement process is thus confirmed.

Résumé—Nous avons déterminé la sépartition locale de la chimie du soluté au voisinage des extrêmités de fissure par spectroscopie Auger à balayage, dans des échantillons d'acier 2¼Cr1Mo soumis a une croissance contrôlée des fissures par rupture intergranulaire à faible ductilité, aux températures élévées. Nous avons montré qu'un enrichissement significatif en soufre dans ces régions était associé à ce type de rupture commun dans les aciers faiblement alliés présentant une fissuration de relaxation de contrainte au cours du traitement thermique après soudure. Nous présentons une analyse théorique de la migration d'atomes de soluté dissous, sous l'influence du champ de contrainte de l'extrêmité d'une fissure, et nous l'appliquons pour expliquer quantitativement la ségrégation de soufre observée près de l'extrêmité de la fissure. Nous confirmons ainsi l'importance du soufre pour le phénomène de fragilisation.

Zusammenfassung—Proben aus Stahl 2¼Cr 1Mo wurden bei erhöhten Temperaturen einem kontrollierten Wachstum von Rissen durch niederduktilen intergranularen Bruch unterworfen. Die lokale Verteilung der gelösten chemischen Substanzen wurde in der Nähe der Rißspitzen mittels Augerelektronenspektroskopie bestimmt. Die aufgefundene bedeutende Anreicherung von Schwefel in diesen Gebieten hängt mit dieser Art von Bruch zusammen. Er wird üblicherweise in niedriglegierten Stählen beobachtet, in denen Rißbildung während der Wärmebehandlung nach der Schweißung durch Abbau von Spannungen auftritt. Eine theoretische Behandlung der Wanderung von gelösten Atomen zum Riß unter dem Einfluß des Spannungsfeldes an der Rißspitze wird vorgelegt. Sie bildet die Grundlage für eine quantitative Erklärung der beobachteten Schwefelsegregation in der Nähe der Rißspitze. Auf diese Weise wird die wichtige Rolle des Schwefels für den Versprödungsprozeß bestätigt.

1. INTRODUCTION

The last decade has witnessed a growing number of reports of slow, low-ductility intergranular fracture in low-alloy steels with an "as-quenched" microstructure when subject to stress at elevated temperatures [1–8]. The majority of cases concern stress-relief cracking in the coarse-grained heat-affected zone of thick-section weldments during post-weld heat treatment. Crack propagation occurs in a slow, but essentially brittle manner under the influence of residual welding stresses which are still high during the heating period of post-weld heat treatment. This mode of cracking generally prevails under high-stress, medium-temperature conditions [1, 2, 6, 8] (350–600°C); at higher temperatures [6–8] the fracture mechanism changes to intergranular microvoid coalescence as the residual stresses relax during heating (e.g. 600–700°C in 2¼Cr1Mo steel) or during the isothermal "hold" period (e.g. 615°C in A533B steel) [9].

Slow, brittle intergranular fracture is observed in laboratory simulated stress–relaxation tests which include the heating period of post-weld heat treatment [4–6, 8] or in isothermal tests which are performed in the medium temperature range (350 to 600°C) [10, 11]. It occurs both in air and vacuum environments [5, 7] and is usually associated with stress-intensifying geometry (e.g. a notch or precrack) [6, 12, 13]. A corresponding mode of fracture has been reported in actual weldments [14, 15]. Although such fractures were initially interpreted as resulting from a "smoothing" of intergranular micro-

†Metallurgy Division, AERE Harwell, Oxfordshire, OX11 0RA, England.
‡Harwell Research Associate July and August 1983; on leave from: Fachbereich Physik der Universität Osnabrück, Postfach 4469, D-4500 Osnabrück, F.R.G.

-/-

voids through surface diffusion [16–18], there is now experimental and theoretical evidence [19] to discount such an explanation.

Investigations of the micromechanisms of slow brittle fracture initially linked this failure mode with several characteristics of the fast low-temperature intergranular fracture induced by temper embrittlement [2, 6, 20]: i.e. thermally activated segregation of embrittling impurities to grain-boundaries, and the precipitation of intergranular carbides. However, there was also indirect evidence to suggest that this mode of fracture may require local stress-induced segregation of impurities to the crack-tip [8]. Subsequently, high resolution scanning Auger analysis has revealed an enrichment of sulphur in the vicinity of crack-tips in $2\frac{1}{4}$Cr1Mo [21] and MnMoNi (A533B) [22] steel alloys.

The first part of this study presents a detailed examination of solute enrichment on crack-surfaces which provides direct evidence for possible stress-induced segregation. The second part gives a theoretical analysis which demonstrates that the proposed interaction between the crack-tip stress field and nearby solute atoms yields a prediction for the segregation of solute that is both physically reasonable and in agreement with observed variations in segregant coverage.

2. CHARACTERISTICS OF LOW-DUCTILITY INTERGRANULAR FRACTURE

Detailed observations of stress-relief cracking in various low-alloy steels have been reported in previous publications [6–8]. The micromechanisms of this mode of cracking in $2\frac{1}{4}$Cr1Mo steel have received particular attention. Four alloys of $2\frac{1}{4}$Cr1Mo steel were examined and, to facilitate reference to previous results [6, 8], will continue in the present discussion to be identified as follows:

A—basic $2\frac{1}{4}$Cr1Mo steel composition but containing very low concentration of residual impurity elements;
B—as "A" doped with 540-ppm phosphorus;
C—as "A" but doped with 500 ppm tin;
D—commercial purity $2\frac{1}{4}$Cr1Mo steel.

Full bulk chemical analyses of alloys A–D are given in Table 1.

Single-edge notched (SEN) specimens of each alloy were given a rapid high-temperature thermal cycle to produce a simulated coarse-grained heat-affected microstructure (predominantly lower bainite) and were then subjected to a stress–relaxation test simulating conditions during the heating period of post-weld heat treatment. It was found that alloys B, C and D exhibited low-ductility intergranular fracture during stress–relaxation in the temperature range 450–600 C. Figure 1 shows fractographs illustrating this type of fracture in alloy D, and demonstrates that it is relatively brittle in nature when compared to a typical creep-cavitation failure in this steel. The high-purity alloy, A, was not susceptible to low-ductility intergranular fracture, exhibiting only the higher temperature, intergranular microvoid coalescence mode, common to all four alloys above ~600 C.

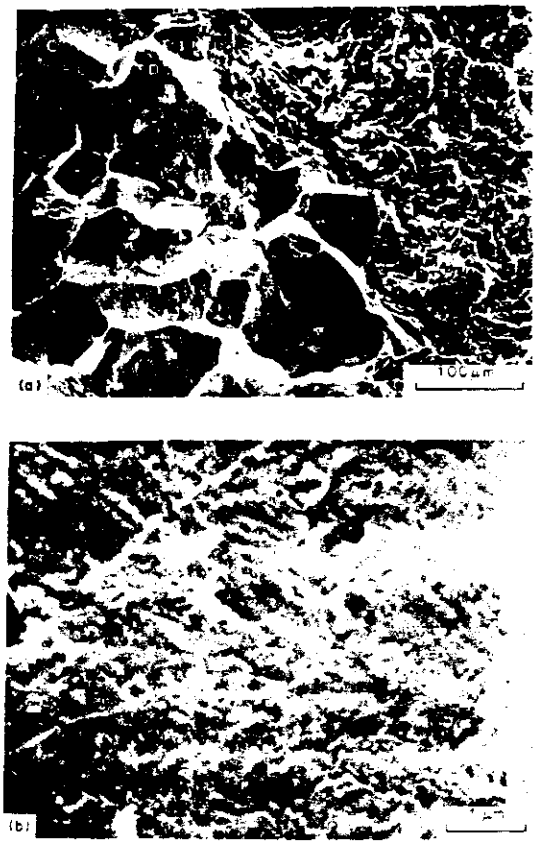

Fig. 1. Low-ductility intergranular fracture morphology in alloy D.

Later work [11] has established that, at fixed

Table 1. Bulk chemical analyses of alloys A–D (in wt%)

Alloy	Cr	Mo	Mn	Si	Ni	Cu	V	W	Nb	As	Sb
A "pure"	2.25	0.97	0.55	0.025	0.02	0.015	<0.01	<0.01	<0.01	<0.01	<0.01
B P-doped	2.25	1.02	0.57	0.02	0.03	0.015	<0.01	<0.01	<0.01	<0.01	<0.001
C Sn-doped	2.23	1.03	0.57	0.03	0.01	0.02	<0.01	<0.01	<0.01	<0.02	<0.001
D commercial	2.12	0.95	0.53	0.17	0.20	0.15	<0.01	<0.02	<0.01	<0.02	<0.005

Alloy	Sn	P	S	Ti	Zr	Bi	Co	Al	C	N	O
A "pure"	<0.01	0.007	0.006	<0.01	<0.01		0.02		0.09	<0.002	
B P-doped	0.007	0.054	0.006	<0.01	<0.01		0.02		0.12	0.005	
C Sn-doped	0.05	0.007	0.005	<0.01	<0.01		0.02		0.10	0.001	0.015
D commercial	0.010	0.015	0.021	<0.01	<0.01	<0.01	<0.01	<0.01	0.13	0.006	

Table 2. Values of the parameters α and β in relation (1) over a range of temperature for alloy D

Temperature (°C)	α (ms^{-1})	β ($m^{3/2}N^{-1}$)
400	6.71×10^{-13}	1.658×10^{-1}
450	1.41×10^{-9}	1.225×10^{-1}
500	1.09×10^{-9}	1.338×10^{-1}
550	3.78×10^{-8}	9.150×10^{-2}
600	9.71×10^{-9}	1.949×10^{-1}

temperature, an exponential relationship exists† between the crack growth rate da/dt and applied stress-intensity K for the low-ductility intergranular fracture mechanism, i.e.

$$da/dt = \alpha \exp(\beta K) \quad (1)$$

with temperature and material dependent parameters α and β; values are given in Table 2. Figure 2 illustrates relationship (1) over a range of temperatures for the commercial alloy, D; both impurity doped alloys, B and C, showed similar behaviour. It is clear from this figure that, although the micromechanism of low-ductility intergranular fracture appears to be of a relatively brittle nature, the rates of crack growth observed are several orders of magnitude lower than those found in brittle low-temperature intergranular fracture, i.e. 10^{-8} to 10^{-5} ms^{-1} compared with $\sim 10^{3}\,ms^{-1}$ for truly brittle fracture.

An initial investigation of the intergranular segregation behaviour in alloys A and B [6] indicated that the embrittlement of grain-boundaries by segregation of residual impurities played a vital role in the fracture mechanism. A maximum in the phosphorus enrichment of grain-boundaries was observed for samples of the doped alloy B which were heat-treated in the absence of applied stress in the temperature range corresponding to the low-ductility intergranular fracture regime (450–600°C). Such heat treatment caused embrittlement of grain-boundaries when fractured at low temperature, thus enabling their surface chemical analysis by Auger electron spectroscopy (AES). However, no such embrittlement was found in the high-purity alloy, A, and it was suggested therefore that impurity segregation of phosphorus by equilibrium or carbide rejection mechanisms was responsible for both the low-temperature and elevated-temperature "brittle" intergranular fracture modes exhibited by alloy B.

Similar segregation patterns were detected in the commercial alloy, D, but the behaviour of the tin-doped alloy C demonstrated that low-ductility intergranular fracture could not be induced by thermally activated segregation alone [8]. Although elevated-temperature intergranular crack growth in alloy C

†This type of behaviour breaks down at crack growth rates of $\lesssim 10^{-8}\,ms^{-1}$, where da/dt becomes independent of K (with decreasing K and temperature) before falling sharply towards a threshold value (G. Gage, AERE Harwell, private communication).

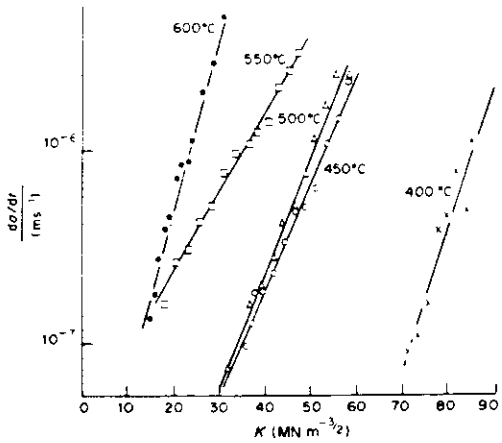

Fig. 2. The variation of crack growth rate with applied stress-intensity in alloy D measured isothermally over a range of temperatures.

showed the same fractographic and K-dependence characteristics as in alloys B and D, samples of the tin-doped alloy, heat-treated in the absence of stress, were not susceptible to low-temperature intergranular embrittlement. Hence, by inference, tin did not segregate to grain-boundaries by equilibrium or carbide rejection mechanisms.

The results summarised above have led to the suggestion that a third mechanism of segregation is involved in low-ductility intergranular fracture of specimens under applied stress, i.e. localised segregation of solute atoms to the crack-tip region possibly driven by the crack-tip stress field [8, 10, 21, 22]. This may enable embrittling solute elements which do not otherwise segregate (e.g. tin) to reach a sufficient concentration at the crack-tip for crack advance under the influence of static applied stress and elevated temperatures (providing solute mobility). Since the proposed segregation is limited to the vicinity of the crack-tip, intergranular embrittlement by the above localised stress-driven segregation mechanism would not induce general grain-boundary fracture on impact at low temperature, i.e. consistent with the behaviour of the tin-doped alloy, C.

3. ANALYSIS OF CRACK-TIP SOLUTE CHEMISTRY

3.1. *Experimental method*

Evaluation of the local segregation hypothesis requires a method for the direct analysis of solute chemistry in the vicinity of a crack-tip. Figure 2 shows that, at a given temperature, a steady-state average crack propagation velocity will be attained in response to an applied stress-intensity. In order to attempt determination of the solute distribution near the crack-tip during crack growth, it was necessary to cool rapidly SEN specimens of alloys B, C and D undergoing low-ductility intergranular fracture while maintaining the applied stress-intensity. It was hoped that a characteristic solute distribution would thus be

"quenched-in" since the segregant species of interest are relatively immobile at room temperature.

Miniature impact specimens were machined from the SEN testpieces to include the intergranular high-temperature crack-tip in their diameter [Fig. 3(a)]. Optical and scanning-electron microscopy of cracks sectioned parallel to the direction of crack growth has shown that, on interruption of specimen tests as described, crack growth may arrest with the crack-tip located partially across a grain-boundary (Fig. 4). Subsequent impact fracture at low temperatures in the AES system may in some cases induce brittle crack propagation across the remaining portion of the grain-boundary, providing it is sufficiently embrittled [Fig. 3(b)]. This operation presents grain-boundary facets within the AES system, part of which are exposed by high-temperature fracture in air, and are thus oxidised, and the remainder of which are free from adsorbed contaminants. A line profile of AES analyses progressing from the "clean" low-temperature region of the intergranular facet to the oxidised region will reveal patterns of solute segregation associated with the high-temperature crack-tip [Fig. 3(c)]. Conventional AES impact specimens were also machined from the "bulk" of SEN testpieces, so

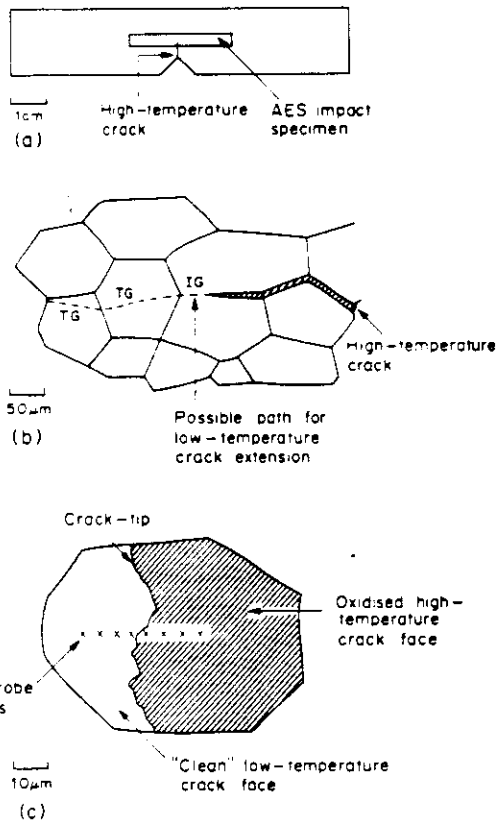

Fig. 3. Schematic illustrations of (a) extraction of AES specimen from SEN testpiece, (b) partial extension of high-temperature crack along grain-boundary (IG) by low-temperature brittle fracture before dominant transgranular cleavage (TG) prevails, and (c) geometry of AES line profile analysis on chosen intergranular facet straddling high/low temperature cracks.

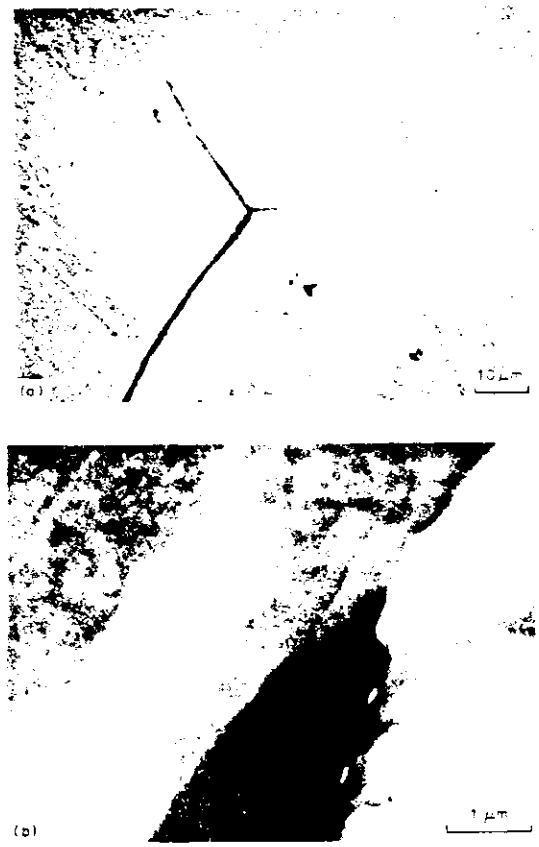

Fig. 4. SEM micrographs of low-ductility intergranular fracture in section showing (a) partial fracture of a grain-boundary and (b) the crack-tip profile.

that the segregation behaviour in unstressed material could be assessed. The AES facility employed was a Vacuum Generators MA500 scanning Auger microprobe. A secondary electron image resolution of ~50 nm was obtainable in low-current mode, which enabled accurate positioning of the ~250 nm diameter Auger analysis probe. Differential spectra were acquired using an accelerating voltage of 10 keV and a probe current of 1 μA.

3.2. Results

In practice, intergranular facets straddling high-temperature/low-temperature fractures were few and were only observed in alloys B and D (i.e. those which exhibited low-temperature intergranular embrittlement). Line profiles of the elements phosphorus, sulphur, carbon and oxygen are shown in Figs 5 and 6 for samples of alloy B (tested at 475°C) and D (tested at 600°C). Surface concentrations are expressed as AES differential peak-height ratios (phr) to the iron (703 eV) peak, while the mean bulk intergranular concentrations of phosphorus and sulphur (estimated from more than 10 analyses) are indicated to the right of each profile for comparison. Figure 7 presents complete AES spectra corresponding to analysis positions 1, 4 and 8 in Fig. 5, taken from alloy B.

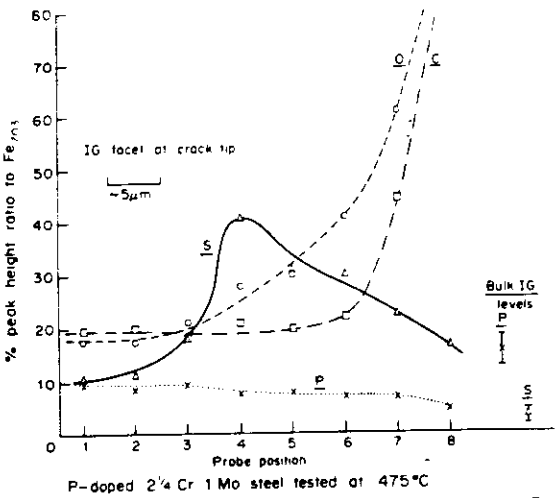

Fig. 5. AES line-profile across a crack-tip facet in alloy B.

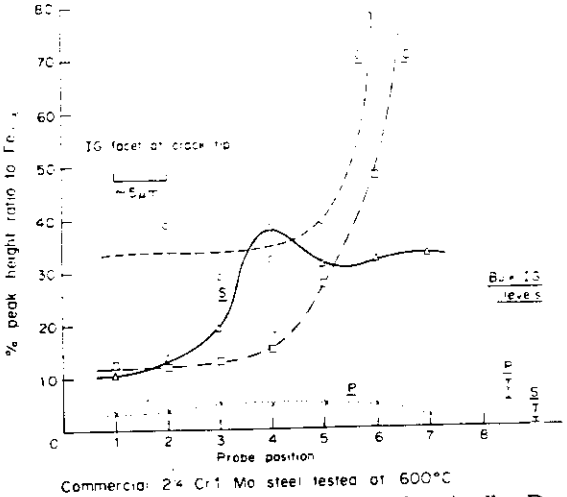

Fig. 6. AES line-profile across a crack-tip facet in alloy D.

The crack-tip is delineated by a sharp rise in oxygen phr due to atmospheric contamination of the high-temperature crack-faces. The carbon phr rises simultaneously with oxygen. Figure 7 indicates that high carbon levels are associated with a change from carbide to graphite form and probably therefore also reflect atmospheric contamination. The embrittling solutes phosphorus and sulphur were also detected on crack-tip facets. No significant enhancement of phosphorus was observed near the crack-tip, the average crack-tip facet phrs generally falling below those found on grain-boundaries in the specimen bulk. However, sulphur levels exhibit a noticeable increase as the vicinity of the crack-tip is approached, rising to concentrations many times greater than those found on grain-boundaries in the absence of stress (Figs 5 and 6). The sequence of spectra in Fig. 7 shows that sulphur levels rise while carbon is still in carbide form, indicating that the enhancement of sulphur is not associated with atmospheric contamination.

No other embrittling agents were detected near crack-tips in samples of alloys B or D, although spectrum noise levels on the tin/antimony region (430–460 eV) correspond to ~3% phr. Grain-boundary concentrations of alloying elements molybdenum and chromium were not significantly affected by proximity to the crack-tip.

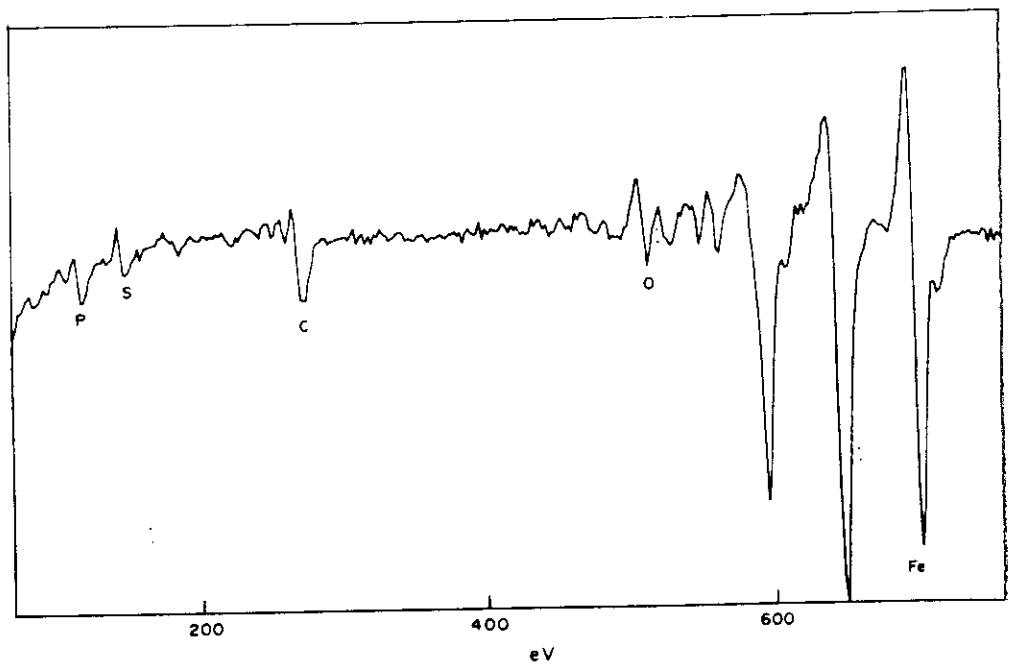

Fig. 7(a).

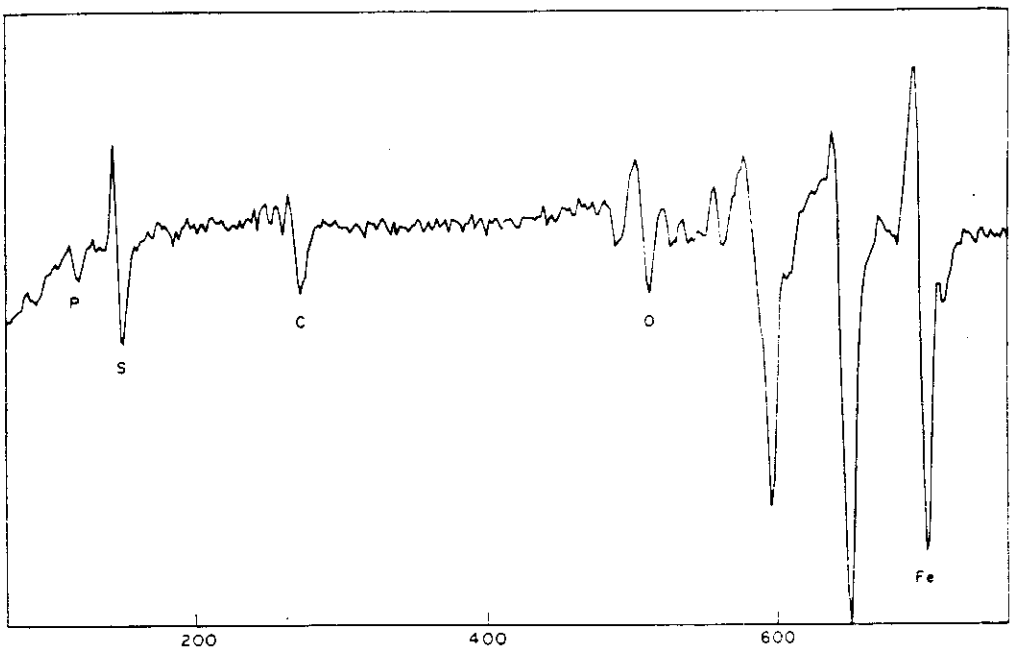

Fig. 7(b).

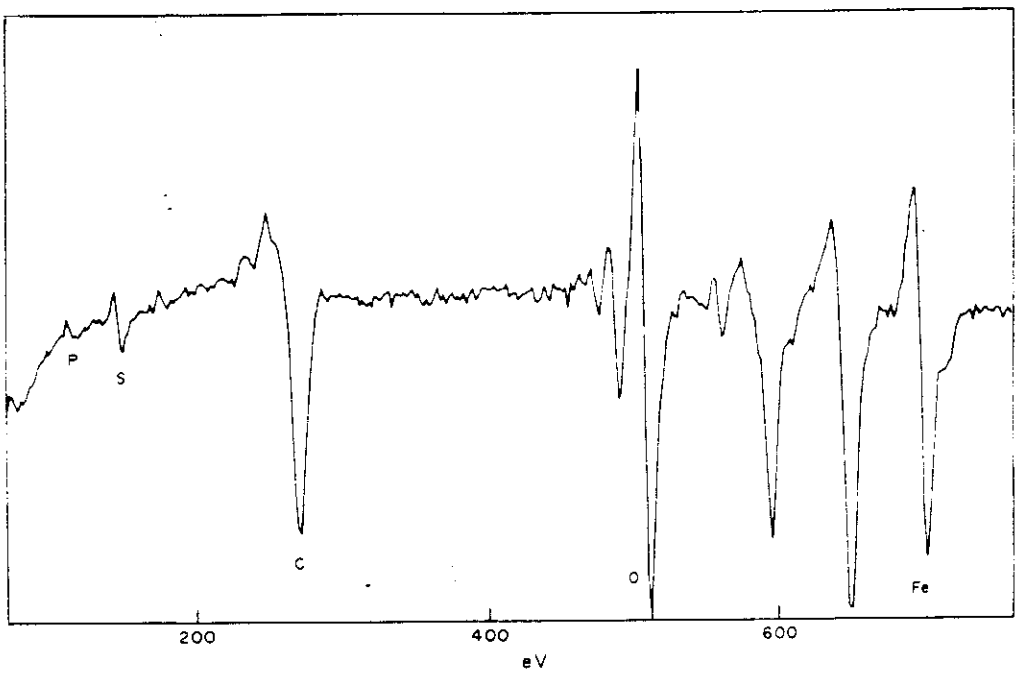

Fig. 7(c).

Fig. 7. AES differential energy spectra (a), (b) and (c) corresponding to positions 1, 4 and 8 respectively in Fig. 5.

Fracture of (tin-doped) alloy C specimens did not provide any grain-boundary facets suitable for AES line profile analysis. The low-temperature crack path became transgranular immediately after the high-temperature intergranular pre-crack. However, some analyses were performed on oxidised intergranular facets as close to the crack-tip as possible, indicating the presence of sulphur together with high oxygen carbon levels. Tin was not detected in these specimens.

Following these initial observations of high-temperature intergranular crack-tip chemistry in alloys B, C and D, a set of controlled tests was performed on three specimens of alloy D at 500, 550

and 600 C. A constant low-ductility intergranular crack growth rate of $\sim 10^{-6}\,ms^{-1}$ was obtained in SEN testpieces by adjusting the applied stress-intensity at each temperature. The specimens were then cooled to arrest the crack, and the solute distribution near the crack-tip analysed (as above). AES line profiles showed significant sulphur enrichment near crack-tips in all three cases. The sulphur phr observed in the vicinity of the crack-tip correspond to atomic percentage coverages of 1.5, 2.0 and 7.5% at 500, 550 and 600 C, respectively (using an approximate S to Fe sensitivity ratio of 4.7). These values will be considered in later discussion of the theoretical model of local segregation to such regions.

3.3. Discussion of experimental results

AES line profile analyses have demonstrated that enrichment of sulphur in the vicinity of the high-temperature intergranular crack-tips was common to all three $2\frac{1}{4}$Cr1Mo steel alloys. The following potential sources of enhanced sulphur detected by AES analysis should be considered:

(i) discrete grain-boundary sulphide particles precipitated by an "overheating" mechanism [23] during high-temperature austenitisation;
(ii) free-surface segregation of sulphur to crack-faces subsequent to fracture;
(iii) segregation of sulphur driven by the crack-tip stress field.

In order to assess the first possibility, a sample of alloy B was transferred to a high-resolution scanning electron microscope after AES analysis. The intergranular facet, from which the line profile shown in Fig 5 is taken, was identified, and a series of micrographs and energy-dispersive X-ray analyses were obtained from each AES spectrum position. No obvious concentration of sulphide particles at the crack-tip was observed micrographically. A set of quantified EDS analyses is given in Figure 8 for the elements chromium, manganese and molybdenum/sulphur. Interpretation is complicated by the superposition of the molybdenum L and sulphur K peaks in the X-ray spectrum. However, it is clear that (a) there is no significant variation in the sulphur/molybdenum level detected across the profile, and (b) if the sulphur/molybdenum peak is

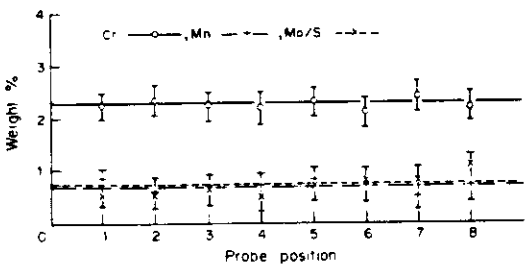

Fig. 8. Quantified energy dispersive X-ray analyses taken from the same probe positions as those in Fig. 5.

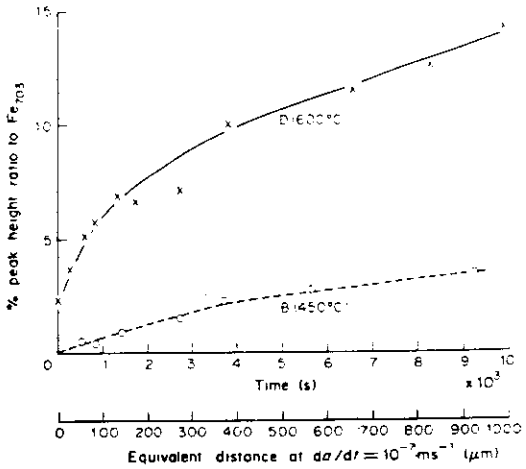

Fig. 9. The segregation behaviour of sulphur to free surfaces in alloy B(450°C) and alloy D(600°C) as a function of time and equivalent distance travelled by a crack front at a velocity of $10^{-7}\,ms^{-1}$.

quantified as arising solely from molybdenum, the average concentrations given in Fig. 8 for molybdenum (together with chromium and manganese) correspond approximately to those present in the specimen bulk (Table 1).

Previous experience of X-ray analysis of small sulphide particles on an iron matrix (within intergranular cavities) has shown that only particles of diameters larger than 0.3 μm contribute significantly to the X-ray signal [6, 19]. Hence the analysis presented in Fig. 8 demonstrates that no sulphides larger than this sensitivity limit were present in the paths of the AES line profile. Some smaller particles were observed micrographically, but these were elongated, of approximate dimensions 0.2 μm × 0.05 μm, characteristic of grain-boundary carbides, and were evenly distributed over the whole facet.

The second possible source of the sulphur found near the crack-tips may be assessed by considering data obtained for the segregation of sulphur to free surfaces in alloys B and D at 450 and 600 C, respectively [21]. The free surfaces were initially polished to 0.25 μm, cleaned by argon-ion bombardment and then analysed using AES. Sulphur levels, expressed as phr to iron (703 eV) are presented in Fig. 9 as functions of time at different temperatures (in a vacuum of 5×10^{-10} torr).

Consider the crack situation: the duration of exposure of crack-surfaces after fracture, and hence the time available for free surface segregation, increases linearly with distance from the crack-tip as a function of crack velocity. Rapid cooling should ideally arrest the crack instantaneously. In practice the maximum cooling rate attainable was ~ 100°C min^{-1} and hence the crack may slow from its original test velocity of $10^{-6}\,ms^{-1}$ before final arrest, and may conceivably be static at temperatures which enable surface segregation to continue.

An equivalent distance from the crack-tip is plotted on the lower horizontal axis in Fig. 9 for a crack velocity of 10^{-7} ms^{-1} i.e. an order of magnitude lower than at the start of cooling. At this reduced velocity it is clear that the levels of sulphur which could be produced by free surface segregation behind the crack-tip at a maximum profile length of 25 μm were negligible when compared to those actually measured in alloys B (475 C) and D (600 C) at exposed crack-tips (Figs 5 and 6). Even allowing a period of, say, 10^3 s during which the crack may be static at elevated temperatures, Fig. 9 shows that free surface segregation could not account for the sulphur levels observed near the crack-tip.

It is therefore reasonable to conclude that the enrichment of sulphur observed near the crack-tips during high-temperature intergranular fracture was produced by the influence of the crack-tip stress field. It is also suggested that stress-induced sulphur segregation contributed towards the mechanism of such low-ductility intergranular fracture. However, since sufficient bulk concentrations of other embrittling impurity elements such as phosphorus and tin have also been shown to be prerequisite for the operation of this fracture mechanism, it would seem that sulphur must act synergistically.

No firm conclusion regarding the expected stress-induced segregation of tin in alloy C can be made at this stage, due to the absence of suitable intergranular facets for AES analysis. It would be difficult to attribute the occurrence of low-ductility intergranular fracture in this alloy to stress-induced sulphur segregation alone, because alloy A (immune to low-ductility intergranular fracture) contains similar bulk sulphur concentrations [8]. It is proposed to induce intergranular fracture ahead of the high-temperature crack-tip by performing slow strain-rate bend tests in hydrogen gas within the AES environment. Further investigation of the possible influence of the crack-tip stress field on tin segregation must await this development.

In view of the unforeseen and apparently major role of sulphur in slow brittle crack extension implied by the results of AES analysis, a short series of stress-relaxation tests was performed to provide more direct evidence for its influence on fracture properties. Two sets of SEN specimens were prepared from the commercial alloy, D, the first being held at 1200 C in vacuum for 0.5 h and directly quenched into oil (DQ) and the second being step cooled, after 0.5 h at 1200 C, to 900 C, held for 1 h and then quenched into oil (SQ). This treatment was intended to provide two different levels of sulphur in solution for specimens of equivalent grain size after final quenching, since the solubility of sulphur in austenite decreases rapidly with temperature from 12.8 ppm at 1200 C (Fe-0.5% Mn alloy) to 0.4 ppm at 900 C [24].

Figure 10 shows the relaxation test results. The severity of cracking is expressed as the final crack length measured from a specimen broken open on concluding the test. In this case a heating rate of 200 C h^{-1} was employed. Specimens were heated to a maximum temperature of 700 C, held for 40 min and then cooled to room temperature. Clearly, stress-relief cracking (known to be dominated by slow brittle fracture in DQ specimens of higher dissolved sulphur content) was dramatically attenuated in the SQ specimens of lower dissolved sulphur content. Hence the importance of the role of sulphur as an embrittling agent acting under the influence of the crack-tip stress is supported.

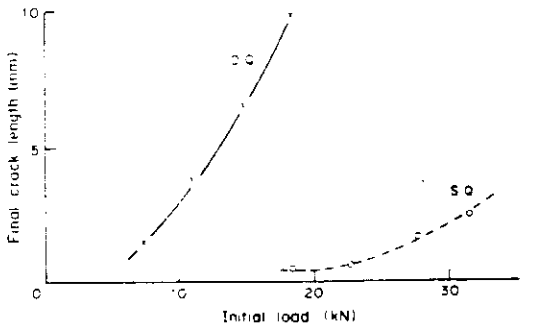

Fig. 10. The relative cracking behaviour of the commercial alloy, D, subject to the stress-relaxation test after direct quenching from 1200 C (DQ), and step quenching from 1200 to 900 C before final quenching to room temperature (SQ).

This result also suggests that the widely reported inhibition of stress relief cracking by refining originally coarse-grained HAZ microstructures [25, 26] is not solely due to the reduction in grain size, but is strongly influenced by the level of sulphur remaining in solution after a second, low-temperature (900–950 C) austenitisation.

4. SOLUTE MIGRATION TO A CRACK

To account for the experimental results reported above, we present a theoretical analysis of the expected migration of solute to a crack in which the respective current density near the crack-tip is assumed to be dominated by the elastic interaction between the stress field of the tip and the solute atoms. The justification for adopting this "pure-drift" approximation and neglecting random diffusion processes stems essentially from the large magnitude of the elastic interaction in the vicinity of the crack-tip and will be amplified in the light of results obtained below. A more extended presentation of this analysis and discussion of other related crack point-defect interaction phenomena is given elsewhere [27].

4.1. Theoretical model

We consider a long straight semi-infinite crack within an isotropic elastic body, occupying the negative x-region of the x–z-plane as indicated in Fig. 11, where x,y,z denote orthogonal Cartesian axes and the crack-tip coincides with the z-axis. When loaded in

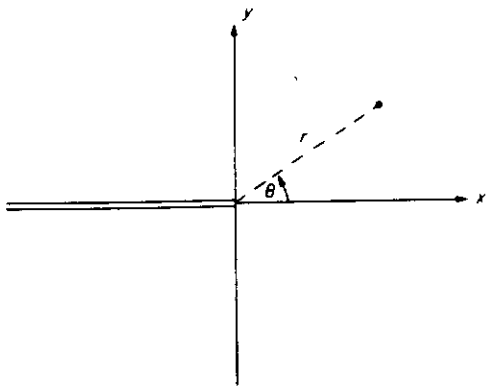

Fig. 11. The long straight semi-infinite crack with its tip occupying the z axis of an orthogonal Cartesian system x,y,z. The definition of cylindrical polar coordinates (r,θ) is indicated.

the opening mode the crack-tip has an elastic stress field characterised by the stress-intensity factor K, and this field interacts with a nearby point-defect, modelled as a misfitting spherical inclusion [28] and located at a position defined in cylindrical polar coordinates (r,θ,z) relative to the tip, with an energy given by [29]

$$E(r,\theta) = -A\cos\left(\frac{\theta}{2}\right)/r^{1/2};\quad -\pi < \theta < \pi. \tag{2}$$

In this expression

$$A = \left(\frac{2}{9\pi}\right)^{1/2}(1+\nu)K\,\Delta V \tag{3}$$

where ν is Poisson's ratio and ΔV is the relaxation volume associated with the point-defect; thus ΔV determines the sign of A and hence of E.

The point-defect current density due to a field of force $-\nabla E$ is in the "pure-drift" approximation

$$\mathbf{j} = -\frac{D}{k_B T}c\nabla E \tag{4}$$

where D is the point-defect diffusion coefficient, k_B denotes Boltzmann's constant, T the absolute temperature and c is the point-defect volume concentration. The continuity equation

$$\frac{\partial c}{\partial t} + \nabla\cdot\mathbf{j} = 0 \tag{5}$$

becomes, from (4)

$$\frac{\partial c}{\partial t} = \frac{D}{k_B T}\nabla E\cdot\nabla c \tag{6}$$

when E is harmonic, as in the present case. With (2), equation (6) takes the explicit form

$$\frac{\partial c}{\partial t} = \frac{AD}{2k_B T r^{3/2}}\left[\cos\left(\frac{\theta}{2}\right)\cdot\frac{\partial c}{\partial r} + \sin\left(\frac{\theta}{2}\right)\cdot\frac{1}{r}\frac{\partial c}{\partial\theta}\right]. \tag{7}$$

We solve this first-order hyperbolic equation for the time dependent point-defect concentration around the crack-tip adopting the simple initial condition

$$c = c_0 > 0 \text{ at } t = 0 \tag{8}$$

with c_0 a constant and the boundary condition

$$c = c_0 > 0 \text{ as } r\to\infty \tag{9}$$

at any time $t \geqslant 0$. Equation (7) has a suitable solution which satisfies the requirements (8) and (9) and which is consistent with the crack-tip or the crack-surfaces acting as sinks for the point-defects arriving there. This solution may easily be obtained by the method of characteristics. Depending on the sign of ΔV, it consists of two regions separated by a characteristic that expands with time; in the inner region the solution is identically zero and in the outer region it remains at its initial value c_0.

When $\Delta V > 0$, the expanding characteristic has the polar equation

$$r(\theta,t) = \bar{r}(t)\frac{\sin^2\left(\frac{\theta}{2}\right)}{\left[3(\sin\theta + (\mathrm{sgn}\theta)\pi - \theta) + 2\sin\theta\,\sin^2\left(\frac{\theta}{2}\right)\right]^{2/3}};\quad -\pi \leqslant \theta \leqslant \pi \tag{10}$$

and when $\Delta V < 0$, it has the equation

$$r(\theta,t) = \bar{r}(t)\frac{\sin^2\left(\frac{\theta}{2}\right)}{\left[3(\sin\theta - \theta) + 2\sin\theta\,\sin^2\left(\frac{\theta}{2}\right)\right]^{2/3}};\quad -\pi \leqslant \theta \leqslant \pi \tag{11}$$

where

$$\bar{r}(t) = \left(\frac{4|A|Dt}{k_B T}\right)^{2/3}. \tag{12}$$

A "snapshot" (at a particular time $t > 0$) of the characteristic defined by (10) and (11) is illustrated in Figs 12 and 13, respectively, by the single long-dashed line, and the concentration is zero inside the characteristic (shaded region) and equal to its initial value c_0 outside. The figures also show various (short-dashed) equipotentials obtained from (2) together with various (solid) flow lines, on which the arrows indicate the directions of flow. It is immediately clear that when $\Delta V > 0$ (Fig. 12) the point-defects are all flowing only into the precise tip of the crack, whereas when $\Delta V < 0$ (Fig. 13) they all flow into the crack-surfaces behind the actual tip.

Since we wish to discuss the segregation of (under-

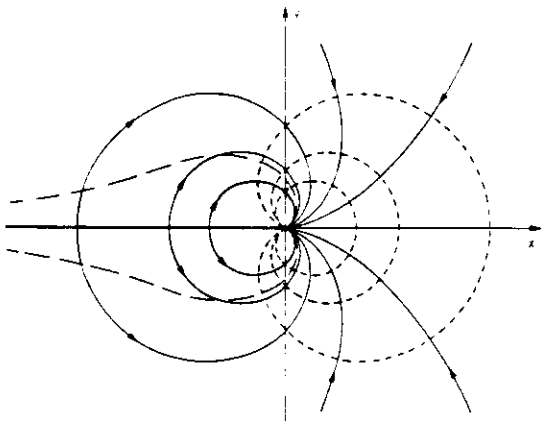

Fig. 12. Equipotentials (– – – –), flow lines (→) and an expanding characteristic (——) in the vicinity of a crack-tip loaded in the opening mode, when the point-defect relaxation volume $\Delta V > 0$. Inside the characteristic (shaded region) the point-defect concentration is zero, and outside it retains its initial value c_0.

sized) substitutional sulphur atoms to a crack it will be convenient to restrict the subsequent analysis to the case $\Delta V < 0$. If $N(t)$ is the total number of point-defects that have reached the crack after time $t > 0$, per unit length in the z-direction in excess of the number deposited at initial time $t = 0$, then we may write

$$N(t) = \int_{-\infty}^{0} n(x,t)\,\mathrm{d}x \tag{13}$$

where $n(x,t)$ defines the spatial distribution of point-defects having entered along the crack $-\infty < x \leqslant 0$ at time t. To deduce $n(x,t)$ we proceed as follows.

The total flux of point-defects to the crack is, from (4) with (2)

$$F(t) = \frac{\mathrm{d}N}{\mathrm{d}t} = \frac{|A|D}{k_B T} c_0 \int_{-\infty}^{\bar{x}(t)} \frac{\mathrm{d}x}{|x|^{3/2}} \tag{14}$$

where

$$\bar{x}(t) = -r(\pi,t) = -\left(\frac{4}{3\pi}\right)^{2/5} \left(\frac{ADt}{k_B T}\right)^{2/5} \tag{15}$$

defines the location of the intersection of the characteristic (11) with the crack, so that for $x \leqslant \bar{x}(t)$ the concentration adjacent to the crack-surfaces remains at its initial value c_0. Inside the characteristic, i.e. for $\bar{x}(t) < x$, the concentration vanishes and the instantaneous flux must be zero.

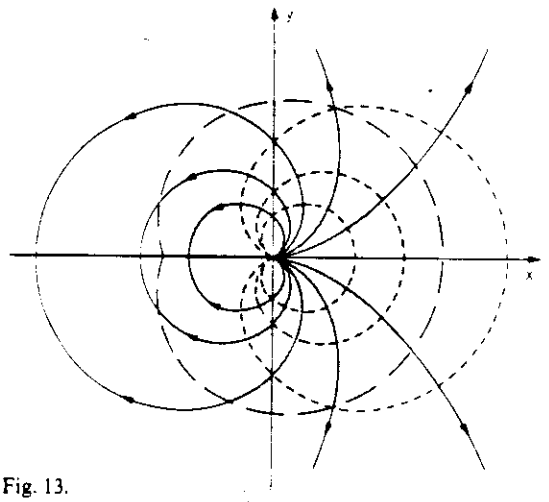

Fig. 13. volume $\Delta V < 0$.

Integrating (14) yields

$$N(t) = \int_0^t \left(\frac{\mathrm{d}N}{\mathrm{d}t'}\right) \mathrm{d}t'$$

$$= \frac{|A|D}{k_B T} c_0 \int_0^t \int_{-\infty}^{\bar{x}(t')} \frac{\mathrm{d}x}{|x|^{3/2}}\,\mathrm{d}t'. \tag{16}$$

The equality between (13) and (16) is easily seen to be satisfied when

$$\frac{n(x,t)}{c_0} = \begin{cases} \left(\frac{3\pi}{4}\right) \frac{|\bar{x}(t)|^{5/2}}{|x|^{3/2}} & \text{for} \quad -\infty < x \leqslant \bar{x}(t) \\ \left(\frac{3\pi}{4}\right) |x| & \text{for} \quad \bar{x}(t) < x \leqslant 0. \end{cases} \tag{17}$$

The variation of this distribution along the crack is shown in Fig. 14 for three times, t, $2t$ and $3t$, where $t > 0$ is arbitrary, and $|\bar{x}(t)|$ is used as the convenient unit of length. On substituting (17) into (13) and performing the integration we find

$$N(t) = \left(\frac{3\pi}{4}\right) c_0 \left\{ 2\,|\bar{x}(t)|^{-1/2} - \frac{1}{2}\,|\bar{x}(t)|^{-1/2} \right\}$$

$$= \frac{5}{2}\left(\frac{3\pi}{4}\right) c_0 |\bar{x}(t)|^{-1/2} \tag{18}$$

which from (15) yields the explicit result

$$N(t) = \frac{5}{2}\left(\frac{3\pi}{4}\right)^{1/5} c_0 \left(\frac{ADt}{k_B T}\right)^{2/5}. \tag{19}$$

It is interesting to note, from the form of $n(x,t)$ in (17) and as indicated in (18), that at any time t precisely *four fifths* of the total number of point-defects which have entered the crack, have done so outside the instantaneous position of the expanding characteristic; that is beyond $x = \bar{x}(t)$. *One fifth* of the total has, of course, entered the crack between the tip at $x = 0$ and $x = \bar{x}(t)$. Finally, since the point-defect concentration is zero within the expanding characteristic and remains at its initial value c_0 outside, it follows that the number of point-defects lost at the crack, $N(t)$, is simply c_0 multiplied by the instantaneous area of the characteristic; i.e.

$$N(t) = \frac{1}{2} c_0 \int_{-\pi}^{\pi} r^2(\theta,t)\,\mathrm{d}\theta \tag{20}$$

with $r(\theta,t)$ given by (11). The integral can readily be evaluated to reproduce exactly the relation (19).

4.2. *Predicted sulphur segregation on the crack*

In order to utilise the above result for discussing the segregation of solute sulphur atoms to the slowly moving crack in the present study, we consider the actual crack propagation to proceed by a periodic sequence of stops and rapid jumps rather that by

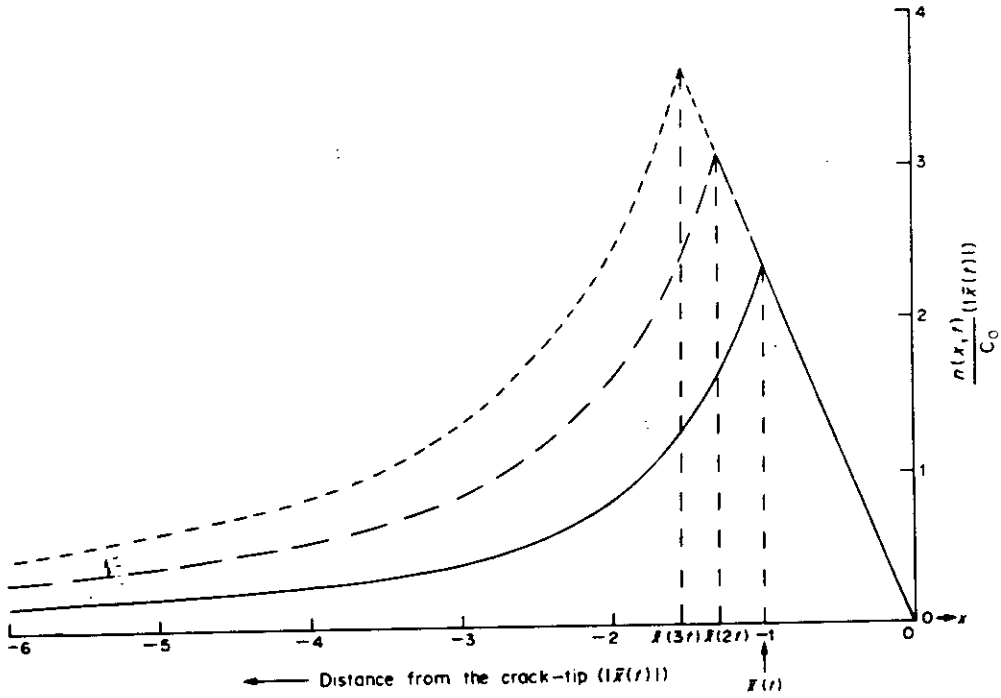

Fig. 14. The distribution of point-defects along the crack for times t (——), $2t$ (— — —) and $3t$ (– – –) in units of $|\bar{x}(t)|$, where $\bar{x}(t)$ defines the location of the intersection of the characteristic in Fig. 13 with the crack at time t.

uniform motion. The average velocity v of the crack is then given by

$$v = d/\Delta t \tag{21}$$

where d denotes the characteristic propagation distance and Δt the time when the crack is stationary between each jump. For $N(\Delta t)$, given by equation (19), to represent the number of segregated solute atoms during Δt, it is necessary that at each step the crack should jump a sufficient distance to immerse its tip in virgin material such that negligible depletion has occurred there; only in this situation is it reasonable to use expression (19) with a constant initial concentration c_0. The required condition on d is therefore

$$d \gg l \tag{22}$$

where l denotes the lateral size of the expanding characteristic after a time Δt. From the polar equation (11) of the characteristic it appears that

$$l = r(0,\Delta t) + r(\theta_0,\Delta t)\,|\cos\theta_0| \tag{23}$$

with $\theta_0 \sim 164°$; this gives

$$l \sim 1.84\left(\frac{AD\Delta t}{k_B T}\right)^{2.5} \tag{24}$$

which implies the condition on the crack resting time Δt

$$\Delta t \gg 2.76\left(\frac{AD}{k_B T}\right)^{2.3}/v^{5.3}. \tag{25}$$

Finally, with this model for the moving crack, the average coverage of solute atoms per unit area of the crack-surfaces would be

$$P = N(\Delta t)/2v\Delta t \tag{26}$$

with $N(\Delta t)$ given by equation (19).

The theoretical dependence of P on temperature has been evaluated, and the result is depicted in Fig. 15 for the physical parameters given in Table 3. The experimentally observed sulphur coverages, also shown in the figure, have been obtained, as described in Section 3.2, by quenching from the respective test temperatures with the applied stress-intensity maintained. To correlate our theoretical model predictions with such observations it is clearly necessary to reduce the crack propagation velocity to a value between the maintained constant low-ductility crack growth rate of $10^{-6}\,\mathrm{ms}^{-1}$ and zero (corresponding to the actual crack-arrest after the quench). We have therefore taken $v = 10^{-7}\,\mathrm{ms}^{-1}$ to represent an average crack propagation velocity prevailing during the initial retardation period of the crack-arrest process. With this value we have obtained the stress-intensity factors covering the temperature range in Fig. 15 by using the empirical form (1) which is fitted to the actual data of Fig. 2. The very close agreement between the predicted and observed sulphur coverage

Table 3. Data used to obtain the theoretical dependence of sulphur coverage on temperature shown in Fig. 15

Sulphur diffusion coefficient [30] $D = D_0\exp(-E_m/k_BT)$: $D_0 = 1.68 \times 10^{-4}\,\mathrm{m^2\,s^{-1}}$, $E_m = 2.13\,\mathrm{eV}$.
Poisson's ratio $\nu = 0.33$.
Atomic volume $\Omega = 11.22 \times 10^{-30}\,\mathrm{m^3}$.

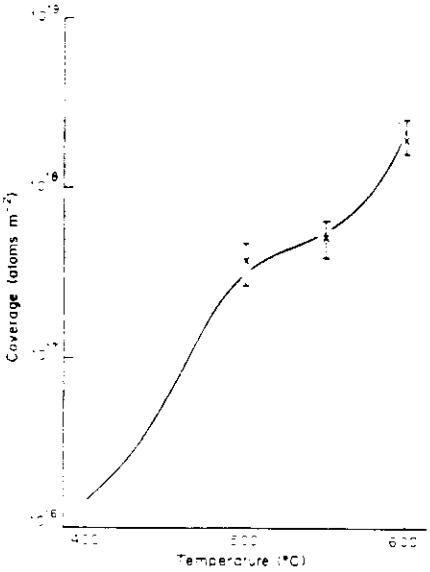

Fig. 15. The theoretically predicted sulphur coverage near the crack-tip as a function of temperature (——) for a crack propagation velocity of 10^{-7} ms^{-1}, together with the available experimental observations (×) and error bars: the measured values of the percent coverage quoted in Section 3.2 have been converted to the appropriate unit by the atomic volume in Table 3.

has been achieved by giving the remaining combination of parameters in (26) the value†

$$c_0 \gamma^{4.5} (\Delta t)^{1.5} = 1.29 \times 10^{24} \text{ atoms} \cdot \text{m}^{-3} \text{s}^{1.5} \quad (27)$$

where

$$\gamma = \Delta V / \Omega \quad (28)$$

is the relaxation volume strain associated with a substitutional sulphur atom and Ω is the atomic volume for b.c.c. iron. Thus the validity of the absolute agreement is conditional upon (27) being reasonable. The actual value of Δt, the stay time between crack jumps, is not known but because it is raised to a low power in (27) its value will only weakly affect the total; therefore we may allow $\Delta t = 1$s. With this choice we see that the necessary inequality (25) is satisfied over the temperature range considered here when $v = 10^{-7}$ ms^{-1}. In addition, the average jump distance defined in (21) is $d = 10^{-7}$ m and therefore, as is clear from Fig. 6, the maximum deposition of sulphur is deemed to occur during the order of ~50 crack-tip jumps, which gives some legitimacy to our use of an average velocity during this period. With $\Delta t = 1$s, we may deduce the variation of c_0 with γ, required to satisfy (27), and the results are given in Table 4. The solubility of sulphur at 1200 C in austenite for alloy D is [24] 1.91×10^{24} atoms·m^{-3} and thus the equality (27) is

†If a higher average crack propagation velocity were to be adopted similar agreement is achievable but with a different value required for the left-hand side of equation (27).

Table 4. Values of sulphur concentration c_0 due to equation (27) over a range of sulphur atom relaxation volume strains γ

γ	c_0 (atoms m^{-3})
−0.2	4.66×10^{24}
−0.4	2.68×10^{24}
−0.6	1.94×10^{24}
−0.8	1.54×10^{24}

reasonable if $|\gamma| \gtrsim 0.6$. A precise value for γ cannot be established since we expect some of the sulphur to precipitate as MnS during the quench: nevertheless we may conclude that the required equality (27) can be satisfied with physically acceptable values for γ and c_0 and therefore, in addition to the agreement with the *form* of the temperature dependence of the sulphur segregation, our model also yields very good *absolute* agreement.

5. GENERAL DISCUSSION

The segregation of sulphur on a crack has been studied theoretically using a "pure-drift" approach. By its very nature, the physical validity of this concept is restricted to small-time depletions from the initial solute concentrations. A more complete analysis would require also random diffusion processes to be accounted for in which the existence of a permanent expanding discontinuity in the concentration solution would be precluded. This calculation would involve the imposition of explicit sink boundary conditions at the crack surfaces and tip and probably would necessitate sophisticated numerical techniques. The present "pure-drift" calculation, on the other hand, has the distinct advantage of transparent analytic simplicity; in addition, such an approach has provided a satisfactory explanation of various analogous phenomena including the kinetics of strain-ageing in steels [31]. In the latter situation we are concerned with the drift of interstitial impurities to dislocations, and exactly the same type of expanding discontinuities exists. However, the interaction between a crack-tip and a nearby point-defect is much greater than the corresponding single dislocation-point-defect interaction, and thus if we accept the validity of the strain-ageing studies the "pure-drift" approach should also be valid for the present problem. However, it is important for the overall applicability of the underlying calculation that the crack does propagate by a sequence of stops and jumps in which each jump takes the crack-tip well into regions of virgin material. In such a region the solute concentration is back at its initial value, and thus the average segregation may be legitimately deduced from the sequence of justified small-time depletions.

The theoretical evaluations presented in Section 4.2 demonstrate that the observed crack-tip enrichment of sulphur can be achieved by solute segregation driven by the crack-tip stress field. The predictions

show a good correlation with experimental results for an average crack velocity of $10^{-7}\,ms^{-1}$, which, although slower than that imposed before specimen cooling, is quite reasonable in the light of the discussion of Sections 3.2 and 4.2.

Our model implies that the crack advances in discrete steps, waiting after each step until sufficient sulphur has been deposited to enable further advance under the conditions of stress-intensity and temperature applied. Evidence to support this assumption can be drawn from the undulations in crack-tip profile illustrated in Fig. 4(b). These are approximately of the same magnitude as the proposed step distance of $10^{-7}\,m$ and are sometimes reflected by ripples of a similar scale on fractured facets [Fig. 1(b)].

If, as now seems likely, sulphur plays an important role in slow, brittle crack propagation, it must both embrittle grain-boundaries in steel and be suitably located at the crack-tip to do so within the overall fracture mechanism envisaged. The efficiency of sulphur as an intergranular embrittling agent has been established in pure iron (fractured at 196°C) [32] where it is free to segregate in the absence of scavenging alloying elements such as manganese and chromium. However, the mode in which embrittlement is achieved by deposition of sulphur *behind* the existing crack-tip, as predicted by the present model, requires clarification.

We have assumed that the relevant crack-tip stress field is that of an ideal sharp crack in a purely elastic medium for which the interaction energy given by equation (2) has its maximum unbounded value precisely at the tip of the crack, i.e. at $r = 0$ (c.f. Fig. 11). In reality, local plastic relaxation alters this ideal distribution such that the interaction energy has its maximum *in front* of the actual crack-tip, where $r \sim 1.9 \times$ (crack root radius) [33] and $\theta = 0$. The deposition of sulphur behind the region of maximum interaction, predicted by the model, can thus take place to unfractured material between the actual crack-tip and $r \sim 2 \times 10^{-7}\,m$. Hence, even if the embrittling action of sulphur necessitates its deposition *in front* of the actual crack-tip the present stress-driven segregation model need not be inconsistent. However, as is apparent from the scale in Figs 5 and 6 the uncertainty of the actual position of the crack-tip is considerable in relation to the scale of the predicted position of sulphur deposition behind the tip as indicated in Fig. 14.

A deficiency of this model is that it is not specific to the *intergranular* solute enrichment and fracture which is consistently observed. Indirect evidence summarised in Section 3.3 suggests that it may be necessary for stress-induced solute enrichment to act synergistically with intergranular segregants such as phosphorus; presumably, the prior segregation of the phosphorous to the grain boundaries under stress free conditions sufficiently depletes the matrix that there is insufficient phosphorus in solution to respond to the stress field of the crack-tip. Alternatively, sulphur enrichment at grain-boundaries may be encouraged by prior precipitation of sulphides during "overheating" which then act as local sulphur sources.

Independently of this investigation, Shin and McMahon [34] have been examining micromechanisms of stress-relief cracking in a MnMoNiCr steel (A508-2). Their findings broadly coincide with those reported here, and in particular, they have identified sulphur enrichment on a smooth intergranular facet which fractured in front of the notch in a loaded SEN specimen. Although their observations were not confined to the vicinity of a crack-tip region as such, they were, in our view, rightly interpreted as evidence in support of stress-induced sulphur segregation. This observation supports the detection of sulphur at a stress-relief crack-tip in a similar steel (A533B) reported previously [22].

Shin and McMahon [34] describe an alternative qualitative mechanism for crack-tip sulphur enrichment in which the crack is considered as a lenticular cavity, growing initially by the deposition of material from the open surface of the crack-faces into the unfractured grain-boundary. They suggest that intergranular sulphides become unstable on exposure to the atmosphere and dissolve on the crack-faces. This provides free sulphur which is deposited on the adjacent grain-boundary as part of the "cavity" growth process, thus embrittling the boundary and enabling "step-wise" growth.

This mechanism for slow brittle crack growth is similar in several aspects to that proposed in the present work, the main difference being in the nature of the free sulphur source, i.e. sulphides dissolving on crack-faces or present in solution after quenching from high temperatures within the material surrounding the crack-tip. There is insufficient experimental evidence to differentiate between the two mechanisms at this time, but it is clearly important to determine

(i) the nature and precise location of sulphides after overheating;
(ii) the stability of sulphides on free surfaces exposed to the atmosphere, and in the ferrite matrix or grain-boundaries at elevated temperature;
(iii) the physical validity of Shin and McMahon's model through a quantitative theoretical analysis.

CONCLUSIONS

1. The controlled propagation of low-ductility intergranular cracks in "as-quenched" $2\frac{1}{4}$Cr1Mo and MnMoNi low-alloy steels at elevated temperatures is associated with localised segregation of sulphur to the vicinity of the crack-tips, driven by the crack-tip stress field. However, it is clear that sulphur is not

solely responsible for the observed embrittlement, but acts synergistically with other intergranular embrittling agents.

2. The coverage of sulphur observed near a crack-tip, which is constrained to move at a constant average velocity, increases with temperature.

3. The predictions of a theoretical analysis, based on a "pure-drift" model of sulphur segregation from solution in the material bulk to the vicinity of the crack-tip, are consistent with experimental observations when physically reasonable starting parameters and a "step-wise" mode of crack growth are adopted.

4. The analysis demonstrates that crack-tip enrichment of available solutes with both positive and negative relaxation volumes in an iron matrix (e.g. tin and sulphur, respectively) can take place by this mechanism.

Acknowledgements—The authors are grateful to Dr B. C. Edwards for useful discussions and to Dr J. Shin and Professor C. J. McMahon for access to their unpublished results.

REFERENCES

1. P. Harris and K. E. Jones, *Proc. Conf. CEGB Welding Research Related to Power Plant*, Southampton, p. 369 (1972).
2. J. C. Ritter and R. McPherson, *Metals Technol.* **1**, 506 (1974).
3. B. L. King, *CEGB Report* RD L R 1945 (1976).
4. S. Debiez and H. Granjon, *Proc. Conf. W.I. Residual Stresses in Welded Construction and Their Effects*, London, p. 231 (19).
5. C. J. McMahon Jr, R. J. Dobbs and D. H. Gentner, *Mater. Sci. Engng.* **37**, 179 (1979).
6. C. A. Hippsley, J. F. Knott and B. C. Edwards, *Acta metall.* **28**, 869 (1980).
7. C. A. Hippsley, J. E. King and J. F. Knott, *Proc. Conf. M.S., Advances in the Physical Metallurgy and Applications of Steels*, Liverpool, p. 147 (1981).
8. C. A. Hippsley, J. F. Knott and B. C. Edwards, *Acta metall.* **30**, 641 (1982).
9. R. Blondeau, R. Boulisset, I. Dottet and B. Viellard-Baron, *Rev. Metall.* CIT No. 1, p. 61 (1980).
10. J. Shin, Jun Kameda and C. J. McMahon Jr, *Micro and Macro Mechanics of Crack Growth* (edited by K. Sadamanda, B. B. Rath and D. J. Michel), p. 149. T.M.E.-A.I.M.E. (1981).
11. C. A. Hippsley, *Metal. Sci.* **17**, 277 (1983).
12. R. C. Miller and A. D. Batte, *Metal Constr.* **7**, 550 (1975).
13. J. D. Murray, *Weld J.* **46**, 447 (1967).
14. B. A. Glossop, N. F. Eaton and T. Boniszewski, *Metal Constr.* **1**, 68 (1969).
15. P. Veron, C. A. Hippsley and J. F. Knott, *Int. J. Press. Vess. Piping* **16**, 29 (1984).
16. T. Boniszewski and N. F. Eaton, *Metal Sci.* **3**, 103 (1969).
17. S. G. Druce and J. A. Hudson, *Harwell Res. Rep.* AERE-R.10418 (1982).
18. D. Burns, D. W. James and H. Jones, *Metal Sci.* **7**, 204 (1973).
19. C. A. Hippsley, Ph.D. thesis, Univ. of Cambridge (1981).
20. R. A. Swift, *Weld J.* **50**, 195 (1971).
21. C. A. Hippsley and B. C. Edwards, *IAEA IWGFR Specialist Meet. Mechanical Properties of Structural Materials Including Environmental Effects*, Chester (1983).
22. B. C. Edwards, C. A. Hippsley and J. A. Hudson, *A.I.M.E. Conf. Ferritic Alloys for use in Nuclear Energy Techniques*, Snowbird, UT (1983).
23. T. J. Baker and R. Johnson, *J. Iron Steel Inst.* **211**, 733 (1973).
24. E. T. Turkdogan, S. Ignatowicz and J. Pearson, *J. Iron Steel Inst.* **180**, 349 (1955).
25. B. L. King, C. J. Middleton and R. D. Townsend, *CEGB Rep. RD L R* 1919 (1975).
26. A. D. Batte and M. C. Murphy, *Metals Technol.* **6**, 62 (1979).
27. H. Rauh and R. Bullough, *Harwell Research Report* TP.1034 (1984).
28. A. H. Cottrell and B. A. Bilby, *Proc. Phys. Soc., Lond.* **62**, 49 (1949).
29. H. W. Liu, *A.S.M.E. J. Basic Engng.* **92**, 633 (1970).
30. N. G. Ainslee and A. E. Seybolt, *J. Iron Steel Inst.* **194**, 341 (1960).
31. R. Bullough and R. C. Newman, *Rep. Prog. Phys.* **33**, 101 (1970).
32. C. Pichard, J. Rieu and C. Goux, *Mem. scient. Rev. metall.* **LXX**, 13 (1973).
33. J. F. Knott, *Fundamentals of Fracture Mechanics*, p. 89. Butterworths, London (1973).
34. J. Shin and C. J. McMahon Jr, *Acta metall.* To be published.

Key Words : Point-defects, stress-driven segregation, crack-tip stress, irradiation, evolving microstructure

POINT-DEFECT MIGRATION TO CRACKS DURING IRRADIATION

R. Bullough, Chief Scientist and Director of Corporate Research
AEA Technology, Harwell Laboratory, Oxfordshire, England

ABSTRACT

The quantitative importance of stress-driven solute segregation to the vicinity of growing crack-tips during high temperature brittle intergranular fracture of low alloy steels has been demonstrated by us. In this present paper we review some of the results of these studies that pertain to the steady state irradiation situation and indicate the probable importance of such crack stresses on the redistribution and loss of intrinsic point-defects at both the crack and in the surrounding evolving microstructure.

INTRODUCTION

It was realised by the earliest researchers into radiation embrittlement that its cause must either be due to hardening of the bulk material when subject to irradiation or to some mysterious loss of cohesive strength of the material, somehow induced by the irradiation. In a series of beautiful experiments in the 1950s the hardening [1] and embrittlement [1,2] mechanisms were identified by exploiting the Hall-Petch relation between grain size and yield stress and grain size and fracture stress respectively. It was concluded that radiation hardening is due to the "dispersion hardening" arising from the clusters or aggregates of the radiation produced point-defects and that such hardening is alone the direct cause of the radiation embrittlement.

In the intervening years both phenomena have been the subject of extensive observational and theoretical studies. Thus, the importance of solute impurities, such as carbon and copper in steels on clustering, the detailed morphologies of both solute precipitates and intrinsic dislocation loop aggregates and the influence of all of these on the hardening process is well understood [3,4,5]. Notwithstanding such complexities the early conclusion, that irradiation hardening is due to the formation of point-defect (solute or intrinsic or both) clusters of some kind leading to "dispersion hardening", remains valid today. On the other hand, whilst this hardening is often the dominant source of radiation embrittlement there is now evidence that irradiation can also cause the segregation of certain embrittling solute to grain boundaries [6] which in turn can enhance the probability of brittle fracture along such boundaries. In addition, in the absence of irradiation, it has been observed that such solute can also migrate under the stress field of an existing crack to embrittle the crack tip zone and thereby again lead to the brittle propagation of an existing crack [7,8]. The purpose of this paper is to present an account of our recent theoretical studies [9,10] of this stress-driven embrittling process and thereby encourage relevant experimental studies to determine its importance in the irradiation environment.

In section 2 we provide a very brief descriptive outline of the effective media and the sink strength representation of typical microstructures. We then describe in sections 3 the effects on the point-defect distributions around a loaded crack in a body containing microstructure and subject to irradiation. We also present explicit expressions for the flux of such point-defects to such a crack in competition with the loss to the sinks that make up the microstructure. Evidence for the importance of such stress driven segregation of solute atoms such as sulphur and hydrogen to loaded cracks in the absence of irradiation will also be cited in this section to reinforce the probable significance of these effect to both intrinsic and solute point-defects under steady state irradiation conditions. Finally in section 4 we discuss the various screening effects of the microstructure on the loss of point-defects to the crack and the concomitant effects of the presence of the crack on the evolution of the surrounding microstructure.

THE SINK-STRENGTH REPRESENTATION OF MICROSTRUCTURES

The theoretical description of the evolving microstructure in irradiated materials by chemical rate theory has developed over the last fifteen years [11-13] and has reached a stage where successful predictions of the detailed microstructural response of technological materials can be made [14]. A typical microstructure of irradiated steel consists of voids, dislocations (loops and network), grain boundaries and precipitates. To study the evolution of this system it is necessary to treat simultaneously the various point-defect loss processes to all the sinks and by bulk recombination.

To obtain a useful representation of such an evolving microstructure we replace the crystalline material, with it spatially varying local point-defect concentrations associated with each of the sinks that make up the total microstructure, by an effective homogeneous continuum. In this effective or lossy continuum the point-defect concentrations are homogeneous and the actual sinks are replaced by effective sinks. The values of these sink strengths for each of the real sink types are deduced by an embedding procedure [13] which is basically analogous to that first used by Maxwell [15] in his analysis of electrical conduction through heterogeneous media. The evolution of the sink-types can then be followed using chemical rate theory [12].

The details of the embedding procedure for the determination of the various sink strengths will not be discussed here; suffice it to say that suitable forms of these sink strengths for inclusion in the rate theory analysis do now exist and can be found in the following references: the network dislocation [16], the interstitial loop [12,17], the vacancy loop [18], the spherical void [12,19], the grain boundary [13,20,21] and the precipitate [21]. This is by no means an exhaustive list and improvements in both the mathematical and physical representation of these sinks continue to be made [22].

STRESS DRIVEN MIGRATION TO A LOADED CRACK

In this section we present results for the flux of point-defects to the tip of a loaded crack in a body subjected to steady state irradiation conditions. We thus consider the crack to be realised in the lossy continuum and permit spatial variation of the generated point-defects around the crack-tip in response to the interaction between the stress field of the crack and the relaxation volume of the point-defects. A long way from the crack-tip the homogeneous conditions of the lossy continuum prevail.

If E is the spatially carrying interaction energy between the crack-tip stress field and a point-defect, then the fractional concentration of c of such point-defects must satisfy the continuity equation[8].

$$\frac{D}{k_B T}\nabla E.\nabla c - Dk^2 c + K = 0 \qquad (1)$$

where k^2 is the total sink strength of the microstructure and K is the point-defect generation rate due to the irradiation; clearly a long way from the crack tip all point-defects created must be lost at sinks within the microstructure and there

$$c \Rightarrow \frac{K}{Dk^2} \qquad (2)$$

In equation (1), D is the diffusion constant of the point-defect, T is the absolute temperature and k_B is Boltzmann's constant. In this analysis bulk combination has been explicitely neglected with the implication that point-defect losses in the microstructure are assumed to be sink dominated and the interaction energy E has been assumed to be sufficiently large to justify the pure drift approximation inherent in the first order form of equation (1) with the concomitant neglect of random diffusion processes [8].

Since we are only concerned with the stress field associated with the tip of the crack we may consider the crack itself to be semi-infinite and occupying the negative x-region of the xz- plane with its tip coinciding the z-axis of a Cartesian coordinate system x,y,z. If the location of a point defect is defined by the polar coordinates (r,θ) where $x = r\cos\theta$, $y = r\sin\theta$ then $E(r,\theta)$ has the explicit form for

(i) Mode I Loading [8].

$$E(r,\theta) = \frac{-AK_I \cos\left[\frac{\theta}{2}\right]}{r^{1/2}} \qquad ; -\pi<\theta<\pi \qquad (3)$$

and for

(ii) Mode II Loading [10]

$$E(r,\theta) = \frac{AK_{II} \sin\left[\frac{\theta}{2}\right]}{r^{1/2}} \qquad ; -\pi<\theta<\pi \qquad (4)$$

where

$$A = \left[\frac{2}{9\pi}\right]^{1/2} (1+\nu)\,\Delta V \qquad (5)$$

In 5, ν is Poisson's Ratio (the body is assumed to be elastically isotopic) and ΔV is the relaxation volume of the point-defect. The quantities K_I and K_{II} are the stress intensity factors for mode I and II respectively.

The required exact solution of equation (1), subject to the boundary condition (2), is for mode I, with $E(r,\theta)$ given by (3) [8]:

$$c(r,\theta) = \left[\frac{K}{Dk^2}\right]\left\{1 - \exp\left[-\left[\frac{k^2}{4L}\right] r^{5/2}\psi(\theta)\right]\right\} \qquad (6)$$

where

$$L = L_I = \frac{AK_I}{k_B T} \qquad (7)$$

and

$$\psi(\theta) = \frac{3(\sin\theta + (\mathrm{sgn}\theta)\pi - \theta) + 2\sin\theta \sin^2\left(\frac{\theta}{2}\right)}{\sin^5\left(\frac{\theta}{2}\right)} \tag{8}$$

if $\Delta V > 0$ or

$$\psi(\theta) = \frac{3(\sin\theta - \theta) + 2\sin\theta \sin^2\left(\frac{\theta}{2}\right)}{\sin^5\left(\frac{\theta}{2}\right)} \tag{9}$$

if $\Delta V < 0$.

For mode II, with $E(r,\theta)$ given by (4) the required solution is also given (6) but with

$$L = L_{II} = \frac{\Delta K_{II}}{k_B T} \tag{10}$$

and the angular function $\psi(\theta)$ now given by

$$\psi(\theta) = \frac{3(\pi - \theta) - 5\sin\theta + 2\sin\theta \sin^2\left(\frac{\theta}{2}\right)}{\cos^5\left(\frac{\theta}{2}\right)} \tag{11}$$

for $\Delta V > 0$ and by (11) with $\theta \rightarrow -\theta$ for $\Delta V < 0$ [10].

These various solutions are shown in the figures 1 to 3 in the form of lines of constant concentration and point-defect flow lines, the latter being the orthogonal trajectories to the equi-potentials defined by the interaction energies (3) or (4) for mode I and II loading respectively.

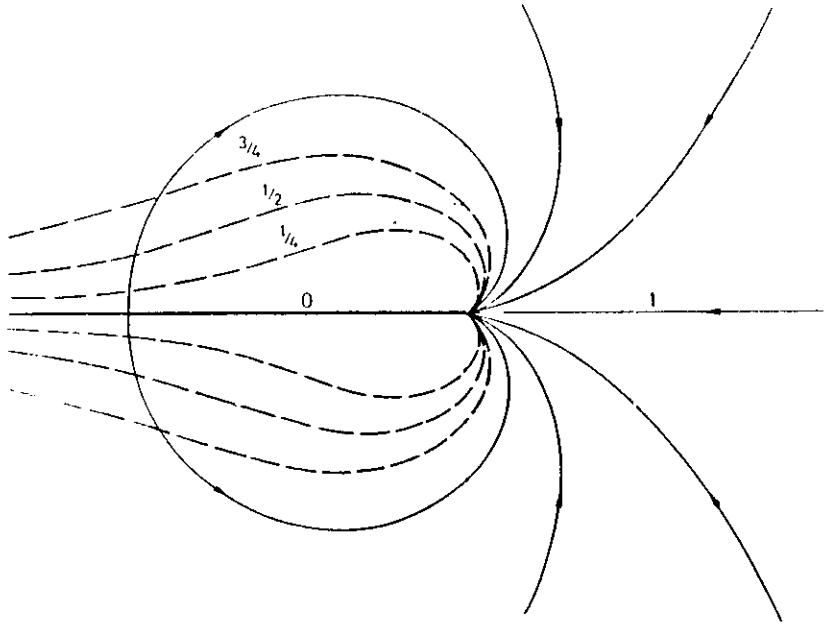

Figure 1 Flow lines (→) and lines of constant concentration (- -), deduced from the solution (6) with (7) and (8), in the vicinity of the crack-tip loaded in mode I during steady-state irradiation when the point-defect relaxation volume $\Delta V > 0$. The values indicated give the concentration in units of K/Dk^2.

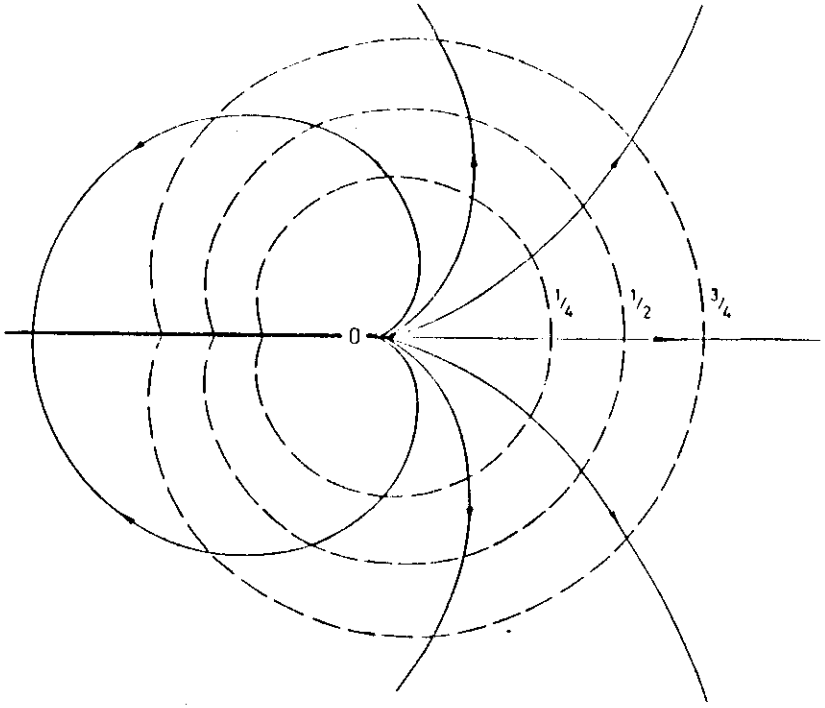

Figure 2 As for figure 1 but when the point-defect relaxation volume $\Delta V < 0$; the lines of constant concentration are now deduced from the solution (6) with (7) and (9).

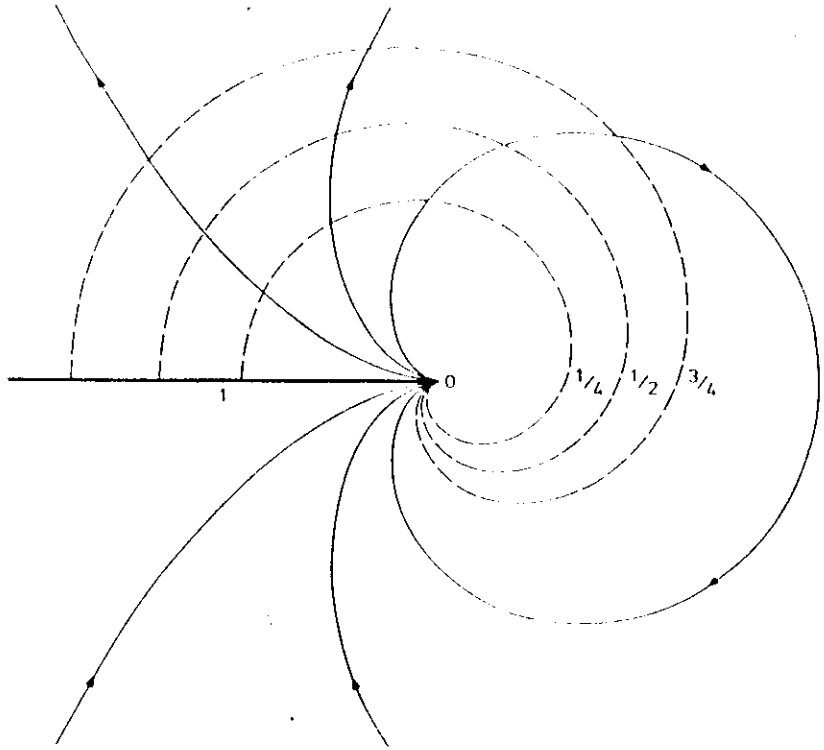

Figure 3 As for figure 1, but when the crack-tip is loaded in mode II; the lines of constant concentration are now deduced from the solution (6) with (10) and (11).

From these analytic solutions we can easily obtain both the distribution of point-defect loss at the crack and its tip after steady state irradiation for a time t and then by simple integration deduce the total excess loss of such point-defects to the crack and its tip. The following results have been obtained [7 - 10]:

Mode I loaded crack and $\Delta V > 0$

In this case the point-defects could be the self interstitials for which $\Delta V > 0$ ($\sim 1.0\Omega$) where Ω is the atomic volume. From figure 1, it is clear that such interstitial atoms will flow only into the crack-tip and we find [8] the number of such interstitials that have entered unit length of the crack at its tip after time t of steady-state irradiation to be

$$N(t) = \frac{5}{2}\left(\frac{3\pi}{4}\right)^{1/5}\Gamma\left(\frac{9}{5}\right)\left(\frac{Kt}{\Omega}\right)\left(\frac{L}{k^2}\right)^{4/5}$$

Where Γ is the Gamma function and with L given by (7) we have explicitly:

$$N_i(t) \cong 1.20\left(\frac{Kt}{\Omega}\right)\left(\frac{\Delta V K_I}{k^2 k_B T}\right)^{4/5} \qquad (12)$$

where $\Delta V = \Delta V_i$ and $k^2 = k_i^2$ are respectively the relaxation volume and total sink strength of the surrounding microstructure for the interstitials.

Mode I loaded crack and $\Delta V < 0$

In this case the point-defects could be the vacancies for which $\Delta V < 0$ ($\sim -0.5\Omega$). From figure 2 we now see that such vacancies will flow only to the two crack faces behind the crack-tip and none will flow to the actual tip. The number of such vacancies that have entered unit length of the crack across its surfaces after time t of steady state irradiation is again given by [8] the expression (12), where now $\Delta V = \Delta V_v$ and $k^2 = k_v^2$ are respectively the relaxation volume and total sink strength of the surrounding microstructure for the vacancies.

Mode II loaded crack [10]

For this mode we see from figure 3 that interstitials ($\Delta V > 0$) will flow only into the underside of the crack-tip whereas vacancies ($\Delta V < 0$) will flow only into the upper side of the crack-tip. The numbers of such point-defects that have entered the crack at its tip after time t of steady- state irradiation is now found to be [10]

$$N_{II}(t) \cong 0.69\left(\frac{Kt}{\Omega}\right)\left(\frac{\Delta V K_{II}}{k^2 k_B T}\right)^{4/5} \qquad (13)$$

where ΔV and k^2 can be interpreted as the relaxation volume and sink strength of the surrounding microstructure respectively for either interstitials or vacancies.

We end this section with a comment on the relationship between these steady state solutions relevant to the irradiation situation and the corresponding transient solutions for the stress driven migration of impurity atoms from an initial constant concentration to such loaded cracks. Mathematically the solutions are related [7,8], the transient solution for the time dependent concentration is discontinuous and is defined by a propagating characteristic (discontinuity) that separates a completely denuded zone from the invariant initial constant concentration; this characteristic is identical in mathematical form to the curves of constant concentration depicted in figures 1 to 3. However, it is perhaps the physical significance of the transient solution that should be emphasised in the present discussion. It has been shown that the transient solution, with its assumption that stress-driven flow to the crack is dominant, yields predictions of the segregation of embrittling impurities such as sulphur or hydrogen in certain steels, that are in excellent agreement with relevant Auger and metallographic data.[7,9]. The agreement between the theory and observation is thus sufficiently good to lend strong support to the validity of the stress-driven segregation mechanism for embrittlement. If this segregation mechanism is thus accepted for such transient situations, there seems no reason to doubt, that in the present irradiation situation, the stress driven migration of the intrinsic point-defects to such cracks will also occur.

DISCUSSION

In this section we discuss some of the probable consequences of the point-defect flows and concentration profiles depicted in figures 1 to 3. The most obvious result is that for mode I the interstitials all flow to the crack-tip (figure 1) whereas the vacancies flow only to the crack surfaces; the extreme nature of this result must be qualified by the realisation that point- defect diffusion has been neglected in comparison to the strong drift flows. Thus one would expect some response to the presence of the concentration gradients shown in the figures which would inevitably yield some interstitial flow to the crack surfaces and some vacancy flow to the crack-tip. However, the tendency for the crack stresses to separate the interstitial and vacancy populations in the vicinity of the crack could well enhance the consistency of the present linear drift solutions since point-defect loss by bulk recombination should be reduced; in addition such a reduction could also be expected to arise from the general loss of both point-defects to the crack. The same separation arguments also apply to the flows and redistributions indicated in figure 3 for interstitials and vacancies.

The functional forms of $N_I(t)$ and $N_{II}(t)$ are of interest. The presence of k^2 in the denominator of these expressions clearly shows the screening effect of the surrounding microstructure. The larger the value of k^2, the fewer point-defects will reach the crack. On the other hand, the greater the relaxation volume of the point-defect, the greater will be the number of such point- defects arriving at the crack. Thus, for example, if dislocations are the dominant sink near the crack-tip in the microstructure then the presence of the ratio $\Delta V/k^2$ in these expressions could well mean that the loss of vacancies and interstitials to a crack may be roughly equal, since in this situation, the ratio $\Delta V/k^2$ could be approximately independent of ΔV and the biassed loss of interstitials to

the dislocations eliminates any biassed flow to the crack! The crack is then essentially a recombination sink since an equal flux of interstitials and vacancies will reach it; needless to say although the total numbers of each point-defect may be equal, their distributions at a mode I loaded crack are quite different. It follows that such different flux distributions could lead to a radical change of shape of the crack with possible blunting processes etc. prevailing. For mode II loaded cracks (figure 3) the arrival locations are on either side of the crack-tip so rather efficient recombination at the tip may be expected. If k^2 is dominated by sinks other than dislocations (such as voids) then the crack becomes a biassed sink for interstitials, through the exposed ΔV in the numerators of (12) and (13). This in turn means that such voids will themselves receive a net flux of vacancies; hence preferential void growth should be seen in the vicinity of such crack-tips. Such growing voids then can have a concommitant effect on the ability of the crack itself to propagate.

It is also expected that during irradiation mobile point-defects other than intrinsic interstitials and vacancies will suffer stress-driven migration to a loaded crack. The results presented in the figures and the expressions (12) and (13) apply equally to transmutation gases such as helium generated during irradiation where now the damage rate K must be interpreted as the gas generation rate and k^2 as the sink strength of the surrounding microstructure for such gas atoms. The precise location of such gas on arriving at the crack depends on its relaxation volume but could lead to the steady state build up of gas pressure within the crack with an obvious propensity to assist its ability to propagate.

Finally, on top of this already complex situation we must include the radiation driven segregation of solute to the crack and the 'transient' stress driven migration of other minor elements present in the material; the latter effects can be treated with suitably lossy terms included in the transient analysis developed for the unirradiated state.

REFERENCES

1. Churchman, A.T., Mogford, I.M. and Cottrell, A.H.: Phil.Mag., 1957,2,1271.

2. Cottrell, A.H.: in Proc. of the November Meeting of British Nucl.Energy Society "The 46th Thomas Hawsksley Lecture",1959,p64.

3. Phythian, W.J. and English, C.A.: AERE Harwell Research Report, R-13632,1989.

4. Williams, T.J.et al: in Proc.of 2nd Intern.Symposium on Environmental Degradation of Materials in Nuclear Power Systems. ASTM, Monteray, 1986.

5. Little, E.A.: Intern.Met.Reviews, 1976, 21,25.

6. Jacobs, A.J., Clausing, R.E., Miller, M.K. and Shepherd, C.: in Proc. of the 4th Intern.Symposium on Environmental Degradation of Materials in Nuclear Power Systems,Water Reactors, Nat.Assoc.of Corrosion Engineers, Georgia, 1989.

7. Hippsley, C.A.,Rauh, H and Bullough, R.: Acta Metall.,1984,32,1381.

8. Rauh, H. and Bullough, R.: Proc.Roy.Soc.Lond.,1985,A397,121.

9. Rauh, H.,Hippsley, C.A. and Bullough, R.: Acta.Metall.,1989,37,269.

10. Rauh, H. and Bullough, R.: Proc.Roy.Soc.Lond.,1990,A427,1.

11. Harkness, S.D. and Li, C.Y.: Metall.Trans.,1971,2,1457.

12. Brailsford, A.D. and Bullough, R.: J.Nucl.Mater.,1972,44,121.

13. Brailsford, A.D. and Bullough, R.: Phil.Trans.Roy.Soc.Lond.,1981,302,87.

14. Bullough, R. and Quigley, T.M.: J.Nucl.Mater.,1983,113,179.

15. Maxwell, J.C.: "A Treatise on Electricity and Magnetism" Clarendon Press,Oxford, 1892.

16. Bullough, R and Quigley, T.M.: J.Nucl.Mater.,1981,103 and 104,1397.

17. Brailsford, A.D. and Bullough, R.: "Vacancy '76", The Metals Society, London, 1977.

18. Bullough, R., Hayns, M.R. and Woo, C.H.: J.Nucl.Mater.,1979,84,93.

19. Brailsford, A.D., Bullough, R. and Hayns, M.R.: Ibid.,1976,60,246.

20. Brailsford, A.D. and Bullough, R.: in Proc.of Conf. "Physical Metallurgy of Reactor Fuel Elements", Berkeley,U.K., Metals Society, 1973.

21. Brailsford, A.D. and Bullough, R.: J.Nucl.Mater.,1976,69 and 70,434.

22. Rauh, H., Matthews, J.R. and Bullough, R.: Phil.Mag.1991, to appear.

PHILOSOPHICAL TRANSACTIONS
OF
THE ROYAL SOCIETY
OF LONDON

A. MATHEMATICAL AND PHYSICAL SCIENCES

ISSN 0080-4614

VOLUME 302 PAGES 87–137 NUMBER 1465

17 July 1981

The theory of sink strengths

by A. D. Brailsford and R. Bullough

PUBLISHED BY THE ROYAL SOCIETY
6 CARLTON HOUSE TERRACE LONDON SW1Y 5AG

PROCEEDINGS AND PHILOSOPHICAL TRANSACTIONS
OF THE ROYAL SOCIETY

Notice to contributors

The Royal Society welcomes suitable communications for publication in its scientific journals: papers estimated to occupy up to 24 printed pages are considered for the *Proceedings* and longer papers and those with numerous or large illustrations for the *Philosophical Transactions*.

Detailed advice on the preparation of papers to be submitted to the Society is given in a leaflet available from the Executive Secretary, The Royal Society, 6 Carlton House Terrace, London SW1Y 5AG. The 'Instructions to authors' are also printed in every fifth volume of the *Proceedings* A and B (volume numbers ending in 0 or 5). The basic requirements are: a paper should be as concise as its scientific content allows and grammatically correct; standard nomenclature, units and symbols should be used; the text (including the abstract, the list of references and figure descriptions) should be in double spaced typing on one side of the paper. A leaflet giving detailed advice on the preparation of illustrations is available from the Executive Secretary; diagrams should be expertly drawn at about twice the proposed final size, preferably with lettering in the correct style but if this is not possible the lettering should be inserted not on the original drawings but on a set of copies; where photographs are essential the layout should be designed to give the most effective presentation.

The initial submission of a paper must be through a Fellow or Foreign Member of the Society, but subsequent correspondence will be conducted direct with the author. The latest lists of Fellows and Foreign Members are to be found in the current edition of the *Year Book of the Royal Society*. A copy of 'Notes for the guidance of Fellows communicating papers' is available from the Executive Secretary. In the event of any difficulty, an author is invited to seek the assistance of the Executive Secretary.

No page charge is levied, and the first 50 offprints of a paper are supplied to the author gratis.

The Editors particularly welcome short communications to *Proceedings*; as far as possible they will be given expeditious treatment both in consideration and in printing, and this will be facilitated if a paper is submitted with a firm recommendation by a Fellow.

THE THEORY OF SINK STRENGTHS

BY A. D. BRAILSFORD† AND R. BULLOUGH‡

† *Scientific Research Staff, Ford Motor Company, Dearborn, Michigan* 48121, *U.S.A.*

‡ *Theoretical Physics Division, A.E.R.E. Harwell, Oxfordshire OX*11 0*RA, U.K.*

(*Communicated by W. C. Marshall, F.R.S. – Received* 4 *August* 1980)

CONTENTS

A formal derivation of the sink strengths to be used in point defect rate theory is presented. Previous models that have been invoked for the approximate evaluation of these parameters are discussed. It is shown that the effective medium approach, as introduced earlier by us, constitutes the best available approach for steady state problems. Sink strengths for voids, straight (and parallel) dislocations, dislocation loops and grain boundaries are considered. It is shown that most recent criticisms of the effective medium method are groundless.

1. Introduction

The theoretical description of irradiation damage (Harkness & Li 1971), and its subsequent annealing (Damask & Dienes 1971), entails analysis of the migration of intrinsic point defects to a spatial distribution of sinks. The latter are almost invariably distributed at random: only rarely is any long range order observed. Even when order does occur, it is generally associated with one type of sink only. Thus spatial disorder in the dispersal of the sinks is the prime characteristic of problems of this general type (Brailsford 1976, Talbot & Willis 1980).

This complexity on the microscale may be contrasted with the quantities most often of interest experimentally, namely the electrical resistivity, sample volume, or creep rate and so on. These are all macroscopic parameters. It is plausible to expect, therefore, that such properties, at least, will be largely insensitive to the finer details of the sink distribution, much as the properties of a gas are independent of the detailed kinetics of its constituent molecules. As ensemble averages suffice for the description of the properties of a gas, so one expects some averaging prescription to achieve a similar end for the defect problem.

Although not explicitly stated, this philosophy, in fact, underlies all theories known to us in this field. From the earliest attempts (Dienes & Vineyard 1957) to the present day, some form of coarse-grained approximation has been used. In general either an idealization of the sink distribution by a periodic array (Bullough & Perrin 1971) is used, or randomness is retained, but only through the conceptualization of an effective homogeneous medium (Brailsford & Bullough 1972*a*). No other method is proven.

The lattice model is widely acknowledged, but the effective medium model less so. Though the disciplines of the latter model have been formulated, some of these appear to be used only if convenient, while others are arbitrarily discarded. As a result, numerous approaches reside in the literature that, though perhaps reaching the same (or nearly the same) result, are nevertheless inconsistent overall. The outcome has been singularly unfortunate in that, since most methods agree to lowest order, legitimate corrections from the most rigorous approach are either overlooked or criticized erroneously (Nichols 1978*a*). It appears to us, therefore, that the time is appropriate to review the subject of sink strength theory, by tracing the sequential steps from the fundamental continuity equations to the evaluation of the sink strength parameters themselves. Such is the theme of the present paper.

It is important to start from first principles to ascertain the precise problem of which the sink strengths are the solution. It is the approach first advocated by Wiedersich (1970) and later pursued on separate occasions by us (Brailsford 1976; Brailsford & Bullough 1972*a*). We shall re-examine this approach in §2. In §3, we discuss the void sink strength. Particular attention is paid to the higher-order correction, which we (in collaboration with Hayns) have obtained previously (Brailsford *et al.* 1976). A new derivation of this correction is given by means of Ham's eigenfunction method (Ham 1958). The result obtained confirms our previous version.

Ham's method is based upon the void's being periodically arranged upon a lattice. As stated above, this is most often an abstraction from reality. Nevertheless, it is useful in answering several questions of principle that arise in general. For example, (i) to what extent can sink strengths derived from steady state be generally applicable? (ii) Is it necessary to allow for sinks, of types other than the one being considered, in computing the sink strength of the latter (Brailsford *et al.* 1976)? By considering a lattice model far more sophisticated than any previously examined, we shall show how these questions may be resolved.

Section 4 is devoted to a study of the sink strength of an infinitely long and straight edge dislocation. We have emphasized previously (Brailsford & Bullough 1976) that we regard this as largely an academic study. For the abstraction from the complex network observed in practice, to the simplistic geometry that is theoretically manageable, is surely such as to overtax the credulity of even the most gullible person. Our view is that *any* such model can indicate only trends. The appropriate parameters must be estimated from the analysis of experiment. But many workers appear still to be unconvinced of this. Thus we shall investigate the matter further here, if only to tread ground which some yet maintain has a semblance of rigour (Nichols 1978*a*).

As with the void sink strength calculation, we shall consider several different models to establish some qualitative features: (i) the effective medium model, with the use of the capture radius concept; (ii) the same model, but with the medium extending to the dislocation core, in which the near-field point defect–dislocation interaction is treated exactly; and (iii) a lattice model, again with use of the capture radius idea. The lattice model considered here is far more sophisticated than any contemplated before. For it is a *mixed* lattice of parallel edge dislocations *and* voids. We shall carry the analysis only far enough to establish the matters of interest. But, we emphasize, the simplifications are mathematically well disciplined, and anyone wishing to carry the analysis further may do so by pursuing the lines we set out. We consider, however, that our analysis is adequate. The sensitivity of the dislocation sink strength to voids, both when voids are ordered in the plane perpendicular to the dislocation axis and when they are completely random, is discussed. We see no point in pursuing the matter further.

The above discussion pertains only to the dislocation sink strength corresponding to the size-effect interaction. Some tentative remarks are also offered concerning the induced interaction, which is the basis of the so-called stress-induced preferential absorption (s.i.p.a.) creep (Heald & Speight 1975; Bullough & Willis 1975; Wolfer & Ashkin 1975; Bullough & Hayns 1975) and stress-induced climb and glide (p.a.g.) creep (Mansur 1979). However, it is included here mainly for completeness, and only at the level of our present treatment. The subject is contentious and may demand sophistication† beyond the scope of this review. Thus it is still being actively investigated (Bullough *et al.* 1981*b*), and the reader is warned that our comments are necessarily provisional. Nevertheless, we feel able to establish certain ground rules, which more detailed analyses must follow. There is some merit, therefore, in addressing the subject for this reason alone.

Like the sink strength for straight dislocations, that for dislocation loops is also currently under study (Bullough *et al.* 1981*b*). Consequently, our remarks upon the subject will be similarly brief. We shall simply highlight the results obtained to date (§5).

† For example, a discussion of more complex geometries.

Section 6 contains a discussion of the sink strength of grain boundaries. The models discussed are the effective medium and the grain boundary lattice with internal sinks. The two approaches are shown to yield the same result, thus confirming, yet again, the value of the former (Brailsford & Bullough 1976, Brailsford & Bullough 1978).

In §§2–6, it most often proves expedient to review the work of others as matters proceed. There are a few cases, however, where this does not arise naturally. Such previously omitted work is therefore considered separately in §7. The whole paper is then summarized in §8.

2. Derivations of rate theory

The purpose of this section is to present a fundamental derivation of the rate theory commonly used in point defect problems. The section is divided into three parts. Part (*a*) is concerned with spatially periodic sink arrays and part (*b*) with completely random arrays. In each case, the methodology to be used in computing sink strengths is established. These are summarized in part (*c*). There we consider also the mathematical models used previously by others. A physical interpretation of such other manipulations is given. It is shown that they do not conform to the prescriptions here derived, though the corrections to lowest order (but that only) may be small. The best approximation scheme for steady state problems is indicated to be that provided by the effective medium model, as defined by us in Brailsford & Bullough (1972*a*).

(*a*) *Periodic sink arrays*

We assume here that the sinks form some type of periodic array. Thus we can divide space into a set of primitive cells. For simplicity, we shall assume that each such cell has inversion symmetry about its centre. As a consequence, the normal components of the point defect fluxes vanish on the cell boundaries. Indeed, this is the main motivation for assuming such an array.

Apart from this symmetry, however, the cell can contain an arbitrary number of sinks of different types. In fact, of *necessity*, it contains more than one sink if more than one type exists in the solid. Otherwise the hypothesis of spatial periodicity becomes inconsistent. It is amazing how often this elementary fact is overlooked.

For such a lattice structure, it is necessary only to consider the point defect equations in the primitive cell. We emphasize from the outset, however, that this is simply a matter of convenience and nothing more. Any number of primitive cells, connected or disjoint, could equally well be envisaged. The ensuing manipulations are equally valid for both, since any larger such volume simply repeats the behaviour of the smallest. This will prove important in §3.

The basic continuity equations for vacancies and self-interstitials are

$$\partial c_{\mathrm{v}}/\partial t + \operatorname{div} j_{\mathrm{v}} = K - \alpha c_{\mathrm{i}} c_{\mathrm{v}}, \tag{1}$$

and

$$\partial c_{\mathrm{i}}/\partial t + \operatorname{div} j_{\mathrm{i}} = K - \alpha c_{\mathrm{i}} c_{\mathrm{v}}, \tag{2}$$

where the c_{v} and c_{i} are the atomic fractions of the defects (in the order introduced), and j_{v} and j_{i} denote the respective fluxes. The quantity K is the defect production rate in displacements per atom per second (dpa s^{-1}), and α is the intrinsic recombination coefficient. For simplicity (only), we shall ignore the possibility of vacancy loop production (Brailsford & Bullough 1972*b*, Bullough *et al.* 1975).

Equations (1) and (2) apply in all parts of the primitive cell outside the internal sinks, which we term the matrix region. These equations are to be solved within the overall cell volume, V_{C}, with boundary conditions of the general type

$$j_{\mathrm{L}l} = v[c(s_{\mathrm{L}l}) - \hat{c}_{\mathrm{L}l}] \tag{3}$$

at the interior surfaces defined by the internal sinks. Each type of the latter is denoted by the symbol L, which is intended to contain all necessary information; that is, whether it is a void or a dislocation, for example, and of what size and so on. The label, l, gives the spatial location of each sink, while $s_{\mathrm{L}l}$ represents either the sink surface itself or, where it appears as the argument of a function, the evaluation of the latter on the particular surface. The other quantities in equation (3) are (i) $j_{\mathrm{L}l}$, the component of the point defect flux along the normal at the sink–matrix interface, directed internally towards the sink, (ii) v, the transfer velocity from matrix to sink, and (iii) $v\hat{c}_{\mathrm{L}l}$, the thermal emission rate from the sink of type L situated at $\mathbf{r}_l$.

Even with periodic arrays, the problem posed is forbidding in general if there is more than one type of sink present. Instead of attempting to solve it, we here look at the first moments of equations (1) and (2). These are obtained by integrating the equations over the cell volume. The result from equation (1) is

$$\int_{V_{\mathrm{M}}} \frac{\partial c_{\mathrm{v}}}{\partial t}\,\mathrm{d}V + \sum_{\mathrm{L},l} J^{\mathrm{v}}_{\mathrm{L}l} = KV_{\mathrm{M}} - \alpha \int_{V_{\mathrm{M}}} c_{\mathrm{i}} c_{\mathrm{v}}\,\mathrm{d}V, \tag{4}$$

where $J^{\mathrm{v}}_{\mathrm{L}l}$ is the integral of $j^{\mathrm{v}}_{\mathrm{L}l}$ over the sink surface $s_{\mathrm{L}l}$, and V_{M} is the volume of matrix within V_{C}. Here, and throughout this section, the corresponding self-interstitial equation can be obtained by interchanging the labels i and v. We remind the reader that there is no point defect loss across the outer boundary, by construction.

We first consider the left-hand side of equation (4). Its leading term may be rewritten as

$$\int_{V_{\mathrm{M}}} \frac{\partial c_{\mathrm{v}}}{\partial t}\,\mathrm{d}V = \frac{\mathrm{d}}{\mathrm{d}t}\int_{V_{\mathrm{M}}} c_{\mathrm{v}}\,\mathrm{d}V - H_{\mathrm{v}}, \tag{5}$$

where

$$H_{\mathrm{v}} = \int_S c_{\mathrm{v}}(S)\, u_{\mathrm{N}}\,\mathrm{d}S - \sum_{\mathrm{L},l}\int_{s_{\mathrm{L}l}} c_{\mathrm{v}}(s_{\mathrm{L}l})\, u_{\mathrm{n}}\,\mathrm{d}s_{\mathrm{L}l}. \tag{6}$$

Here u_{N} is the outward normal velocity of the surface S enclosing the primitive cell, u_{n} the corresponding quantity for each sink–matrix interface. Volume relaxation effects associated with point defects in solution are generally small. Thus the volume V_{M} is constant. Hence the outer surface S must be allowed to expand in response to the volume increase of internal sinks. This is the effect embodied in H_{v}. Even at this stage one can see that in the void swelling problem H_{v} is dependent upon the swelling rate.

However, the main issue here concerns the $J^{\mathrm{v}}_{\mathrm{L}l}$ and the corresponding quantities for self-interstitials. We elect to define each in terms of a *sink strength*, $k^2_{\mathrm{L}l,\mathrm{v}}$, and a *thermal emission rate*, $K_{\mathrm{L}l,\mathrm{v}}$, by the following relation†:

$$J^{\mathrm{v}}_{\mathrm{L}l} = D_{\mathrm{v}} k^2_{\mathrm{L}l,\mathrm{v}} \int_{V_{\mathrm{M}}} c_{\mathrm{v}}\,\mathrm{d}V - K_{\mathrm{L}l,\mathrm{v}} V_{\mathrm{M}}, \tag{7}$$

with a corresponding definition for interstitial quantities. In equation (7), D_{v} is the vacancy diffusivity. Evidently, at this point we have only one relation for two parameters. Thus we

† The introduction of the factor V_{M} is, of course, arbitrary. It is included here so that production terms consequent upon emission have the same dimensionality as the basic production process.

complete the prescription for determining each separately by the stipulation that $K_{\mathrm{L},\mathrm{v}}/D_{\mathrm{v}}$ must vanish as the temperature approaches absolute zero.

The reader may have gathered by now that we are seeking a constitutive equation for the volume integral of c_{v}. Thus we express the final term in equation (4) in the amenable form

$$\alpha \int_{V_{\mathrm{M}}} c_{\mathrm{i}} c_{\mathrm{v}} \mathrm{d}V = \alpha V_{\mathrm{M}} \langle c_{\mathrm{i}} \rangle \langle c_{\mathrm{v}} \rangle + I, \tag{8}$$

where here, for brevity, we introduce the notation

$$\langle c \rangle = V_{\mathrm{M}}^{-1} \int_{V_{\mathrm{M}}} c \mathrm{d}V \tag{9}$$

for both defects. The quantity I is therefore

$$I = \alpha \int_{V_{\mathrm{M}}} (c_{\mathrm{i}} - \langle c_{\mathrm{i}} \rangle)(c_{\mathrm{v}} - \langle c_{\mathrm{v}} \rangle) \mathrm{d}V. \tag{10}$$

It is a measure of the joint mean of the deviations of the defect concentrations from their spatial averages.

Thus, upon rearranging the terms in equation (4), and using the subsequent definitions, we arrive at the following moment equation:

$$\frac{\mathrm{d}\langle c_{\mathrm{v}} \rangle}{\mathrm{d}t} + \sum_{\mathrm{L}} (D_{\mathrm{v}} k_{\mathrm{L}\mathrm{v}}^2 \langle c_{\mathrm{v}} \rangle - K_{\mathrm{L}\mathrm{v}}) - K + \alpha \langle c_{\mathrm{i}} \rangle \langle c_{\mathrm{v}} \rangle = V_{\mathrm{M}}^{-1} (H_{\mathrm{v}} - I). \tag{11}$$

It should be noted that we have here introduced the two new quantities $k_{\mathrm{L}\mathrm{v}}^2$ and $K_{\mathrm{L}\mathrm{v}}$. These are defined as

$$k_{\mathrm{L}\mathrm{v}}^2 = \sum_{l} k_{\mathrm{L}l,\mathrm{v}}^2 \tag{12}$$

and

$$K_{\mathrm{L}\mathrm{v}} = \sum_{l} K_{\mathrm{L}l,\mathrm{v}}. \tag{13}$$

They are, therefore, being sums over all locations of each sink type within the cell, average properties. They are the sink strength and emission rate of the sinks of type L, as they are commonly understood.

It is seen from equation (11), and its counterpart for self-interstitials, that a simple rate theory follows from these manipulations if it can be argued that the right-hand side of this equation is negligible. Now, where volume swelling does occur, its time dependence *is* usually small. Thus H_{v} can be neglected to a high degree of precision. Moreover, I can usually be neglected on the basis of self-consistency. That is, one assumes it is small, solves the problem at hand, and then checks the initial premise. It is usually consistent because in the cases explored c_{i} and c_{v} differ substantially from their volume averages only very near to any sink. Since at the sink surfaces themselves, c_{i} and c_{v} are of order $\bar{c}_{\mathrm{L}}$, it follows that the ratio of I to the recombination term that *is* retained is of order $V_{\mathrm{int}}/V_{\mathrm{M}}$ at the most, where V_{int} is an 'effective volume of influence' of each sink. (The $\bar{c}_{\mathrm{L}}$ are generally small compared with the $\langle c \rangle$.) Thus I may also be discarded.

The end result is, then, the two rate equations

$$\frac{\mathrm{d}\langle c_{\mathrm{v}} \rangle}{\mathrm{d}t} + \sum_{\mathrm{L}} (D_{\mathrm{v}} k_{\mathrm{L}\mathrm{v}}^2 \langle c_{\mathrm{v}} \rangle - K_{\mathrm{L}\mathrm{v}}) - K + \alpha \langle c_{\mathrm{i}} \rangle \langle c_{\mathrm{v}} \rangle = 0, \tag{14}$$

and

$$\frac{\mathrm{d}\langle c_{\mathrm{i}} \rangle}{\mathrm{d}t} + \sum_{\mathrm{L}} (D_{\mathrm{i}} k_{\mathrm{L}\mathrm{i}}^2 \langle c_{\mathrm{i}} \rangle - K_{\mathrm{L}\mathrm{i}}) - K + \alpha \langle c_{\mathrm{i}} \rangle \langle c_{\mathrm{v}} \rangle = 0. \tag{15}$$

These are to be solved, numerically if need be, to obtain the $\langle c_{\mathrm{v}} \rangle$ and $\langle c_{\mathrm{i}} \rangle$ as functions of time for some prescribed initial conditions. Such a procedure is straightforward, in principle at least, if the sink strength k_{L}^2 and thermal emission rate K_{L} are known for each defect and each sink type.

It is clear then what the subsequent procedure must be. One must solve the continuity equations within each cell to compute the $J_{\mathrm{L}}^{\mathrm{v}}$ and hence derive the $k_{\mathrm{L}l,\mathrm{v}}^2$ and $K_{\mathrm{L}l,\mathrm{v}}$ for each sink type. The same must be done for self-interstitials. Only then is one able to address equations (14) and (15). We shall take up the matter again in §2(*c*).

(*b*) *Random arrays of sinks*

The periodic array is useful as background for the more complex random sink distributions which we now discuss. The development parallels that already given as closely as possible.

There are, however, two prime differences that arise when considering random sink arrays. These are, first, that there are no natural internal surfaces where the defect fluxes may be presumed to vanish. Secondly, any volume over which spatial averages are to be formed must be large if such quantities are to be, in any sense, representative of the whole. This does *not* imply that nothing less than the volume of the entire body will suffice. Nevertheless the volume must be large in extent compared with the mean inter-sink spacing. Once this is appreciated, the manipulations that follow become comparatively straightforward to comprehend.

On the scale alluded to above, therefore, we consider a closed surface containing a volume, V. As before, the matrix contribution to this is V_{M}. We can perform all the steps leading to equation (11) except that now we must also incorporate the surface flux contribution

$$J_{\mathrm{N}} = \int_{S} \boldsymbol{J} . \boldsymbol{N} \mathrm{d}S, \tag{16}$$

in the left-hand side of equation (4) and in the appropriate equations after it. The result is that equation (11) is replaced by

$$\frac{\mathrm{d}\langle c_{\mathrm{v}} \rangle}{\mathrm{d}t} + \sum_{\mathrm{L}} (D_{\mathrm{v}} k_{\mathrm{L}\mathrm{v}}^2 \langle c_{\mathrm{v}} \rangle - K_{\mathrm{L}\mathrm{v}}) - K + \alpha \langle c_{\mathrm{i}} \rangle \langle c_{\mathrm{v}} \rangle = V_{\mathrm{M}}^{-1} (H_{\mathrm{v}} - I - J_{\mathrm{N}\mathrm{v}}), \tag{17}$$

the additional subscript on J_{N} denoting that it here refers to vacancies. The definitions, equation (7) and what follows have precisely the same significance as for the periodic array, but for the larger volume.

This, it must be appreciated, is exactly the problem. For equation (17), as it stands, refers to one specific configuration of sinks. Thus it contains far more information than we could possibly expect to need. What is required is an average over all possible configurations, i.e. an ensemble average. Performing this average is therefore the next crucial step.

At this juncture the choice of sample volume V, comes to the fore. Clearly, if it is too small, the variation of the mean concentration within S could vary enormously from one configuration to another. Indeed, some configurations may not even be permissible within it. On the other hand, if it is sufficiently large, then each defect will already sense many different regions where one or other sink types is spatially isolated, where it is locally correlated with others, and so forth. This has the following consequence. Suppose we define the probability of a particular sink configuration as $P(\ldots; \boldsymbol{r}_1^{\mathrm{L}}, \ldots \boldsymbol{r}_k^{\mathrm{L}}, \ldots \boldsymbol{r}_{\mathrm{N}_{\mathrm{L}}}^{\mathrm{L}}; \ldots)$, where the positions $\boldsymbol{r}_k^{\mathrm{L}}$ of the N_{L} sinks of

type L alone have been explicitly enumerated. The rest are to be understood by the sequences of dots within the argument. Thus the ensemble average of $\langle c_v \rangle$, for example, is given by

$$\langle c_v \rangle = \int \langle c_v \rangle P(\ldots; \mathbf{r}_1^L, \ldots \mathbf{r}_{N_L}^L; \ldots) \prod_{L,l} \mathrm{d}\mathbf{r}_l^L. \tag{18}$$

Then the consequence of the argument given above is the expectation that

$$\langle \dot{c}_v \rangle \approx \langle c_v \rangle, \tag{19}$$

if the sample volume V is large enough. Similarly we expect that

$$\int \langle c_l \rangle \langle c_v \rangle P(\ldots; \mathbf{r}_1^L, \ldots \mathbf{r}_{N_L}^L; \ldots) \prod_{L,l} \mathrm{d}\mathbf{r}_l^L \approx \langle c_l \rangle \langle c_v \rangle. \tag{20}$$

Thus, in forming the ensemble average of equation (17) (that is, multiplying by P and integrating over the $\mathbf{r}_l^L$), the only remaining crucial issues are the evaluations of

$$\int k_{Lv}^2 \langle c_v \rangle P(\ldots; \mathbf{r}_1^L, \ldots \mathbf{r}_{N_L}^L; \ldots) \prod_{L,l} \mathrm{d}\mathbf{r}_l^L \tag{21}$$

and the analogous integral of K_{Lv}. But, by virtue of equation (19), the expression (21) is also, approximately, $\overline{k_{Lv}^2} \langle c_v \rangle$, where

$$\overline{k_{Lv}^2} = \int k_{Lv}^2 P(\ldots; \mathbf{r}_1^L, \ldots \mathbf{r}_{N_L}^L; \ldots) \prod_{L,l} \mathrm{d}\mathbf{r}_l^L, \tag{22}$$

while, from equation (12)

$$\overline{k_{Lv}^2} = N_L \overline{k_{Ll,v}^2}, \tag{23}$$

because the average for each sink of the same type must be the same. Similarly, it follows that

$$\overline{K_{Lv}} = N_L \overline{K_{Ll,v}}. \tag{24}$$

Therefore we are led to ensemble averages of one sink of each type only. Moreover, we now take the ensemble average of equation (7) and use equations (23) and (24) to find

$$\overline{k_{Lv}^2} \approx [(N_L/V_M) J_{Ll}^v + K_{Lv}]/D_v \langle \dot{c}_v \rangle, \tag{25}$$

where J_{Ll}^v is the ensemble average of J_{Ll}^v. Thus we can not only identify the terms produced by ensemble averaging here but also, by virtue of equation (25), understand how they are to be derived.

It is worth digressing for a moment to emphasize the simplification introduced by the last equation. The quantity J_{Ll}^v is the vacancy flux to the sink, of type L, situated at $\mathbf{r}_l$. In any one configuration it will depend upon what other sinks neighbour it, their type and their relative location. But after ensemble-averaging as in equation (18), all such detail is obviously smeared out. Furthermore, while averaging over the positions of all other sinks may yet leave some dependence upon $\mathbf{r}_l$ (because of the relative position of the sink in question *vis-à-vis* the bounding surface S), upon integrating over $\mathbf{r}_l$ itself, this too is removed. Thus J_{Ll}^v is independent of l; this subscript may be dropped; provided, yet again, the volume V is large enough for all these considerations to apply.

The end result therefore is that the ensemble average of equation (17) is given by

$$\frac{\mathrm{d}\langle c_v \rangle}{\mathrm{d}t} + \sum_L (D_v \overline{k_{Lv}^2} \langle \dot{c}_v \rangle - \overline{K}_{Lv}) - K + \alpha \langle \dot{c}_i \rangle \langle \dot{c}_v \rangle \approx V_M^{-1} (\bar{I}_v - \bar{I} - J_{Nv}), \tag{26}$$

the approximations to this point being purely statistical. We now focus upon the right-hand side of equation (26). Inasmuch as the arguments leading to the neglect of $\bar{I}_v$ and $\bar{I}$ for the periodic array were independent of this periodicity, they hold equally well here for their ensemble averages. Moreover, since the sample volume we have chosen is large, the total production rate of defects within V, i.e. KV_M, will be almost entirely mitigated by flow to sinks *within* V. That is, J_{Nv} will be negligible compared with KV_M. As a result, we arrive, finally, at precisely the same rate equations, (14) and (15), as already derived for the periodic array, the only changes being ones of interpretation. Namely, the quantities $\langle c_v \rangle$ and $\langle c_i \rangle$ are to be replaced by the ensemble averages $\langle \dot{c}_v \rangle$ and $\langle \dot{c}_i \rangle$, respectively, while the sink strengths and emission rates are to be found from the ensemble average of the flux to a particular sink type as prescribed by equation (25).

(*c*) *Methodology for sink strength calculations*

We next turn to the question of how these sink strengths are to be evaluated in any particular system. First, we shall invoke one simplification, which is invariably adopted, namely the concept of so-called steady state growth. It is to be understood here in the following sense: all characteristic dimensions entering the sink strengths are to be treated as time-independent. Thus the sink size and the distance to the outer bounding surface are regarded as fixed for solving the rate equations. Obviously, since there are fluxes to the sinks, this cannot be strictly legitimate. Voids and dislocation loops, for example, will grow. Nevertheless, it is assumed that the concentrations, or more importantly, the fluxes, may be estimated at each instant by using the sink and boundary sizes at that instant. The basis of this approximation may be traced to the solution of an idealized problem by Zener (1949), and we shall adopt it without further enquiry. The only alternative would be to confront partial differential equations with moving boundary conditions in a finite domain. Generally, these are unmanageable. It is fortunate that, as Zener has shown, this is usually unnecessary for the problems we consider.

Subject to this simplification, if the production rate is independent of time, the time derivatives in the rate equations are of no importance except for deriving initial transients. For the moment we shall ignore the latter. The rate equations are then simple algebraic relations which can be solved for the concentrations, with the sink strengths and emission rates entering as parameters (Harkness & Li 1971; Brailsford & Bullough 1972*a*; Wiedersich 1970).

Reviewing the derivations given in §§2(*a*), (*b*), one sees that the parameters are to be found from the defect fluxes to each sink type under the following conditions:

(i) point defect generation is to be included;
(ii) intrinsic recombination is to be included;
(iii) the flow to each sink is to be computed with allowance for the presence of all other sinks;
(iv) in periodic arrays, the flux at the primitive cell boundary must vanish;
(v) in random arrays, the sample volume must be large compared with the inter-sink spacing.

It is informative to contrast these conditions with those of the models that have actually been used by workers in this field in computing the strengths of sinks of various types (see table 1). It is not our intent here to dismiss any of these, but rather to indicate their broad variety. Our overall classification into periodic or random arrays has been solely dictated by whether condition (iv) above was invoked or not. If it was not, and the authors did not at the same time explicitly state that they intended there to be surface sources or sinks (as the case may be)

at the appropriate outer boundary, we have presumed that their intention was to consider a random configuration. Usually this is not made clear, explicitly, but their later applications to real materials usually infer it.

A further comment on table 1 is in order. It should be understood that the works cited do not universally address the question of sink strengths *per se*. For example, in Bullough & Perrin (1971) and Ham (1958) these quantities are not even mentioned. But this is not the point. What we are alluding to is whether the methods used in each case are adaptable straightforwardly to the problem at hand. In some instances this is still to be shown by detailed analysis, in others the lack of consistency is immediately apparent.

TABLE 1. METHODS USED FOR COMPUTING VACANCY SINK STRENGTHS

	defect generation	recombination	other sinks	configuration	consistent overall
Wiedersich (1970)	yes	yes	no	lattice	no
Bullough & Perrin (1971)	yes	no	yes	lattice	yes
Nichols (1978*a*, *b*)	yes	no	no	lattice	no
Ham (1958)	no	no	no	lattice	yes
Damask & Dienes (1971)	no	no	no	lattice	no
Brailsford & Bullough (1972*a*)	yes	no	yes	random	yes†
Heald & Speight (1975)	no	no	no	random	no
Wolfer & Mansur (1978)	no	no	no	random	no

† See also Brailsford *et al.* (1979) and Hayns (1979).

Confronted by this diversity of approaches, it is natural to ask how critical are the various ingredients that each discarded for some reason. How important is intrinsic recombination, or the presence of other sinks, or the distinction between a regular array and a random one, for example? There appears to be no viable alternative to exploring each in detail, simple models being used to focus upon the point at issue. This is the approach followed recently by Brailsford *et al.* (1979) to confirm that intrinsic recombination corrections to the sink strengths are indeed usually small (see also Hayns 1979). It will be further adopted in subsequent sections.

The problem posed for periodic arrays is straightforward though difficult; that for random arrays still requires further comment. To compute the sink strengths, configurational averages of the fluxes to the sinks are needed. This process has in fact been completed in only one case, namely for a void in an array of like voids (Brailsford 1976). The intent there was to justify an approximate alternative scheme, which we had introduced earlier: the effective medium approach (Brailsford & Bullough 1972*a*). Such justification was deduced for the model problem considered.

The synthesis of the effective medium model is the following. One does not compute the J_L^v configuration by configuration and then average, but focuses first upon the physical content of equation (26) (with H_v, $\bar{I}$ and J_{Nv} neglected). Being independent of the spatial coordinate, clearly equation (26) can be conceived of as defining the concentration in a homogeneous lossy continuum containing all sink types distributed uniformly. To find the appropriate strength of any sink it is necessary therefore to link the true local behaviour around any one sink type to the mean behaviour in this continuum. In reality each sink is surrounded by some

matrix region. Thus one considers a model in which the correct local distribution is connected to the ensemble mean by surrounding the sink-plus-matrix region by this continuum and computing the flux to the central sink that ensues. For consistency, this flux is then made such that the sink strength so deduced is equal to that first assumed in the medium. This determines the sink strength. Clearly the calculation has to be performed for a large volume for reasons given in §2(*b*); comments to the contrary (Nichols 1978*a*) are simply ill conceived. The method as here advocated was first suggested by Brailsford & Bullough (1972*a*).

We have recognised recently, however, that the self-consistency step will be automatically satisfied if we use the definition equation (25) and ignore intrinsic recombination. For in steady state this equation states that

$$\langle c_v \rangle \approx (K + K_v)/D_v k_v^2, \tag{27}$$

where

$$k_v^2 = \sum_L k_{Lv}^2, \; K_v = \sum_L K_{Lv}. \tag{28}$$

Thus $\langle c_v \rangle$ is precisely the quantity we previously denoted (Brailsford & Bullough 1972*a*) by c_∞, so that equation (25) may be placed in the form

$$D k_{Lv}^2 c_\infty - K_{Lv} = (N_L/V_{at}) J_L^v. \tag{29}$$

This, therefore, is simply a statement of the self-consistency in mathematical language. Consequently, and more to the point, equation (25) automatically satisfies this constraint as a matter of definition. Thus appeal to self-consistency need not be explicitly mentioned subsequently.

Particular examples of the lattice and effective medium models are explored later. There is still one further frequently used approach to be mentioned. Instead of invoking a zero-current outer boundary condition, such as is appropriate for a lattice, or a finite concentration at infinite distance, as is truly appropriate for the effective medium, a fixed concentration at a *finite* distance from the sink in question is imposed (Heald & Speight 1975). Strictly speaking, then, this is a hybrid model. By using this model, the flux to the sink under discussion is computed and a strength is ascribed to it in terms of the ratio of flux to boundary concentration. We know of no way in which the sink strength so deduced can be justified for direct substitution in rate theory. For the problem that this procedure in fact solves is one in which the region under discussion is surrounded by a continuum with a total sink strength that *tends to infinity*. To appreciate the point, suppose the region has spherical symmetry and let its boundary be a distance R from its centre. Then, if the surrounding continuum has a total sink strength q^2, the solution of

$$\frac{D_v}{r^2}\frac{\mathrm{d}}{\mathrm{d}r} r^2 \frac{\mathrm{d}c_v}{\mathrm{d}r} - D_v q^2 c_v + K \approx 0 \tag{30}$$

appropriate to it (when thermal emission is omitted) is

$$c_v = c_\infty - (c_\infty - c_b)(R/r)\, \mathrm{e}^{q(R-r)}, \tag{31}$$

where c_b is the concentration at the boundary and, here, $c_\infty = K/D_v q^2$. Thus the logarithmic derivative of the internal solution, at the boundary, must be such that

$$R\left(\frac{1}{c_v}\frac{\mathrm{d}c_v}{\mathrm{d}r}\right)_R = \frac{c_\infty - c_b}{c_b}(1 + qR). \tag{32}$$

But if the flux to the central sink is to originate from defect flow *within* $r < R$ only, the left-hand side of equation (32) must vanish for arbitrary $c_{\rm h}$, $D_{\rm v}$ and K. Evidently, from equation (31), this is possible only if $q \to \infty$. For this reason, we believe that this hybrid approach is inconsistent, though the results it yields in isolated cases may, in fact, be to some degree correct.

We conclude this section with a brief comment upon the question of initial transients or time-dependent point defect production in general. Our central attention will be upon neither; the steady state with constant production rate will usually be understood. We shall address the broader issue only in relation to the question of the sink strengths of voids in the section following, and there mainly to the extent of highlighting one limitation (Gösele 1978) of the higher-order sink strength correction that we derive. Our intention was formerly, and continues to be, to focus on the question of rate theory application to the uniform void swelling problem. For this it appears that the constant production rate model is adequate (Mansur *et al.* 1979). In other areas of defect kinetics†, however, the sink strength theory developed here may require modification.

3. The sink strength of voids

Part (*a*) of this section sets the stage for what follows in the remainder. In it, we consider the result obtained from the effective medium approach and explore some of its facets with relation to the conditions exposed in §2(*c*). In §3(*b*) we then explore some aspects of void lattice models to highlight the points already raised.

Henceforth in this paper, we repeat, we shall neglect intrinsic recombination entirely. We give three reasons. First, when it dominates, the sink strengths are in any case of relatively minor importance (Brailsford & Bullough 1972*a*). Secondly, in previous analyses (Brailsford *et al.* 1979, Hayns 1979) it has been shown to produce only minor corrections. Thirdly, to retain it would render further analytical progress virtually out of the question. Nevertheless, we would point out, that while the last is the most pressing reason, we do not believe it the most significant.

(*a*) *The effective medium approach*

In a previous study (Brailsford *et al.* 1976) it has been shown that the void sink strength is only slightly sensitive to the thickness of the matrix shell that is considered to surround each void. Thus, for simplicity, we shall omit such a region entirely. The void, of radius $r_{\rm c}$, is to be imagined as embedded directly in the effective medium.‡

The effective medium has the same properties as the continuum abstracted from rate theory. Inspection of equation (26) shows therefore that the sink strength appropriate to it is $\Sigma_{\rm I} k^2_{\rm I,v}$; the emission rate, $\Sigma_{\rm L} \bar{K}_{\rm I,v}$, for vacancies, with these quantities is to be obtained from equation (25). We shall now simplify the notation. We drop the bar sign over these quantities, ensemble-averaging having been incorporated within the model itself. Also, the index i, or v, need no longer be continually repeated since intrinsic recombination effects on the sink strengths are being neglected. The following analyses are the same for both defects except where an explicit distinction is drawn.

† Pulsed irradiation, for example, deserves further study.

‡ The criticism (Nichols 1978*a*) of our first derivation (Brailsford & Bullough 1972*a*) is fallacious. The approximation $kR_1 \ll 1$ invoked by Nichols (1978*a*) (where k^2 is the total sink strength, R_1 the radius of the outer boundary of the sink-free region) is one of low void volume fraction only. It is explicitly stated after equation (9) of Brailsford & Bullough (1972*a*) that an accuracy of $O(r_{\rm c}/R_1)$, with R_1 small, is intended. The limit inferred by Nichols (1978*a*, equation (187*a*)) is erroneous mathematically.

Our problem then is to find the flux to the central cavity embedded in the medium. The concentration, now written simply as c, is the solution of

$$\frac{D}{r^2}\frac{\mathrm{d}}{\mathrm{d}r} r^2 \frac{\mathrm{d}c}{\mathrm{d}r} - Dk^2 c + K + K_{\rm e} = 0, \tag{33}$$

and $k^2 \equiv \Sigma_{\rm L} k^2_{\rm L,v}$, $K_{\rm e} \equiv \Sigma_{\rm L} \bar{K}_{\rm L,v}$, in the former detailed notation (for vacancies). The boundary condition at the medium–sink interface is obtained from equation (3). We have

$$j_{\rm e} \equiv D \left.\frac{\mathrm{d}c}{\mathrm{d}r}\right|_{r_{\rm e}} = v(c(r_{\rm e}) - \hat{c}_{\rm e}). \tag{34}$$

Here the L label has been assigned the symbol e (for cavity). As noted earlier, the *l* label is redundant after the ensemble-averaging, which is the basis of this model.

The solution of this problem is readily found to be

$$c = c_\infty - \frac{(c_\infty - \hat{c}_{\rm e})\, vr_{\rm e}/D}{1 + kr_{\rm e} + vr_{\rm e}/D} \frac{r_{\rm e}}{r} \mathrm{e}^{-k(r - r_{\rm e})}, \tag{35}$$

where $c_\infty = (K + K_{\rm e})/Dk^2$. We use it to compute the quantities appearing in equation (25). First, consider the volume average of the concentration, $\langle \bar{c}_{\rm v} \rangle$ as it there occurs. Because $c - c_\infty$ is localized about $r \approx r_{\rm e}$, it is evident that $\langle \bar{c}_{\rm v} \rangle \equiv \langle c \rangle$ is simply c_∞, the volume being large. Secondly, the surface integral of the flux (i.e. the quantity $\bar{J}_{\rm e}$) is

$$J_{\rm e} = \frac{4\pi (c_\infty - \hat{c}_{\rm e})\, vr_{\rm e}^2 (1 + kr_{\rm e})}{1 + kr_{\rm e} + vr_{\rm e}/D}. \tag{36}$$

Hence, with $k_{\rm e}^2$ denoting the void sink strength and $K_{\rm e}$ the void emission rate, equation (25) becomes

$$k_{\rm e}^2 = \frac{1}{c_\infty}\left[C_{\rm e} \frac{4\pi (c_\infty - \hat{c}_{\rm e})\,(1 + kr_{\rm e})\, vr_{\rm e}^2/D}{1 + kr_{\rm e} + vr_{\rm e}/D} + \frac{K_{\rm e}}{D}\right], \tag{37}$$

where $C_{\rm e} = N_{\rm e}/V_{\rm M}$ is the volume concentration of voids in the low swelling régime. We now apply the low temperature limit when, by definition, $K_{\rm e}/D$ vanishes. The quantity $\hat{c}_{\rm e}$ also tends to zero†, whence equation (37) yields

$$k_{\rm e}^2 = 4\pi r_{\rm e} C_{\rm e} (1 + kr_{\rm e}) \frac{vr_{\rm e}/D}{1 + kr_{\rm e} + vr_{\rm e}/D}. \tag{38}$$

Furthermore, since equation (37) must hold at all temperatures, it now follows that

$$K_{\rm e} = Dk_{\rm e}^2 \hat{c}_{\rm e} \tag{39}$$

with $k_{\rm e}^2$ given by equation (38).

These are the general results of this model for the most general form of boundary condition, as embodied in equation (3). The transfer velocity influences the sink strength, and the emission term $v\hat{c}_{\rm e}$ determines $K_{\rm e}$. Henceforth we shall adopt two simplifications to aid brevity. First, it will be taken as understood that all flow is diffusion-controlled, by which we mean that the last jump into the sink is not *substantially* different from defect jumps within the matrix. Then

† This is true on general thermodynamic grounds. Specifically, for vacancies, $\hat{c}_{\rm v} = c_{\rm v}^{\rm e} \exp[(2\gamma/r_{\rm c} - p)\,\Omega/k_{\rm B}T]$ where $c_{\rm v}^{\rm e}$ is the thermal equilibrium bulk concentration appropriate to the temperature T, γ is the specific surface free energy, Ω is the atomic volume, $k_{\rm B}$ is Boltzmann's constant and p is the pressure due to any enclosed gas. For interstitials $\hat{c}_{\rm i}$ is negligible because of the much larger formation energy (i.e. negligible $c_{\rm i}^{\rm e}$).

v will be of the order of D/lattice spacing, so that for voids of any significant size, $vr_c/D \gg 1$. Then

$$k_c^2 = 4\pi r_c C_c(1 + kr_c) \tag{40}$$

follows from equation (38). Secondly, we shall henceforth neglect emission processes as far as possible, so that here, for example, $\dot{c}_v$ and K_v become negligible. This, we emphasize, is solely to curtail endless repetition as far as possible in comparing one method with another. The sink strengths alone contain all the necessary physics for this purpose. The emission rates, if required, can always be found by duplicating the processes given above.

We turn now to some of the points, (i) to (v), listed in §2(*c*). Concerning the inclusion or exclusion of point defect generation, one can easily see that in fact it is immaterial in this approach. Incorporating it simply serves to determine what c_∞ actually is in terms of it. One might equally well have left c_∞ as some arbitrary given parameter and solved the production-free problem subject to the condition $c \to c_\infty$ as $r \to \infty$. It is easy to show that the k_n^2 so derived is the same. Point (ii), relating to intrinsic recombination, has been discussed earlier, whereas (iv) is not relevant here. The size of the sample volume, point (v), is an intrinsic part of this method, and point (iii) is paramount when kr_c is comparable with unity. For k, by definition, contains not only the sink strengths of voids but also dislocations, for example (Brailsford *et al.* 1976). The ability to incorporate the effect of other sinks in a random array, known as the higher order correction, is a prime virtue of this method.

(*b*) *Void lattice models*

Because we have several new results to present, our treatment of the void lattice will be comparatively extensive. In subsection (i) we shall adapt Ham's method to the sink strength problem for arbitrary time-dependent, but spatially uniform, point defect production. The presence of sinks other than voids is included in an average sense specified in more detail. In subsection (ii) we will show how the results of the effective medium approach are confirmed by this method. Here we also make reference to the approach of Bullough & Perrin (1971). Subsection (iii) contains an analysis of the voids-only lattice. It shows, specifically, the importance of including all sink types by pointing out the internal inconsistencies that can arise when they are ignored.

(i) *The eigenfunction expansion*

We imagine now the voids to lie on the points of a lattice (simple cubic will suffice). Further, it will be *assumed* that any other sink, e.g. straight dislocations or dislocation loops, can be represented in an average sense. Thus, external to the voids, a loss rate of defects exists of the form $Dk_n^2 c$, where c is the local concentration. For now, this assumption may be understood as simply defining a mathematical problem; we shall give the physical justification later (see §3(*b*iii). With this model we wish to evaluate the void sink strength using the formalism of §2(*a*).

We follow the usual Wigner–Seitz construction and replace the unit cell by a sphere of the same volume with the void at its centre. The radius of this sphere, R, is

$$R = (3V_c/4\pi)^{\frac{1}{3}}, \tag{41}$$

where V_c is the sample volume per void. Between $r = r_c$, and $r = R$, we have therefore

$$\frac{D}{r^2}\frac{\partial}{\partial r}\left(r^2\frac{\partial c}{\partial r}\right) - Dk_n^2 c + K = \frac{\partial c}{\partial t}, \tag{42}$$

where, in line with our earlier remark, we now ignore all emission processes ($K_v \to 0$) and assume diffusion-controlled flow ($c \to 0$ at $r = r_c$). We allow for the possibility of K depending upon time by incorporating the term $\partial c/\partial t$ in equation (42). Here, it is perhaps worth re-emphasizing, the term in k_n^2 is simply an *approximate* representation of the effects of other sink types within the cell. In the *real* lattice system, no such term exists. We should in fact be solving a *sink-free* equation within the matrix region, with certain prescribed boundary conditions at these other sink surfaces. Thus equation (42) really embodies a model of a model! Nevertheless, it is a convenient place to start.

To compute the void sink strength we need the flux to the void and the volume average of the concentration. In accordance with the method of Ham (1958), but with a trivial generalization, we shall suppose that the eigenfunctions ψ_n ($n = 0, 1, 2, \ldots$) satisfying

$$\frac{1}{r^2}\frac{\mathrm{d}}{\mathrm{d}r}\left(r^2\frac{\mathrm{d}\psi_n}{\mathrm{d}r}\right) - (k_n^2 - \lambda_n^2)\psi_n = 0 \tag{43}$$

are known for the boundary conditions

$$\psi_n(r_v) = 0, \quad (\mathrm{d}\psi_n/\mathrm{d}r)_R = 0; \tag{44}$$

λ_n^2 is the corresponding eigenvalue. The eigenfunctions form a complete set; we assume they are normalized to unity within the matrix volume V_M. We now substitute an expansion of c in terms of these functions, namely

$$c(r, t) = \sum_n a_n(t)\,\mathrm{e}^{-D\lambda_n^2 t}\psi_n(r) \tag{45}$$

into equation (42), which leads to

$$\sum_n \psi_n \frac{\mathrm{d}a_n}{\mathrm{d}t}\,\mathrm{e}^{-D\lambda_n^2 t} = K. \tag{46}$$

Thus, since the ψ_n are orthonormal, upon multiplying equation (46) by a particular ψ_m and integrating over the matrix volume between r_c and R we find

$$\mathrm{d}a_m/\mathrm{d}t = KI_m\mathrm{e}^{D\lambda_m^2 t}, \tag{47}$$

where, here, $I_m = \int_{V_M}\psi_m \mathrm{d}V$. We remind the reader that equations (46) and (47) apply only within the 'steady state' growth approximation. The $\psi_n(r)$ clearly must contain r_c and R as parameters. The time dependence of these has been ignored.

When K is time-independent, the solution of equation (47) is simply

$$a_m(t) - a_m(0) = \frac{KI_m}{D\lambda_m^2}\left(\mathrm{e}^{D\lambda_m^2 t} - 1\right), \tag{48}$$

where the initial value of a_m is to be obtained from equation (45):

$$a_m(0) = \int_{V_M} c(r, 0)\,\psi_m \mathrm{d}V. \tag{49}$$

The concentration within the cell is then

$$c(r, t) = \sum_n \left[a_n(0)\,\mathrm{e}^{-D\lambda_n^2 t} + \frac{KI_n}{D\lambda_n^2}\left(1 - \mathrm{e}^{-D\lambda_n^2 t}\right)\right]\psi_n(r). \tag{50}$$

In this, the final steady state is apparent.

When K is time-dependent, on the other hand, the solution becomes more complicated. Suppose, for example, we represent $K(t)$ by the Fourier integral

$$K(t) = \frac{1}{(2\pi)^{\frac{1}{2}}} \int_{-\infty}^{\infty} \tilde{K}(\omega)\, e^{i\omega t}\, d\omega. \tag{51}$$

Then integration of equation (47) leads to

$$a_m(t) - a_m(0) = \frac{I_m}{(2\pi)^{\frac{1}{2}}} \int_{-\infty}^{\infty} \tilde{K}(\omega)\, \frac{e^{(i\omega + D\lambda_m^2)t} - 1}{i\omega + D\lambda_m^2}\, d\omega, \tag{52}$$

so that

$$c(r,t) = \sum_n \left[a_n(0)\, e^{-D\lambda_n^2 t} + \frac{I_n}{(2\pi)^{\frac{1}{2}}} \int_{-\infty}^{\infty} \tilde{K}(\omega)\, \frac{e^{i\omega t} - e^{-D\lambda_n^2 t}}{i\omega + D\lambda_n^2}\, d\omega \right] \psi_n(r). \tag{53}$$

Equation (50) is just a special case of equation (53), for $\tilde{K}(\omega) = (2\pi)^{\frac{1}{2}} K\delta(\omega)$, with K a constant and δ the Dirac delta function.

The initial transients will not concern us here. We assume a time such that $D\lambda_0^2 t \gg 1$, where λ_0^2 is the smallest eigenvalue. Then the volume integral of c is

$$\langle c \rangle = \sum_n \frac{I_n^2}{(2\pi)^{\frac{1}{2}}} \int_{-\infty}^{\infty} \frac{\tilde{K}(\omega)\, e^{i\omega t}}{i\omega + D\lambda_n^2}\, d\omega, \tag{54}$$

while the total flux to the void is

$$J_c = 4\pi r_c^2 D \sum_n \frac{I_n}{(2\pi)^{\frac{1}{2}}} \left(\frac{d\psi_n}{dr}\right)_{r_c} \int_{-\infty}^{\infty} \frac{\tilde{K}(\omega)\, e^{i\omega t}}{i\omega + D\lambda_n^2}\, d\omega, \tag{55}$$

as follows from equation (53). Thus, the void sink strength we determine via equation (7) is

$$k_c^2 = 4\pi r_c^2 \sum_n I_n \left(\frac{d\psi_n}{dr}\right)_{r_c} \int_{-\infty}^{\infty} \frac{\tilde{K}(\omega)\, e^{i\omega t}}{i\omega + D\lambda_n^2}\, d\omega \Big/ \sum_n I_n^2 \int_{-\infty}^{\infty} \frac{\tilde{K}(\omega)\, e^{i\omega t}}{i\omega + D\lambda_n^2}\, d\omega. \tag{56}$$

This relation embodies the main fact motivating our digression into time-dependent production rate problems, namely that the sink strength depends upon the mode of irradiation. Two simple examples will suffice to make the point. Suppose first that the irradiation is time-independent at the rate K. Then $\tilde{K}(\omega) = (2\pi)^{\frac{1}{2}} K\delta(\omega)$, as specified previously. In this instance, equation (56) yields

$$k_c^2 = 4\pi r_c^2 \sum_n \frac{I_n}{\lambda_n^2} \left(\frac{d\psi_n}{dr}\right)_{r_c} \Big/ \sum_n \frac{I_n^2}{\lambda_n^2}. \tag{57}$$

However, suppose instead that $K(t) = 2K\cos^2(\frac{1}{2}\omega_0 t)$. This has the same mean as the uniform case but it fluctuates in time. Then the inverse of equation (51),

$$\tilde{K}(\omega) = \frac{1}{(2\pi)^{\frac{1}{2}}} \int_{-\infty}^{\infty} K(t)\, e^{-i\omega t}\, dt, \tag{58}$$

indicates that $\tilde{K}(\omega) = (2\pi)^{\frac{1}{2}} K\{\delta(\omega) + \frac{1}{2}[\delta(\omega+\omega_0) + \delta(\omega-\omega_0)]\}$. Consequently, when this is inserted in equation (56), we find a sink strength, $k_c^2(\omega_0)$, say, given by

$$k_c^2(\omega_0) = 4\pi r_c^2 \sum_n \frac{I_n}{\lambda_n^2} \left(\frac{d\psi_n}{dr}\right)_{r_c} F_n(\omega_0) \Big/ \sum_n \frac{I_n^2}{\lambda_n^2} F_n(\omega_0), \tag{59}$$

where

$$F_n(\omega_0) = \frac{2 + (\omega_0/D\lambda_n^2)^2}{1 + (\omega_0/D\lambda_n^2)^2}. \tag{60}$$

Evidently, the two forms for the void sink strength will be the same only if F_n is independent of n. Two possibilities arise: either $\omega_0 \ll D\lambda_0^2$ or $\omega_0 \gg D(\lambda_n^2)_{max}$, where $(\lambda_n^2)_{max}$ is the greatest possible eigenvalue. The latter, as we shall show shortly, is impossible: the eigenvalues are unbounded with increasing n. Thus only the first can arise. In that case alone can the steady state analysis be justified rigorously to this point.

There is however one loop-hole in this argument. It resides in the following fact. Suppose that in both numerator and denominator one particular mode could be said to dominate in some sense. Then the value of F_n would be immaterial for this mode since it would simply cancel out. This indeed can happen, as we now proceed to show. It is convenient to discuss it along with the higher order-void sink correction found in §3 (*a*) of this section.

(ii) *Evaluation of the void sink strength*

We turn then to the eigenvalues and eigenfunctions for the void lattice model. The details, many of which are but slight extensions of Ham's analysis, are given in Appendix A. We shall quote here only the final approximate results. These are, for the eigenfunctions

$$\psi_n = A_n r^{-1} \sin[(\lambda_n^2 - k_0^2)^{\frac{1}{2}} (r - r_c)], \tag{61}$$

where

$$A_0 \approx (4\pi r_c)^{-\frac{1}{2}}, \tag{62}$$

$$A_n \approx (2\pi R)^{-\frac{1}{2}} \quad (n \geqslant 1); \tag{63}$$

and for the eigenvalues

$$\lambda_0^2 \approx k_0^2 + 3r_c/R^3, \tag{64}$$

and

$$\lambda_n^2 \approx k_0^2 + [(n + \tfrac{1}{2})\pi/R]^2 \quad (n \geqslant 1). \tag{65}$$

The approximations involved here depend partly upon the assumption that r_c/R be small compared with unity and partly upon the fact that we wish to render the sums in equation (57) amenable to direct analytical evaluation, even if approximate. The reader is referred to Appendix A for details.

The other quantities needed are

$$I_n = 4\pi r_c A_n / (\lambda_n^2 - k_0^2)^{\frac{1}{2}}, \tag{66}$$

(see Appendix A, also), and

$$\left(\frac{d\psi_n}{dr}\right)_{r_c} = \frac{A_n}{r_c} (\lambda_n^2 - k_0^2)^{\frac{1}{2}}, \tag{67}$$

which follows from equation (61). It ensues then that

$$\frac{I_0}{\lambda_0^2} \left(\frac{d\psi_0}{dr}\right)_{r_c} \approx \frac{1}{r_c(k_0^2 + 3r_c/R^3)} \tag{68}$$

while (for $n \neq 0$)

$$\frac{I_n}{\lambda_n^2} \left(\frac{d\psi_n}{dr}\right)_{r_c} \approx \frac{2}{R[k_0^2 + [(n + \tfrac{1}{2})\pi/R]^2]}. \tag{69}$$

Consequently, for $r_c \ll R$, the lowest-mode contribution dominates the sum in the numerator of equation (57). Similarly, we have

$$\frac{I_0^2}{\lambda_0^2} \approx \frac{4\pi R^3}{3(k_0^2 + 3r_c/R^3)}, \tag{70}$$

while (for $n \neq 0$)

$$\frac{I_n^2}{\lambda_n^2} \approx \frac{8Rr_c^2}{\pi(n + \tfrac{1}{2})^2 [k_0^2 + [(n + \tfrac{1}{2})\pi/R]^2]}. \tag{71}$$

Here, also, the lowest mode dominates the sum in the denominator of equation (57). Therefore, if we retain only the contributions from the lowest mode we have

$$k_0^2 \approx \frac{4\pi r_c^2}{I_0}\left(\frac{\mathrm{d}\psi_0}{\mathrm{d}r}\right)_{r_c} \approx \frac{3r_c}{R^3} \approx 4\pi r_c C_c \tag{72}$$

a result that we can trace back as far as Dienes & Vineyard (1957).

Now compare this with the effective medium result, equation (40). The results are the same if kr_c is small compared with unity, but differ otherwise. The higher-order correction is missing. Clearly it must reside in the contributions of the higher-order modes if, as we are here assuming, $r_c/R \ll 1$. Thus we must look at all contributions to k_0^2 in equation (57). However, it is apparent from a comparison of equations (68) and (69), or (70) and (71), that the major correction arises from the numerator in k_0^2. We include this extension of the previous analysis only, with the result that

$$k_0^2 \approx \frac{3r_c}{R^3}\left\{1+\frac{2r_c}{R}(k_0^2+3r_c/R^3)\sum_{n=1}^{\infty}\frac{1}{k_0^2+[(n+\tfrac{1}{2})\pi/R]^2}\right\}, \tag{73}$$

or upon performing the indicated sum (Gradshteyn & Ryzhik 1975), that

$$k_0^2 \approx 4\pi r_c C_c\left\{1+k_0 r_c\left(1+\frac{3r_c}{k_0^2R^3}\right)\left[\tanh k_0 R-\frac{8k_0R}{\pi^2+(2k_0R)^2}\right]\right\}. \tag{74}$$

To the extent that, owing to the algebraic approximations used here, a comparison with equation (40) is warranted, equation (74) is virtually identical with it. The voids have been assumed small in the above, thus k, where it appears in equation (40), becomes the same thing as k_0. Equation (74) indicates that in the lattice model k_0^2 spans the range from $4\pi r_c C_c$ to $4\pi r_c C_c(1+k_0 r_c)$ as $k_0 R$ ranges between values small and large compared with unity (with, of course r_c always small compared with R). But if $k_0 r_c$ is to be significant in any event, and r_c yet small compared to R, then $k_0 R$ must be large. The two results are thus synonymous.

By this means, therefore, we have established that the higher-order sink correction of the effective medium model resides in the total contribution of other than the lowest mode in the lattice eigenfunction approach. Our earlier (Brailsford *et al.* 1976) surmise to the contrary was incorrect, and we here retract it.

In retrospect, this now seems obvious. For the uniform production model we have examined here is precisely that investigated by Bullough & Perrin (1971). It can be solved directly without any recourse to the eigenfunction expansion. Since the effective medium method was shown (Brailsford *et al.* 1976) to yield the same limits as this direct solution, and the eigenfunctions form a complete orthonormal set, any differences of this method from the direct solution could only have arisen because insufficient such functions were included in the analysis. This is the sole reason why the zero-order result in equation (72) is incomplete. That it is, while incorrect in detail, as good as it is, is solely a consequence of the near uniformity (Ham 1958) of $\psi_0(r)$ over most of the matrix region within the cell, when $r_c \ll R$. For with spatially uniform defect production, I_0 thereby projects out most of the driving term on the system. And with this, the zero-order result follows. The higher-order modes account for what still remains, in the way we have indicated.

At this juncture, we can now return briefly to the matter of time-dependent defect production. We indicated in §3(*bi*) that if one mode were to dominate the sums, then the void sink strength would be independent of this time dependence. To the extent that the lowest-order

void sink strength is adequate, we see that this situation does prevail. It is in the higher-order correction that such dependence will show up, therefore, in the manner prescribed by equation (56). Each case must then be taken on its own merits, with allowance, in general, for time- and possible space-dependent generation (Mansur *et al.* 1980) as well†. But to explore this topic in detail would take us too far afield. We shall leave the matter with the claim that the eigenfunction method for the lattice, and the effective medium approach for the random array, have been shown to yield the same void sink strength when the production rate varies slowly on a time scale $(D\lambda_0^2)^{-1}$, for either interstitials or vacancies. This but substantiates an earlier surmise on this subject by one of us (Brailsford 1976). It is also in agreement‡ with an independent later observation by Gösele (1978).

(iii) *The role of 'other' sinks*

In the effective medium approach it is abundantly clear that sinks of a type other than that of the one considered must be taken into account. In the preceding subsection we have shown, also, that if these other sinks are incorporated in the average manner there used, the same conclusion follows. Yet it should be clearly understood that the nature of the approximation involved in these two cases is *not* the same. In the effective medium approach, the use of a continuum sink loss rate is consequent upon ensemble averaging. In the lattice model, on the other hand, it merely represents an attempt, in an approximate way, to mimic the effect of sink surfaces, in an otherwise *sink-free* region, by dispersing a uniform loss rate term (namely $D\lambda_0^2 c$) homogeneously within it. Clearly, the motivations in the two approaches are different.

It would be pleasing if the distinction between the two approaches could simply be disregarded, as many previous investigators have in fact done. But obviously this is wrong in principle. If there is more than one sink type, it *must* be present in the basic lattice cell. Otherwise, how could the structure possibly have the periodicity assumed? There is, then, no alternative but to confront the issue.

Unfortunately, the problem posed by considering long straight dislocations arranged about one void appears to be about the most difficult task of this type one could envisage. First, the spherical symmetry is lost. Secondly, how does one handle the internal stress field properly? It seems propitious to start elsewhere.

In situations like this, it is often useful to complicate purposely a simple problem, of which the solution has already been obtained. This is the line we shall follow here. A simple cubic lattice of voids, alone, is considered (see figure 1). But instead of regarding it as simply a Bravais lattice with spacing a, we shall view it now as having a lattice constant $3a$ and a basis comprised of 27 atoms per unit cell. Our Wigner–Seitz sphere, therefore, here has a radius R_b given by

$$R_b = (3n_c V_c/4\pi)^{\frac{1}{3}} \tag{75}$$

where $n_c = 27$ and $V_c = a^3$, the latter being as before. Obviously, whether we elect to view the lattice in this more complicated way or not has to be immaterial. The void sink strength must be the same!

† The generalization for spatial dependence is trivial. In place of $K(t)I_n$, simply read $\int_{V_n} K(r,t)\,\psi_n(r)\,\mathrm{d}V$.

‡ Our analysis shows, however, that the assertion by Gösele (1978), that the higher-order corrections have nothing to do with the overlap of diffusion fields, is incorrect.

Let us then focus attention on all the voids in the larger cell and redetermine the sink strength. The lowest-order result will suffice, so we concentrate exclusively on the eigenfunction.

We can proceed in two ways once we have paid heed to how the sink strength is defined in our rate theory. Note that in equation (12), the sink strength is, by *definition*, the sum of that for *all* sinks of the same type located within the cell. Thus we may, if we wish, partially beg the question at hand and simply assert that the strength for each is the same. Thus, the void

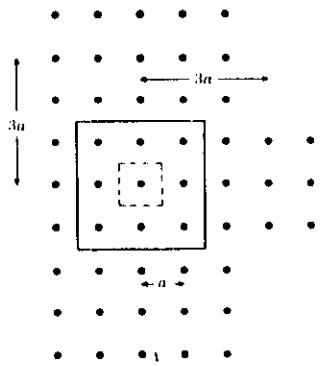

FIGURE 1. A simple cubic void lattice. The boundaries of a cell containing 27 voids per unit cell are indicated.

sink strength as it appears in the rate theory is $k_v^2 = n_c k_c^2$, where k_c^2 is the sink strength that we compute for any one of them. Obviously, the central one is the simplest, and we will look at that. For this purpose, then, suppose we simply adopt the procedure of others and now disregard the presence of the other voids. The further analysis becomes trivial, for the only change is that of a variable: R is replaced by R_b. Hence we can immediately extract from equation (75) the form for k_c^2 with the result that

$$k_c^2 = n_c(3r_c/R_b^3) = 3r_c/R^3. \tag{76}$$

This result *is* the same as that obtained previously.

However, by this process of neglecting the other sinks, we have in fact produced a comedy of errors that have simply cancelled out each other in the end. We shall demonstrate this by looking at the physical quantities involved, particularly their dependence upon the cell radius. Consider first the steady state flux, at the void surface. From equations (50) and (68) (the latter with $k_b^2 \to 0$), this is seen to be proportional to the cube of the cell radius. Thus the flux to the same central void is supposed to be n_c times larger with the larger cell than with the smaller. This is nonsense! Next look at the concentration at the cell boundary. With the aid of the equations already referred to, and equations (61), (62) and (66), this too is proportional to the cube of the cell radius. Hence the concentration at the outer boundary is similarly supposed to be n_c times larger with the larger cell than with the smaller one. This cannot be, for the former is obtained by simply stacking the latter in a bunch, and they each duplicate one another. Clearly, then, the error is one of scale. Both the flux and the concentration are

incorrect by the same factor†. It is only because the sink strength involves the *ratio* of flux to volume integral of the concentration that the correct result was finally obtained.

It is obvious that this method of neglecting the other sinks in the cell, relying as it does upon the cancellation of large errors, is not to be trusted. We now develop an alternative approach.

The eigenfunction method of §3(*bi*) is legitimate for both large and small cells. It is the eigenfunctions of equation (61) *et seq.* that are inappropriate. What is needed for the problem at hand are new eigenfunctions, $\phi_n(r)$, that are the solutions of

$$\nabla^2\phi_n + \mu_n^2\phi_n = 0, \tag{77}$$

subject to the conditions that (i) the flux at the cell boundary vanish, and (ii) that ϕ_n be zero at every internal sink surface. Apart from the central void surface, there are $n_c - 1$ ($= 26$), other such surfaces. These correspond to the six voids centred at a (100) positions, the twelve at $a\,2^{\frac{1}{2}}$(110) and the eight at $a\,3^{\frac{1}{2}}$(111).

Problems of the same general character are encountered in neutron scattering off nuclei, and there the analysis is well developed (Goldberger & Seitz 1947). We shall adapt this treatment to the case at hand.

The starting point is the observation that, in the single void problem, the lowest eigenfunction is of the form

$$\psi_0 \sim a_{-1}(1 - r_c/r) \tag{78}$$

when $r_c/R \ll 1$. The quantity $a_{-1}r_c$ is, by definition, the coefficient of $(-r)^{-1}$. Thus ψ_0 is also the solution of

$$\nabla^2\psi_0 = 4\pi a_{-1}r_c\,\delta(r) \tag{79}$$

if we consider *all* space within the cell and choose to stipulate that $\psi_0(r_c)$ vanishes only later. That option is open. Now it is to be expected that $\phi_0(r)$ will have the character of ψ_0 but now near *every* void. Thus, in place of equation (77) *and its associated boundary conditions*, we can equally well look for solutions of

$$\nabla^2\phi_0 + \mu_0^2\phi_0 = 4\pi a_{-1}r_c \sum_l \delta(r - r_l) \tag{80}$$

as far as the lowest eigenfunction is concerned. Here r_l denotes the location of the centre of the void labelled l (with $l = 1, 2, \ldots, 26$) and $a_{-1}r_c$ is now the coefficient of $(-r)^{-1}$ in an expansion of $\phi_0^l(r)$ at small r. By convention, $l = 0$ will correspond to the central void which, to link up with what has gone before, we shall treat as a finite object. Apart from this, equation (80) is to be solved over *all* space between central void and cell boundaries. The δ-functions already account for the presence of the remaining voids.

To this point, both the equation itself and its associated boundary conditions have only cubic symmetry. The Wigner-Seitz procedure corresponds to replacing the true environment by a spherically symmetric one. We use the same approximation here. The cubic cell outer boundary is replaced by a sphere of radius R_b and the angular average of equation (80) is performed. In this way we obtain

$$\frac{1}{r^2}\frac{\mathrm{d}}{\mathrm{d}r}\,r^2\frac{\mathrm{d}\phi_0}{\mathrm{d}r} + \mu_0^2\phi_0 = a_{-1}r_c\sum_\sigma \frac{n_\sigma}{a_\sigma^2}\,\delta(r - a_\sigma). \tag{81}$$

† A direct solution of the problem, with recourse to the eigenfunction expansion being avoided, yields the same conclusion.

Here σ, which can assume the values 1, 2 or 3, is the shell number, a_σ is the distance of the shell σ from the origin, and n_σ is the number of voids on each shell. Thus, if we label the shells successively by the numbers 1 to 3 moving outwards, $a_\sigma = a\sigma^{\frac{1}{2}}$, while $n_1 = 6$, $n_2 = 12$ and $n_3 = 8$. In obtaining equation (81) we have used the fact that

$$\delta(r - r_i) = (r_i^2 \sin\theta_i)^{-1}\delta(r - r_i)\,\delta(\theta - \theta_i)\,\delta(\phi - \phi_i), \tag{82}$$

in spherical coordinates, r_i, θ_i and ϕ_i having their usual significance in this system. On general grounds we know that ϕ_0 will be an s-state, as implied by the form of equation (81).

Equation (81) can be solved readily as it stands. The detail engendered by the three distinct δ-functions serves only to mask the central issue. None of the physics essential to us is lost if we now coalesce the three shells and simply assert that $a_\sigma = r_0$ for all σ. Henceforth, therefore, we shall suppose that the right-hand side of equation (81) has been replaced by $(n_c - 1)(a_{-1}r_c/r_0^2)\,\delta(r - r_0)$.

For $r_c < r < r_0$ and $r_0 < r < R_b$ the δ-function so obtained contributes nothing to the equation. The solutions in these regions are, respectively,

$$\phi_0(r) = (a_{-1}/\mu_0 r)\sin\mu_0(r - r_c), \tag{83}$$

and

$$\phi_0(r) = (B/r)[\mu_0 R_b \cos\mu_0(R_b - r) - \sin\mu_0(R_b - r)]. \tag{84}$$

In the inner region ϕ_0 has been chosen to vanish at $r = r_c$ as required, and its coefficient satisfies the prescription for a_{-1}. The derivative of ϕ_0 in equation (84) vanishes at $r = R_b$.

The δ-function at $r = r_0$ introduces a discontinuity into the derivative of ϕ_0 at this point. Multiplying the simplified version of equation (81) by r^2 and integrating between $r_0 - \epsilon$ and $r_0 + \epsilon$ lead to the following

$$r_0^2\left[\left(\frac{d\phi_0}{dr}\right)_{r_0+\epsilon} - \left(\frac{d\phi_0}{dr}\right)_{r_0-\epsilon}\right] = (n_c - 1)\,a_{-1}r_c \tag{85}$$

as $\epsilon \to 0$. Thus the condition that $\phi_0(r)$ itself be continuous at $r = r_0$ yields a relation between B and a_{-1}, whereas equation (85), being then homogeneous in a_{-1}, becomes a relation from which the eigenvalue μ_0^2 is to be obtained.

The result of these manipulations is that

$$B = \frac{a_{-1}}{\mu_0}\,\frac{\sin\mu_0(r_0 - r_c)}{\mu_0 R_b \cos\mu_0(R_b - r_0) - \sin\mu_0(R_b - r_0)} \tag{86}$$

and, after some algebra, that

$$\sin\mu_0(R_b - r_c) - \mu_0 R_b \cos\mu_0(R_b - r_c) = [(n_c - 1)r_c/r_0][\mu_0 R_b \cos\mu_0(R_b - r_0) - \sin\mu_0(R_b - r_0)]. \tag{87}$$

Comparison of the last result with Ham's analysis (Appendix A, equation (A 5)), shows that they are the same when $n_c = 1$, as they must be. We see from Appendix A, that the lowest eigenvalue is such that $\mu_0 R_b \ll 1$, if $r_c \ll R_b$. It then follows by an expansion of equation (87) that

$$\mu_0^2 \approx 3n_c r_c/R_b^2 = \lambda_0^2. \tag{88}$$

The lowest eigenvalue is *unchanged*. It is *not* a factor of n_c smaller with the larger cell, as the neglect of other cell sinks would erroneously indicate.

It takes a few more lengthy but straightforward algebraic steps to compute the void sink strength by this method. We shall simply indicate what these are and omit the details. First, a_{-1} is determined by the normalization condition, $\int_{r_c}\phi_0^2 dV = 1$, and equation (86). Then the flux to the central void is computed, hence allowing evaluation of k_0^2. The flux to each void is the same, because the construction of equation (80) implies that each has the same local environment. Thus $k_c^2 = n_c k_c^2$ is here deduced. The end result of all this analysis is a rederivation of equation (72), but now by a correct line of reasoning. The other sinks in the larger cell have been included.

There are several physical checks on this that are worth emphasis. First, it removes a blatant inconsistency which the neglect of other sinks introduces. This is brought to light by comparing the rate theory, equation (11), and the detailed solution within the cell, equation (50), for uniform defect production. When we take cognizance of all the simplifying physical assumptions appropriate to the present analysis (i.e. no intrinsic recombination or thermal emission, one type of sink only, and H_v and I neglected, of course) the following emerges. The volume average, $\langle c\rangle$, approaches steady state with a characteristic time $(Dk_c^2)^{-1}$ according to rate theory. On the other hand, the eigenfunction approach, when the lowest mode is dominant, indicates that at each point in the cell the characteristic time approaches $(D\xi_0^2)^{-1}$, where here the eigenvalue has been denoted by ξ_0^2 to emphasize that it is for *any* cell size. With one void only per unit cell, there is no problem, for then $\xi_0^2 = \lambda_0^2 = k_c^2$. Both times are the same. Consider now the larger cell. If the central void alone is considered in finding the eigenvalue, then the eigenvalue is a factor of n_c smaller, while the void sink strength is unchanged. Thus we get the absurd result that the volume average of a function varies with time at a different rate from that at which its value at each point in space does! The correct eigenvalue, equation (88), which accounts for all sinks in the cell, removes this contradiction.

Indeed, this may provide a check on the consistency of other sink strength problems that might arise in the future. For if one sorts through the details, it turns out that provided the lowest mode dominates the sink strength, the latter is *independent* of the eigenvalue provided only that the eigenvalue is small (i.e. $\xi_0 R_b \ll 1$ in our case). Thus, if the sink strength (to lowest order) is determined in any model, it must agree with the lowest eigenvalue predicted by the same model.

The remaining physical checks on the above analysis relate to the flux to the central void and to the value of the concentration at the cell boundary. These are found to be exactly the same irrespective of cell size. This must be so, of course, if the array is periodic.

With this acquired perspective on the Goldberger-Seitz method, we now wish to back-track a little and re-examine the isolated void problem afresh. We have two purposes in mind. One is the matter of smearing out the other sinks in the cell, as done by Bullough & Perrin (1971). This has still to be resolved. The other is that we shall later need to know how to deal with voids when we discuss the dislocation sink strength in §4.

In the Wigner-Seitz approximation, the concentration, c, within the cell of radius R, is to satisfy

$$\frac{D}{r^2}\frac{d}{dr}\left(r^2\frac{dc}{dr}\right) + K = 0, \quad r_c < r < R. \tag{89}$$

This is trivial to solve exactly

$$c(r) = \frac{KR^3}{3Dr_c}\left(1 - \frac{r_c}{r}\right) - \frac{K}{6D}(r^2 - r_c^2). \tag{90}$$

The concentration at the cell boundary is therefore

$$c(R) \approx KR^3/3D r_c, \tag{91}$$

provided $r_c \ll R$. Thus $c(r)$ is, in this approximation, also a solution of

$$D\nabla^2 c + K = D4\pi r_c \delta(r) c(R) \tag{92}$$

where the range of r is unrestricted (boundary conditions being imposed later). But within the cell, $c(r)$ is virtually constant except near $r = r_c$. Thus, we suspect, it should not matter whether we use $c(R)$ or the *local* value $c(r)$ in the right-hand side of equation (92). It ought to lead ultimately only to errors of order r_c/R at most.

In the context, again, of the multi-void cell, one can now repeat the void sink strength analysis based upon the above conjecture. That is, one solves *not* equation (80), but

$$D\nabla^2 c(r) + K = [4\pi r_c \sum_i \delta(r - r_i)] D c(r). \tag{93}$$

The conjecture is that to lowest order in r_c/R it should make no difference. Indeed, if one follows all the steps given before†, it is possible to show that, to this order, it does not.

Suppose, finally, we replaced the factor in square brackets in equation (93) by its volume average:

$$[4\pi r_c \sum_i \delta(r - r_i)]_{\mathrm{av}} = 4\pi r_c C_c (n_c - 1)/n_c. \tag{94}$$

Then the spherically symmetric solution of equation (93) would be exactly the same as the steady state solution of equation (42), but now with $\lambda_0^2 = 4\pi r_c C_c (n_c - 1)/n_c$. We already know this from equation (61) *et seq*! In particular, the lowest eigenvalue for the large cell, but with the spatially 'smeared-out' voids (via equation (94)), is

$$\lambda_0^2 = 4\pi r_c C_c \frac{n_c - 1}{n_c} + \frac{3r_c}{R_0^3} \tag{95}$$

by virtue of equation (64). Whence, upon substituting for R_0^3, we obtain the by now familiar result for the eigenvalue, which is the same thing as the sink strength (as we have proved above), to the order of r_c/R of current interest.

This closes the argument for substantiating the Bullough–Perrin averaging procedure for other sinks, as far as we are able to prove it. We have shown that it is exact when the other sinks are voids themselves, and when only the lowest-order void sink strength is considered. The agreement in the higher-order correction with the effective medium result suggests that it may have wider applicability, but the proof eludes us. The extension to other sink types such as dislocations can only be answered by asking any detractors a question. Namely, if it is applicable to one type of sink, why not also to another? Faced with the contingency of having to incorporate these other sinks somehow, of which by now, it is hoped, the reader is convinced, there seems currently no logical alternative if lattice models are to be used at all in the void sink strength problem.

4. The sink strength of dislocations

Any discussion of dislocation sink strengths brings to prominence one of the central problems in the whole field. Namely, how are internal stress fields to be handled properly? In neither periodic arrays nor random configurations is the answer known completely. Only the hybrid

† The central void is considered as before. The approximate scheme of equation (93) is intended only for the 26 other voids.

model defined in §2(*c*) has been analysed exactly (Heald & Speight 1975). This model may partly evade one issue by definition. For, by invoking an infinite sink strength external to the domain investigated at the microscopic level, the influence of external dislocations will, to some extent, be rendered impotent. In the cases to be discussed, the matter is simply avoided. The ruse used is the introduction of a local capture radius concept extracted from an analysis of an isolated dislocation in an otherwise sink-free body. Quite clearly, this is a further abstraction which ought to be avoided if at all possible. It is unfortunate that, it sometimes appears impossible to make progress without it. This is the only excuse we will offer for using it where we do, though we can in one case justify it.

The organization of this section parallels the preceding one. Thus part (*a*) is concerned with random sink arrays, and part (*b*) with dislocation-void lattices, both when the dislocation–point defect size effect interaction alone is considered. Consequences of the stress-induced interaction are discussed briefly in part (*c*).

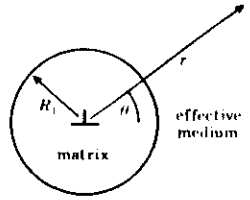

Figure 2. The geometry for a dislocation, plus its matrix environment, in the effective medium.

(*a*) *Random arrays*

To compute the dislocation sink strength, we need the ensemble-average of the flux to any one dislocation. As in the void problem, the flux is not computed configuration by configuration and then averaged. We use, instead, the concept of an effective medium again. One dislocation, plus its surrounding sink-free region, is embedded in the medium itself. As we shall see, the crucial question evolves into deciding how large this sink-free region actually is. For now we will leave the matter open.

The size effect interaction of a point defect a radial distance r from the axis of an infinitely long, straight, edge dislocation is expressed by the energy per unit length, E, where (Cottrell & Bilby 1949)

$$E = (Gb/\pi) v c (\sin\theta/r). \tag{96}$$

Here θ is the angle between the position $\boldsymbol{r}$ of the point defect and the Burgers vector, $\boldsymbol{b}$, v is the volume of the spherical inclusion representing the defect, ϵ the relaxation volume strain associated with it, and G is the shear modulus. Thus, when the effective medium method is adapted to the dislocation problem we are confronted by the following equation for the concentration, c

$$\nabla^2 c + (1/k_{\mathrm{B}}T)\,\mathrm{grad}\, c \cdot \mathrm{grad}\, E - k^2\theta(r - R_1)c + K/D = 0. \tag{97}$$

The θ-function used here is defined to be zero when its argument is negative and unity otherwise. R_1 represents the radial distance to the matrix-medium boundary, as shown in figure 2. Note also, that because the angular average of E is zero, only the interaction with the central dislocation appears in this model.

Since thermal emission is being ignored, equation (97) must be solved subject to the conditions $c(r_0) = 0$, where r_0 is the dislocation core radius, and $c(\infty)$ be bounded. We have been unsuccessful in a search for even an approximate solution unless $R_1 = r_0$. When this *is* the case, we proceed as follows. Let (Ham 1959)

$$c(r) = c_\infty + \phi(r)\, e^{-K/2k_0 T}, \qquad (98)$$

where $c_\infty = K/Dk^2$ as before. Then ϕ must satisfy

$$\frac{1}{r}\frac{\partial}{\partial r}\left(r\frac{\partial\phi}{\partial r}\right) + \frac{1}{r^2}\frac{\partial^2\phi}{\partial\phi^2} - \left(\frac{L^2}{4r^4} + k^2\right)\phi = 0, \qquad (99)$$

in which

$$L = GbVc/\pi k_0 T, \qquad (100)$$

subject to the conditions

$$\phi \to 0 \quad \text{as} \quad r \to \infty$$

and

$$\phi(r_0) = -c_\infty e^{(L/2r_0)\sin\theta}. \qquad (101)$$

To curtail the analysis as much as possible we shall now appeal to the solutions of closely related problems (Ham 1958, Heald & Speight 1975). These show that the greatest contribution to the current comes from the cylindrically symmetric part of the solution to equations such as (99) *et seq*†. We denote this by $\bar{\phi}$. Thus, $\bar{\phi}$ must satisfy

$$\frac{1}{r}\frac{\mathrm{d}}{\mathrm{d}r}\left(r\frac{\mathrm{d}\bar{\phi}}{\mathrm{d}r}\right) - \left(\frac{L^2}{4r^4} + k^2\right)\bar{\phi} = 0, \qquad (102)$$

with

$$\bar{\phi}(\infty) = 0$$

and

$$\bar{\phi}(r_0) = -c_\infty I_0(L/2r_0). \qquad (103)$$

Here I_0 is the Bessel function of order zero and imaginary argument: the last result follows from use of the generating function (Morse & Feshbach 1953).

We can construct an approximate solution of equation (102) by noting that, for $r < (L/2k)^{\frac{1}{2}}$, the dislocation stress field effects are more important than losses to sinks in the medium, whereas for values of r greater than $(L/2k)^{\frac{1}{2}}$ exactly the converse obtains (Brailsford & Bullough 1976). The *approximate* solution‡ is therefore (Brailsford & Bullough 1976)

$$\bar{\phi} \approx AK_0(kr), \quad r > (L/2k)^{\frac{1}{2}}, \qquad (104)$$

and

$$\bar{\phi} \approx BI_0(L/2r) + CK_0(L/2r), \quad r < (L/2k)^{\frac{1}{2}}, \qquad (105)$$

where K_0 is the zero-order Bessel function of the second kind and imaginary argument. We then make $\bar{\phi}$ and its derivative continuous at $r = (L/2k)^{\frac{1}{2}}$, and also impose the second of equations (103) to find the constants A, B and C. Only A is needed here, so this alone will be given

$$A = \frac{-c_\infty I_0 L/2r_0}{2\beta K_0(\beta)\,[I_0(L/2r_0)\,K_1(\beta) + K_0(L/2r_0)\,I_1(\beta)] - K_0(L/2r_0)}, \qquad (106)$$

$$\approx \frac{-c_\infty}{2\beta K_0(\beta)\,K_1(\beta)}, \qquad (107)$$

the last step following because (Heald & Speight 1975) $L/2r_0 \gg 1$. The parameter β is given by $\beta = (kL/2)^{\frac{1}{2}}$. (The Wronksian relation (Morse & Feshbach 1953) has been used to obtain equation (106)).

† The precise condition here is that $(kL/2)^{\frac{1}{2}}$ be small compared with unity.

‡ Additional mathematical details can be extracted from Brailsford & Bullough (1976).

From equations (98) and (104) we may write the spherically symmetric part of the concentration at large r as

$$c(r) \approx c_\infty[1 + (A/c_\infty)\, I_0(L/2r)\, K_0(kr)]; \quad r > (L/2k)^{\frac{1}{2}}. \qquad (108)$$

Evidently, this rapidly tends to c_∞ as $r \to \infty$. Using it, we compute the surface integral of the flux crossing the surface $r = (L/2k)^{\frac{1}{2}}$. Denoting this by J_d, we have

$$J_d = -2\pi DA, \qquad (109)$$

per unit length of dislocation. And since our mathematical approximations correspond to the neglect of other than flow to the dislocation, when $r < (L/2k)^{\frac{1}{2}}$, this must also be the flow to the latter. Moreover, again for a large volume, the volume average of c is just c_∞. Thus we can now evaluate equation (25) to find the dislocation sink strength, k_d^2. We have

$$k_d^2 = Z^{\mathrm{e.m.}}\rho_d \approx -(2\pi A/c_\infty)\rho_d, \qquad (110)$$

where ρ_d is the dislocation density and equation (110) serves to define the bias factor $Z^{\mathrm{e.m.}}$ (e.m. implying 'effective-medium'). The latter can now be found from equation (107). It is given by

$$Z^{\mathrm{e.m.}} \approx \pi/K_0(\beta) \qquad (111)$$

for $\beta \ll 1$, as is usually the case. This result has been given by us earlier (Brailsford & Bullough 1976), although point defect generation was not there included. Evidently this omission makes no difference, if the effective medium is considered to extend inwards all the way to the dislocation core†.

Equation (111) subsumes succintly the combined effects of the dislocation–point defect interaction and the influence of other sinks. If there are only dislocations and voids present, then $k^2 = k_c^2 + k_d^2$. Thus β becomes

$$\beta = (\tfrac{1}{2}kL)^{\frac{1}{2}} = [\tfrac{1}{2}L(k_c^2 + Z^{\mathrm{e.m.}}\rho_d)^{\frac{1}{2}}]^{\frac{1}{2}}. \qquad (112)$$

Equation (111) is in reality, therefore, a transcendental relation from which $Z^{\mathrm{e.m.}}$ must still be determined. We shall postpone that determination. For now we wish only to note that $Z^{\mathrm{e.m.}}$ depends upon L, the interaction strength. This, being different for interstitials and vacancies, will ultimately require the addition of the subscripts i or v to $Z^{\mathrm{e.m.}}$.

We think all would agree that even though we have pruned the derivation of $Z^{\mathrm{e.m.}}$ down to its barest essentials, it remains complicated nevertheless. The question arises whether a simpler physical model could duplicate the essential result. The answer is that there is indeed one such; it was presented by us several years ago‡. The central idea is to mimic the internal stress effect by considering diffusion in a stress-free environment, but with the final jump of the defect, as it enters the dislocation core, being enhanced appropriately to its character. The earliest application (Brailsford & Bullough 1972*a*) was to the $Z^{\mathrm{e.m.}}$ values for isolated dislocation loops, values for straight dislocation lines being inferred by extrapolation. Since then, the straight dislocation problem has been analysed directly by this method (Brailsford *et al.* 1976), with other sinks incorporated as well. The result obtained was

$$(Z^{\mathrm{e.m.}})_{\mathrm{model}} \approx 2\pi\eta/[1 + \eta K_0(kr_0)] \qquad (113)$$

† Brailsford & Bullough (1976) introduced the nomenclature of a 'pseudo-effective' medium. It implies a physical distinction when all that is really involved is a mathematical approximation. Henceforth we shall discard this name.

‡ The argument presented by Nichols (1978*b*) for discarding it is a *non sequitur*.

for $kr_0 \ll 1$. Here η is a factor describing the enhancement of the final jump of the defect upon entering the dislocation core. Inasmuch as $K_0(kr_0)$ is large, equation (113) is virtually independent of this quantity. Such gross behaviour is consistent (in essence) with equation (111), because the dependence of K_0 upon its argument is logarithmic. Indeed, if we consider only this functional dependence, we see that whereas $Z^{\text{c.m.}} \sim 2\pi/\ln(2/kL)$, $(Z^{\text{c.m.}})_{\text{model}} \sim 2\pi/\ln(1/kr_0)$. At the same time, we have exposed one deficiency of the approach. Namely that the absolute value of the mode Z will be too small, because $L/2r_0$ exceeds unity. Consequently, if the model is to be used, it appears safest to use it for determining the *ratio* of bias factors of interstitials to vacancies rather than absolute values. This is the recourse explored in more detail in Brailsford *et al.* (1976) and Brailsford & Bullough (1976). For such ratios, the model is shown to be adequate.

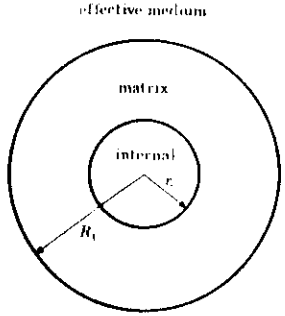

FIGURE 3. The geometry envisaged for the capture radius model.

We now turn to the vexing question of the extent of the matrix region that should be considered to surround each dislocation. In the void problem it was possible to demonstrate directly that such a region was of negligible significance. Here we have simply assumed that this is the case and proceeded from there. Further, we cannot establish the point in like fashion, because we have not yet discovered a method of solving† equation (97) for arbitrary R_1. Some acceptable simplification seems warranted.

The alternative approach we shall adopt is the capture radius concept introduced by Ham (1959). His analysis of the flow of defects to an isolated dislocation illustrated that the effect of the stress field on the defect could be simulated by *stress-free* diffusion to an ideal concentric cylindrical sink of radius here denoted by r_s. Ham's result for r_s is

$$r_s = (L/4)e^{\gamma}, \tag{114}$$

where $\gamma = 0.5772$ is Euler's constant. We shall use this idea below, but not in the precise form Ham advocates. With point defect generation taking place, one has defects being formed *within* the sink if the notion is adopted directly. We find it simpler, instead, to envisage the defect diffusivity within the capture radius as being fictitiously large at some 'internal' value D_1. Obviously, this achieves the same physical end. The zero concentration boundary condition may then be applied at the core radius, r_0, exactly as before.

† Numerical methods always exist, of course, but these seem to us a trifle Draconian for resolving such a qualitative point.

Thus, as a simulation of the solution of equation (97), we consider the system illustrated schematically in figure 3. In the internal region,

$$\frac{D_1}{r}\frac{\mathrm{d}}{\mathrm{d}r}\left(r\frac{\mathrm{d}c}{\mathrm{d}r}\right) + K = 0, \tag{115}$$

and elsewhere,

$$\frac{D}{r}\frac{\mathrm{d}}{\mathrm{d}r}\left(r\frac{\mathrm{d}c}{\mathrm{d}r}\right) - Dk^2\theta(r-R_1)c + K = 0. \tag{116}$$

The solution in the three regions therefore has the form

$$c = -\frac{K}{4D_1}(r^2 - r_0^2) - B\ln\frac{r}{r_0}, \quad r < r_0, \tag{117}$$

$$c = -\frac{K}{4D}(r^2 - r_0^2) - \frac{BD_1}{D}\ln\frac{r}{r_0}, \quad r_0 < r < R_1, \tag{118}$$

and

$$c = c_\infty - \left[\frac{K}{4D}(R_1^2 - r_0^2) + \frac{BD_1}{D}\ln\frac{R_1}{r_0} + c_\infty\right]\frac{K_0(kr)}{K_0(kR_1)}, \quad r > R_1, \tag{119}$$

once D/D_1 has been assumed negligible. To curtail the equations, all boundary conditions have been satisfied in the above except that of the continuity of flux at $r = R_1$. This determines the constant B:

$$\frac{BD_1}{D} = -\left\{\frac{\zeta[c_\infty + (K/4D)(R_1^2 - r_0^2)] + KR_1^2/2D}{1 + \zeta\ln(R_1/r_0)}\right\}, \tag{120}$$

where

$$\zeta = kR_1K_1(kR_1)/K_0(kR_1). \tag{121}$$

The next step follows the established routine. We compute the flux at r_0 and hence determine k_0^2 via equation (25), whence

$$k_0^2 = \frac{-2\pi\rho_0 D_1}{Dc_\infty}\left[B + \frac{Kr_0^2}{2D_1}\right]. \tag{122}$$

Now note that B in equation (120) contains c_∞ as a parameter. By inspection of equation (116) this is seen to be $c_\infty = K/Dk^2$, and therefore also dependent upon k_0^2. We shall take it that voids are the only other sinks present, for illustration; thus $k^2 = k_0^2 + k_c^2$. Consequently, equation (122) can be rearranged as follows, after some algebra

$$\frac{k_0^2}{\rho_0} = Z^{\text{e.m.c.}} = \frac{2\pi\{\zeta + \frac{1}{2}k_c^2[R_1^2 + \frac{1}{2}(R_1^2 - r_0^2)\zeta]\}}{\{1 - R_1^2/R^2 + \zeta[\ln(R_1/r_0) - (R_1^2 - r_0^2)/2R^2]\}}, \tag{123}$$

where the new length, R, appearing in the above is defined by $R = (\pi\rho_0)^{-\frac{1}{2}}$. Terms of order r_0^2/r_s^2 have been dropped. The letters attached to Z indicate that it is obtained by the effective medium approach, with the use of the capture radius concept.

Since ζ depends upon $Z^{\text{e.m.c.}}$, equation (123) is also a transcendental equation for this quantity. It can be solved for any R_1, but before doing so, it is more useful to have another meaningful physical scale in which to express it.

So as not to digress too far from the main argument, the interested reader is here referred to Appendix B for details of the next step. The rationale for what is done there is based upon the observation that the parameter R is approximately one half the mean distance one must travel from the dislocation of interest before encountering another one. (Recall that they are all presumed to be parallel in this 'random' arrangement.) In the intervening space between

dislocations there are voids. Therefore it makes no sense to allow the radius, R_1, of the sink-free region to float arbitrarily. Purely on geometrical grounds it must be related to the chance of an encounter with a void as one moves outward. This is the basis of the model developed in Appendix B, where we show that a more pertinent variable is the void concentration. Specifically, we relate R_1 to C_c as follows

$$R_1 = \frac{1}{2}\left[(\tfrac{4}{3}\pi)^{\frac{1}{2}}\frac{1}{\Gamma(\frac{3}{2})}\right]^{\frac{1}{3}} C_c^{-\frac{1}{3}}, \tag{124}$$

where $\Gamma(z)$ is the gamma-function (Jahnke *et al.* 1960). In this way we can transform the initial question of how large is R_1 compared with R into the more meaningful one of the variation of $Z^{\text{e.m.c.}}$ with an appropriate measure of sink number density ratios†.

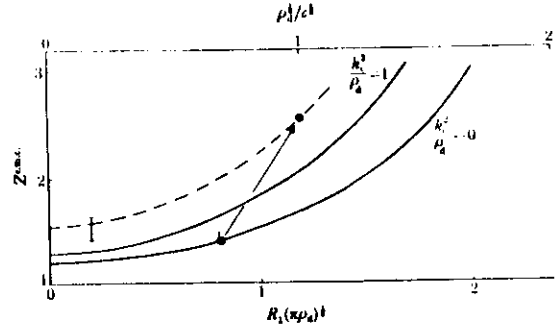

FIGURE 4. The bias factor for an edge dislocation, when obtained from the effective medium method, as a function of the extent of the matrix region. The bar indicates the spread derived from the lattice model; full line for $r_w/R = 0.01$, broken line for $r_w/R = 0.02154$.

With these mutual prescriptions, the variation of $Z^{\text{e.m.c.}}$ obtained from a numerical solution of equation (123) is shown in figure 4 for two different values of k_c^2/ρ_d, the full curves for $r_w/R = 0.01$, as an example. The variation in $Z^{\text{e.m.c.}}$ is modest as long as R_1 is about one half the mean dislocation spacing or less, irrespective of whether one includes point defect losses to voids or not. For reference, the marker in the figure also gives the spread (of different origin) that is later derived for lattice models. The two are thus seen to be comparable. The upper abscissa exhibits the variation of $Z^{\text{e.m.c.}}$ as it is reflected in the geometrical constraint of the voids being present. Here we note simply that, if $\rho_d \approx 10^{14}$ m^{-2} and $C_c \approx 10^{21}$ m^{-3} then $\rho_d^{\frac{1}{2}}/C_c^{\frac{1}{3}} \approx 1$.

What we personally conclude from all this is that it is best to forget the entire matter and regard the Z as empirical parameters to be obtained from the analysis of experiment. The notion of parallel, infinitely long, and straight dislocations is so far removed from the complex networks actually observed that all the analysis of this section so far serves only to rationalize the notion that effective Z exist. Yet others differ, we realize. For their benefit, therefore, we add the following: extending the effective medium to the core boundary will not be significantly in error if in reality R_1 is less than about $0.5R$. If it is greater than this, all manner of

† Note that $kR_1 = (R_1/\pi^{\frac{1}{2}}R)[Z^{\text{e.m.c.}} + (k_c^2/\rho_d)]^{\frac{1}{2}}$. Thus both sink density ratios *and* sink strength ratios appear.

complications may arise. We have illustrated one such in figure 4. Presume we start from a condition where $\rho_d = 10^{13}$ m^{-2} and $C_c = 10^{20}$ m^{-3}, and, as the irradiation proceeds, reach a point where both of these increase by an order of magnitude. (This was suggested by inspection of some experimental observations (Hudson *et al.* 1971).) We thus repeat the determination of $Z^{\text{e.m.c.}}$ with the new parameter set, which yields the broken line in figure 4. Presuming the void sink strength is initially small, but ends at $k_c^2 = \rho_d$ (because the void radius increases), thus leads to an excursion of Z as indicated by the arrow in the figure. Though this is small when compared with the increase in ρ_d, C_c and k_c^2 themselves, believers in the idealized geometry considered here should take note. We have therefore, at this stage, exposed our own viewpoint, yet also, as rigorously as possible, considered the alternative. With that, we shall let this matter rest for the moment.

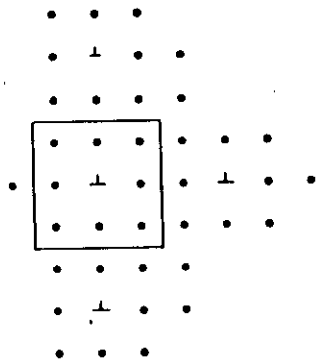

FIGURE 5. An idealized mixed dislocation and void lattice.

(*b*) *A lattice model*

It is important that the reader should not be misled into believing that all the features we have discussed for parallel dislocations in a random array are peculiar to this randomness. For this reason we shall here consider a periodic dislocation arrangement. Since we are interested in void swelling and not strain-ageing, for example, we must also incorporate these sinks. Otherwise our model cannot fill all space. Thus we consider a case where these too are located periodically. This mixed lattice is shown in figure 5. The precise geometry, however, is immaterial. We wish simply to convey a notion and nothing more.

The first problem encountered with any such model is the determination of the stress at each point in space within one cell. The interaction energy, equation (9·5), is long ranged. The result must vary from one lattice structure to another. To our knowledge, no-one has properly considered the matter. Nor shall we. Instead, we immediately resort to the capture radius model.

The second problem is how to handle the voids. If they are small, these can be dealt with by our extension of the Goldberger–Seitz approach, which was given in § 3. We assume this to be the case.

Thus, to compute the flux to the central dislocation we start from the equation for each cell

$$\operatorname{div} \boldsymbol{j} + 4\pi r_c D \sum_l \delta(\boldsymbol{r} - \boldsymbol{r}_l)\, c(r) - K = 0. \tag{125}$$

The void distribution along the direction parallel to the dislocation axis (the z-direction) is taken to be periodic with spacing a_z. We first average over an interval z of this length, symmetrically disposed relative to the voids. In cylindrical coordinates

$$\delta(\boldsymbol{r} - \boldsymbol{r}_l) = \frac{1}{r_l}\,\delta(r - r_l)\,\delta(\theta - \theta_l)\,\delta(z - z_l). \tag{126}$$

Therefore this process leads to

$$a_z^{-1} \int \operatorname{div} \boldsymbol{j}\, \mathrm{d}z - K + (4\pi r_c D/a_z) \sum_l r_l^{-1}\,\delta(r - r_l)\,\delta(\theta - \theta_l)\, c(r, \theta, z_l) = 0. \tag{127}$$

Without writing out all the details, one can appreciate that the flux along the z-direction will give no contribution to the integral. In the remaining components, since they are linear in c, we can simply take the integral as done, if c is replaced by its z-average, $\tilde{c}$. The l-label in the sum is compound, running over all void sites in one plane and over each plane in the z-direction, namely $l = (l_p, l_z)$, where p implies sites in one plane. It is assumed that

$$\sum_{l_z} c(r, \theta, z_{l_z}) \approx n_z\, \tilde{c}(r, \theta), \tag{128}$$

where n_z is the number of void planes per cell. Consequently equation (127) evolves into

$$\operatorname{div} \boldsymbol{j}_p - K + (4\pi r_c n_z D/a_z) \sum_{l_p} r_{l_p}^{-1}\,\delta(r - r_{l_p})\,\delta(\theta - \theta_{l_p})\, \tilde{c}(r, \theta) \approx 0, \tag{129}$$

where the p suffix on $\boldsymbol{j}$ denotes the planar component.

The sole purpose of these manipulations, of course, is to change the problem from one involving point sinks to one involving 'tube' sinks, with the correct strength. We make no other claim for it than that. Now we incorporate the capture radius concept explicitly and use the Wigner–Seitz approximation to get the following problem†:

$$D_1 \left(\frac{1}{r} \frac{\partial}{\partial r} r \frac{\partial}{\partial r} + \frac{1}{r^2} \frac{\partial^2}{\partial \theta^2} \right) c + K = 0, \quad r_0 < r < r_s, \tag{130}$$

and

$$D \left[\frac{1}{r} \frac{\partial}{\partial r} r \frac{\partial}{\partial r} + \frac{1}{r^2} \frac{\partial^2}{\partial \theta^2} - (4\pi r_c n_z/a_z) \sum_l r_l^{-1}\,\delta(r - r_l)\,\delta(\theta - \theta_l) \right] c + K \approx 0, \quad r_s < r < R, \tag{131}$$

where again $R = (\pi\rho_d)^{-\frac{1}{2}}$. The tilde on c, and the suffix on l, have been dropped now that the two-dimensional nature of the problem has been made clear.

Evidently, we are still not out of the woods, because of the angular dependence of the void sink term. But since all boundaries have full circular symmetry, and only the c-component of this symmetry contributes to the flux, it is reasonable to suppose that this sink term may, to a first approximation, be replaced by its angular average‡. Then only radial δ-functions corresponding to the different void shells remain. The final simplification is thus obvious: collapse

† Naturally it is assumed that the voids lie outside the capture radius. Otherwise it is difficult to see how they could ever form in this model.

‡ A difficult but more rigorous procedure would be to expand the sink term and concentration in trigonometric series and solve the coupled set of partial differential equations which ensue.

all shells into a single unit and investigate the consequences. This, in fact, is what we shall do first.

The above motivations have brought us then to the model problem actually solved:

$$\frac{D_1}{r} \frac{\mathrm{d}}{\mathrm{d}r} \left(r \frac{\mathrm{d}c}{\mathrm{d}r} \right) + K = 0, \quad r_0 < r < r_s, \tag{132}$$

and

$$D \left[\frac{1}{r} \frac{\mathrm{d}}{\mathrm{d}r} \left(r \frac{\mathrm{d}c}{\mathrm{d}r} \right) - \frac{2r_c n_c}{a_z r_v}\,\delta(r - r_v)\, c \right] + K = 0, \quad r_s < r < R, \tag{133}$$

where n_c is the total number of voids within one cell and r_v is the single shell radius. We have exposed the origin of this model at length because we believe there is a general lack of awareness of what lattice models actually demand. Admittedly our final problem is itself greatly simplified. But at least it contains all the essential physics of the system, something that the neglect of voids entirely certainly cannot claim.

The solution of equations (132) and (133) is straightforward but tedious. The two external boundary conditions are $c(r_0) = 0$ and $(\mathrm{d}c/\mathrm{d}r)_R = 0$. Interior boundaries are at r_s and r_v. Across both, c must be continuous, while the flux is to be continuous across the first but is to have a jump discontinuity across the second, analogously to equation (85) (but here for two-dimensional analysis). The following describe the intermediate forms when $D_1/D \gg 1$

$$c = -\frac{K}{4D_1}(r^2 - r_0^2) - B \ln \frac{r}{r_0}, \quad r_0 < r < r_s, \tag{134}$$

$$c = -\frac{K}{4D}(r^2 - r_s^2) - \frac{BD_1}{D} \ln \frac{r}{r_s}, \quad r_s < r < r_v, \tag{135}$$

$$c = \frac{K}{2D} \left[R^2 \ln \frac{r}{r_v} + \tfrac{1}{2}(r_v^2 - r^2) \right] - \frac{BD_1}{D} \ln \frac{r_v}{r_s}, \quad r_v < r < R. \tag{136}$$

Here B is a constant of integration that is determined from the condition

$$r_v \left[\left(\frac{\mathrm{d}c}{\mathrm{d}r} \right)_{r_v + 0} + \left(\frac{\mathrm{d}c}{\mathrm{d}r} \right)_{r_v - 0} \right] - \frac{2r_c n_c}{a_z} c(r_v) = 0. \tag{137}$$

Therefore,

$$B = -\frac{K}{2D_1} \left[\frac{R^2 + (n_c r_c/a_z)(r_v^2 - r_0^2)}{1 + (2n_c r_c/a_z) \ln (r_v/r_0)} \right]. \tag{138}$$

From this point on the calculation is routine. One calculates the flux to the dislocation and evaluates the volume integral of the concentration. The sink strength, $k_0^2 = Z^{1,v} \rho_d$, so determined is eventually found to be obtained from

$$Z^{1,v} \approx \frac{2\pi(1 + n_c r_c r_v^2/a_z R^2)}{\ln (R/r_0) - \frac{3}{4} - (n_c r_c/a_z R^2)\left[2(\frac{3}{4}R^2 - R^2 \ln (R/r_v) - r_v^2) \ln (r_v/r_0) + \frac{1}{2}r_v^2/R^2 \right]}, \tag{139}$$

where $R^2 = (\pi\rho_d)^{-1}$ as before. In obtaining the above, terms of order r_0^2/r_v^2 have been dropped to render the result to as simple a form as possible.

In the absence of voids (i.e. $n_c = 0$) equation (139) reduces to a standard result (Wiedersich 1970). Voidage effects are contained in the parameter $n_c r_c/a_z R^2$, which is the same thing as $\frac{1}{4}k_c^2$, since the voids are small. The bias $Z^{1,v}$ is plotted as a function of k_c^2/ρ_d in figure 6 for two different values of r_v. Evidently the change in $Z^{1,v}$ with k_c^2/ρ_d is a modest, essentially linear, one in both cases.

The bias $Z^{1,v}$ arises from lumping all voids in one lattice cell onto a single shell. A possible

alternative approximation scheme is obviously to smear them out over the whole cell. This would be the counterpart of the Bullough–Perrin procedure in the void sink strength problem, where, the dislocations were spatially averaged. The result is not obvious, because sink strengths depend upon the ratio of two field quantities. There is no recourse but to start anew.

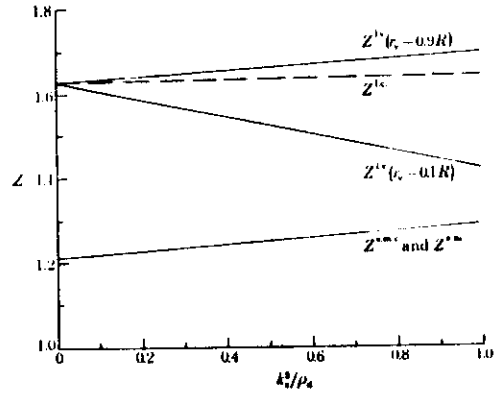

FIGURE 6. The variation of various dislocation bias factors with the ratio of void sink strength to dislocation density for $R = 100r_a$.

Thus we revert to equation (125) and simply take the volume average of the factor multiplying $c(r)$. The result is the new equation

$$\operatorname{div} \boldsymbol{j} + Dk_0^2 c(r) - K = 0, \tag{140}$$

where k_0^2 is understood to be the lowest-order void sink strength†. This we solve with the two-diffusivity model as before, with the same boundary conditions as have been given previously. The pertinent results are

$$c(r) = -\frac{K}{4D_1}(r^2 - r_a^2) - B \ln \frac{r}{r_a}, \quad r_a < r < r_c, \tag{141}$$

and

$$c(r) = \frac{K}{Dk_c^2} + A\left\{I_0(k_c r) + \frac{I_1(k_c R)}{K_1(k_c R)} K_0(k_c r)\right\}, \quad r_a < r < R, \tag{142}$$

where A and B are constants. These are determined from the continuity of flux and concentration at $r = r_a$. Such conditions give

$$\frac{BD_1}{D} = -\frac{Kr_a}{Dk_c^2 \nu}(1 + \tfrac{1}{2}k_c r_a \nu), \tag{143}$$

where

$$\nu = \frac{I_0(k_c r_a) K_1(k_c R) + I_1(k_c R) K_0(k_c r_a)}{I_1(k_c R) K_1(k_c r_a) - I_1(k_c r_a) K_1(k_c R)}, \tag{144}$$

and

$$A = -\frac{K}{Dk_c^2} \frac{K_1(k_c R)}{I_0(k_c r_a) K_1(k_c R) + I_1(k_c R) K_0(k_c r_a)}. \tag{145}$$

The limit $D_1/D \gg 1$ has been invoked.

† Strictly, it would make more sense to average between r_a and R, but, since r_a/R is taken small compared with unity, the distinction is ignored.

From these we compute the dislocation sink strength $k_d^2 = Z^{l.c.}\rho_d$, where the letter c implies continuum voids. Again neglecting powers of r_a^2, we now find

$$Z^{l.c.} = \frac{2\pi k_c r_a (1 + \frac{1}{2}k_c r_a \nu)}{\nu[1 - r_a^2/R^2 + 2r_a \xi / k_c R^2]}, \tag{146}$$

where

$$\xi = \frac{I_1(k_c r_a) K_1(k_c R) - I_1(k_c R) K_1(k_c r_a)}{I_0(k_c r_a) K_1(k_c R) + I_1(k_c R) K_0(k_c r_a)}. \tag{147}$$

The bias $Z^{l.c.}$ is also shown in figure 6.

It is apparent, therefore, that no matter how one elects to disperse the voids within the cell, the dislocation sink strength is not significantly different. The largest difference, in fact, resides in the Z-values for a regular and random array. Figure 6 illustrates this. $Z^{e.m.}$ is the sink strength obtained for the latter, by using equation (111), with L re-expressed in terms of the capture radius via equation (114). In this the internal stress problem was handled explicitly. $Z^{e.m.c.}$ was obtained by using the capture radius from the outset, equation (123). The result is for $R_1 = r_a$ in figure 6. These two, $Z^{e.m.}$ and $Z^{e.m.c.}$, cannot be distinguished visually. Thus we may conclude that the difference that exists between $Z^{e.m.}$ and $Z^{l.c.}$, for example, resides completely in the different dislocation distributions to which they relate. This is not surprising, for two-dimensional isolated sinks have no bounded steady state solutions around them. In the end this only brings us back to our earlier point. Variations dependent upon geometry have now been shown to exist, whereas the geometry itself is a highly idealized abstraction. Resort to experiment seems the only recourse for determining the dislocation bias parameters in each real case.

(c) *Sink strengths with the induced interaction*

The induced interaction between a point defect and an edge dislocation has been found to have important consequences in theories of irradiation creep (Heald & Speight 1974, 1975; Wolfer & Ashkin 1975; Bullough & Hayns 1975; Mansur 1979). It arises when a point defect is conceptualized as a deformable elastic inclusion that distorts in response to the combined effect of an external stress and the stress due to a dislocation. The end result is the appearance of a stress-dependent term, in addition to that given by equation (96), of the form (Bullough & Willis 1975)

$$\delta E = (Gb\sigma v A / E\pi) \sin\theta / r, \tag{148}$$

where E is the Young modulus, σ is the applied stress, and A is a parameter that depends upon the point defect type and upon the orientation of the Burgers vector relative to the external stress axis. The reader is referred to Bullough & Willis (1975) for further details.

The mere mention of relative orientation, of course, immediately raises a problem. For no-one knows how to describe adequately real configurations even in the absence of stress. All we can do is immediately resort to an abstraction. As before, we align the dislocations along one direction, and then suppose the stress to be oriented normal to it.

In the otherwise random array, therefore, the ultimate change is only one of the parameter L to

$$L = L_0(1 + A), \tag{149}$$

where L_0 is identical with the form given in equation (100) and

$$A = \sigma A / cE. \tag{150}$$

This compact form subsumes all details of defect type and dislocation orientation. Further analysis of physical effects will therefore be contained in a modified value for $Z^{v,m.}$ for each such orientation, with the appropriate density of this component. (Of course, to complete the description, thermal emission processes must also be included.) The quantity A is small compared with unity. Accordingly, let us suppose we have just two dislocation types, which we label by $n = 1$ or $n = 2$. Suppose that δz_n denotes the fractional change in $Z_n^{v,m.}$:

$$Z_n^{v,m.} = Z_0^{v,m.}(1 + \delta z_n). \tag{151}$$

Then, upon expanding equation (111) to first order, we eventually arrive at†

$$\delta z_1 \approx \frac{1}{2}\left[\frac{Z_0^{v,m.}}{\pi} A_1 + \frac{(Z_0^{v,m.})^2}{2\pi k^2}(\delta z_1 \rho_d^{(1)} + \delta z_2 \rho_d^{(2)})\right], \tag{152}$$

where $\rho_d^{(1)}$ and $\rho_d^{(2)}$ are the densities of the two groups, and $k^2 = Z_0^{v,m.}(\rho_d^{(1)} + \rho_d^{(2)}) + k_c^2$ (this is the sink strength obtained by ignoring the induced interaction). There is another equation analogous to (152) that can be obtained by simply interchanging the labels 1 and 2. Solving the pair, we find then that

$$\delta z_1 = \frac{Z_0^{v,m.}}{2\pi}\left[\frac{A_1 - (Z_0^{v,m.})^2 \rho_d^{(2)}(A_1 - A_2)/4\pi k^2}{1 - (Z_0^{v,m.})^2(\rho_d^{(1)} + \rho_d^{(2)})/4\pi k^2}\right], \tag{153}$$

with δz_2 given by interchanging subscripts 1 and 2. Much of this complexity can now be removed, since $(Z_0^{v,m.})^2 \ll 4\pi$, and $\rho_d^{(1)} + \rho_d^{(2)}$ must always be less than k^2. The essential result is therefore contained in

$$Z_n^{v,m.} \approx Z_0^{v,m.}[1 + (Z_0^{v,m.}/2\pi)A_n], \tag{154}$$

with an appropriate label added for each point-defect type.

When periodic dislocation arrays, and voids, are envisaged as an alternative mathematical model, the analysis is far more complicated. It remains so even if voids are neglected, and the long range stress effects of other dislocations discarded also. For, of necessity, there must now be at least two types of dislocations per unit cell. Nor does the appeal to the capture radius model ameliorate the situation. To our knowledge, the problem has not been solved.

5. The sink strength of dislocation loops

The assignment of sink strengths for dislocation loops is still being actively investigated. It would therefore be premature to presume that the results given here in any sense constitute the last word. We wish simply to survey the field and highlight the previous methods of attack that we and others have adopted.

Doubtless, the simplest approach imaginable is the last-jump model (Brailsford & Bullough 1972) introduced in §4(*a*). It has the virtue also of being immediately transformable to a three-dimensional problem that is already solved. This step is strictly justifiable for the effective medium approach only. Thus we shall consider again random sink arrays first.

(*a*) *Effective medium method*

A loop and its sink-free local environment is to be placed in the effective medium. Again, the extent of this sink-free region is unknown. We will assume it such that, if the loop has radius r_l, there is a negligible probability that any other sink lies within a spherical volume of

† Consistent with equation (111), it is taken that $(kL_0/2)^{\frac{1}{2}}$ is small compared with unity.

radius r_l containing the loop as one diameter. This implies, for example, that $\frac{4}{3}\pi r_l^3 C_c \ll 1$. The geometry is depicted in figure 7.

With the last-jump model, the problem as outlined may now be transformed to one already encountered with the void. For suppose the flux at the loop surface is $c_l v_n$, where v_n is the transfer velocity on the toroidal surface of the loop and c_l the concentration there. Then since, by hypothesis, there are no sinks within the sphere, its value on the latter must be $\pi r_0 c_l v_n / r_l$.

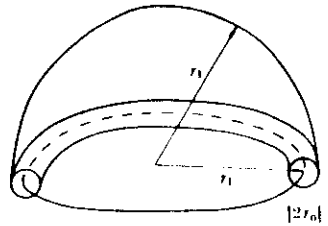

Figure 7. The geometry investigated for a dislocation loop.

This can be re-expressed as an effective transfer velocity v_{eff} across the spherical boundary as follows

$$v_{eff} = \frac{\pi r_0}{r_l}\frac{c_l}{c(r_l)} v_n, \tag{155}$$

where $c(r_l)$ is the concentration on the sphere. Now we refer back to the analysis of §3, specifically equation (38). The result for this model will here follow if we replace r_c by r_l, C_c by the volume density of loops, and v by v_{eff}. The resulting sink strength, k_l^2, is then

$$k_l^2 = [2\rho_d^l(1 + kr_l)]/[1 + (1 + kr_l)w], \tag{156}$$

where $w = D/v_{eff} r_l$. Equation (38) is based upon the presumption that the medium extends inward to the void surface. Hence the above k_l^2 implies that the effective medium starts at the surface $r = r_l$.

The parameter w appearing in equation (156) is independent of loop size if the ratio $c_l/c(r_l)$ is also. Without solving the complete problem, it is impossible to say if this is true or not. The weakness of the following argument resides in our simply assuming it to be true. Should it be so, this model indicates that, with $v_n = \lambda D/b$, where λ is the jump-enhancement factor at the core:

$$k_l^2/\rho_d = Z_l \approx 2\lambda/\{\lambda + [bc(r_l)/\pi r_0 c_l]\} \tag{157}$$

for $kr_l \ll 1$. With the assumptions noted, this is independent of loop radius, a result that initially motivated us (Brailsford & Bullough 1972*a*) to infer that the bias factors for the dislocation network, in general, should be regarded as constants. More recently, one of us (and colleagues) (Bullough *et al.* 1979) has explored the consequences of retaining the kr_l-terms, assuming w is independent of r_l. It is clear from equation (156) that the mathematical limit, as $kr_l \to \infty$, is simply $Z_l \to Z^{v,m.}$, where the latter should be the value obtained earlier for a straight dislocation. Thus the form suggested (Bullough *et al.* 1979) for the loop of radius r_l is

$$Z_l = Z^{v,m.}/[1 + Z^{v,m.}/2(1 + kr_l)] \tag{158}$$

which varies between the limits $2Z^{c.m.}/(2+Z^{c.m.})$ and $Z^{c.m.}$, as kr_1 is increased. Since $Z^{c.m.} \sim 1.2$, as we have seen in §4, this range is roughly from 0.75 to 1.2. The salient aspect of this variation is that it allows one to rationalize the growth of *vacancy* dislocation loops in irradiated materials. Interested readers may consult Bullough *et al.* (1979) for details.

To assess the merit of regarding the concentration ratio as independent of loop radius, one can avoid the approximation entirely if one is interested in the lowest-order result only. As we have pointed out earlier, the specific inclusion of point defect generation is immaterial if the effective medium extends to the sink surface. We can simply prescribe a general c_∞ and compute the total flux. The volume average of the concentration is always c_∞ if we have a large enough sample volume. Moreover, provided $kr_1 \ll 1$ here, we can also neglect other sinks. The simplified problem at hand is then to solve

$$\nabla^2 c = 0, \tag{159}$$

subject to the conditions $c \to c_\infty$, as $r \to \infty$, and

$$\partial c/\partial n = c_1 v_n/D \tag{160}$$

on the toroidal surface. This has an electrostatic analogue (Flynn 1972). For we can take c as the counterpart of the potential and $\partial c/\partial n$ as the magnitude of the electric field at the surface of a metal torus. Thus, we are given that the 'electric field' is $c_1 v_n/D$, where c_1 is the metal potential. But we know that it is also equal to 4π times the 'surface charge', that is, to $C_t(c_\infty - c_1)/\pi r_0 r_1$, where C_t is the capacitance of the torus. From this we find c_1

$$c_1 = \frac{C_t c_\infty}{\pi r_0 r_1 (v_n/D + C_t/\pi r_0 r_1)} \tag{161}$$

and hence we can now calculate the total flux to the torus and, thereby, the sink strength. With

$$C_t = \pi r_1/\ln(8r_1/r_0), \tag{162}$$

and $v_n = D\lambda/b$ as before, we find in this way that

$$Z_1 = 2\,\frac{\pi}{\ln(8r_1/r_0)}\,\frac{\lambda}{\lambda + b/r_0 \ln(8r_1/r_0)}. \tag{163}$$

The major differences between this result and that for the last jump model reside only in a modest change of scale and a very slight dependence upon loop radius. Moreover, equation (163) is restricted to $kr_1 \ll 1$, whereas equation (158) is not. It is reasonable then to adopt the latter as the best approximation for random arrays, pending an exact analysis of the stress-induced drift problem.

(*b*) *Dislocation loop lattices*

The foregoing has served to substantiate partially the notion that dislocation loops will mimic three-dimensional sinks to some extent. The higher-order sink correction appropriate to lattices is therefore likely to be significant. It follows then that cognizance will have to be taken of voids and straight dislocations. As a first approximation, the Bullough–Perrin continuum 'other-sink' procedure is necessary. If and when such is done for the size effect interaction, the induced interaction will need study. A further complication will ensue because then there will have to be at least two loops per unit cell. These requirements being fulfilled, such a calculation should be fairly reliable because the stress field from a loop, as distinct from that from a straight dislocation, is quite short ranged. The stress field from loops external to the cell of interest ought to be negligible.

Some progress towards this goal has been made and further work is under way (Bullough *et al.* 1981*b*). Suffice it to say that these calculations indicate a bias for such loops that increases with increasing loop radius; a feature necessary to explain observations of large vacancy loops in irradiated materials when genuinely neutral sinks such as voids are not present.

6. The sink strength of grain boundaries

The main thrust of the present section will be to establish that grain boundaries are sinks with a unique character, namely, that the higher-order sink strength corrections are, for them, the dominant source of their sink-strength. The zero-order result (Damask & Dienes 1971; Nichols 1978*a*) is most often useless. We consider here samples containing grains of random size, and a grain boundary lattice. In both cases internal sinks such as voids and dislocations are incorporated.

(*a*) *Random grains*

The analysis of grain boundary sink strengths was performed several years ago (Brailsford & Bullough 1972*b*), but only recently have the details been made available (Brailsford & Bullough 1978). The model used is a natural outgrowth of the effective medium approach. One particular grain (assumed spherical) is embedded in a medium characterized by a total sink strength incorporating the combined effects of other sinks *and* grain boundaries themselves. The flow to the external surface of the central sink is computed. The total flow is composed of this contribution and that arising from defect production within the grain itself. To obtain the latter, the interior sinks are continuously distributed in the manner of the Bullough–Perrin procedure. This last topic has already been rationalized for the void and dislocation problems separately.

In the present overall context, where thermal emission is being ignored for simplicity, the problem evolves into determining the concentration satisfying the following, for a grain of radius R_g:

$$\frac{D}{r^2}\frac{\mathrm{d}}{\mathrm{d}r}\left(r^2\frac{\mathrm{d}c}{\mathrm{d}r}\right) - Dk^2 c + K = 0, \quad r > R_g, \tag{164}$$

and

$$\frac{D}{r^2}\frac{\mathrm{d}}{\mathrm{d}r}\left(r^2\frac{\mathrm{d}c}{\mathrm{d}r}\right) - Dk_{s.c.}^2 + K = 0, \quad r < R_g. \tag{165}$$

Here $k_{s.c.}^2$ is the 'single-crystal' sink strength, namely

$$k_{s.c.}^2 = k_d^2 + k_c^2, \tag{166}$$

while

$$k^2 = k_{s.c.}^2 + k_{g.b.}^2, \tag{167}$$

$k_{g.b}^2$ being the grain boundary sink strength. Equations (164) and (165) are to be solved subject to $c(0)$ and $c(\infty)$ being bounded, while $c(R_g) = 0$.

The interior and exterior solutions are, respectively:

$$c = \frac{K}{Dk_{s.c.}^2}\left[1 - \frac{R_g}{r}\,\frac{\sinh k_{s.c.} r}{\sinh k_{s.c.} R_g}\right], \quad r < R_g, \tag{168}$$

and

$$c = \frac{K}{Dk^2}\left[1 - \frac{R_g}{r}\,e^{-k(r-R_g)}\right], \quad r > R_g. \tag{169}$$

The volume average of c is again $c_v = K/Dk^2$, if the sample volume is large. The one tricky point is deciding exactly what flux to apportion to the grain volume $\frac{4}{3}\pi R_g^3$. Each boundary is, in reality, fed by two grains. Thus we see† that, per volume of *one* of them, we should take the arithmetic mean of the fluxes derived from equations (168) and (169). The result for the sink strength, $k^2_{g,b.}(R_g)$, then follows from equation (25):

$$k^2_{g,b.}(R_g) = 2\pi R_g C_g \left[\frac{k^2}{k^2_{s.c.}}(k_{s.c.}R_g \coth k_{s.c.}R_g - 1) + (1 + kR_g)\right], \tag{170}$$

where C_g is the volume concentration of grains of radius R_g.

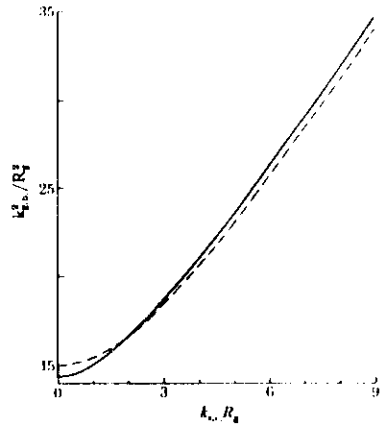

FIGURE 8. The variation of the grain boundary sink strength with the sink strength of internal sinks. The full line is obtained by the effective medium method, the broken line from a grain boundary lattice.

Since $k^2_{g.b.}$ depends upon R_g, for complete generality we would next have to specify the distribution of grain sizes to obtain the formal solution of equation (170). Here we shall ignore this statistical spread and treat $k^2_{g.b.}$ as though it referred to the mean. Then $C_g = 3/4\pi R_g^3$, where now R_g is the mean size, and we drop the R_g-argument of $k_{g.b.}$. In this manner, after some rearrangement, a quadratic equation for $k^2_{g.b.}R_g^2$ is obtained from equation (170) upon substituting for k. Its solution is (Bullough *et al.* 1980)

$$k^2_{g.b.} = \frac{3}{2R_g^2}\left\langle 3 + 4\beta - \frac{6\beta(\beta-1)}{\alpha^2} + \left\{\left[3 + 4\beta - \frac{6\beta(\beta-1)}{\alpha^2}\right]^2 - 4(\beta^2 - \alpha^2)\left[2 - \frac{3(\beta-1)}{\alpha^2}\right]\right\}^{\frac{1}{2}}\right\rangle \Big/ \left[2 - \frac{3(\beta-1)}{\alpha^2}\right]^2, \tag{171}$$

where

$$\beta = \alpha \coth \alpha, \tag{172}$$

and

$$\alpha = k_{s.c.}R_g. \tag{173}$$

† Brailsford & Bullough (1972*b*) and Bullough *et al.* (1980) obtained the same result by slightly different reasoning.

This function varies between

$$\text{when } k_{s.c.}R_g \ll 1, \text{ and} \qquad k^2_{g.b.} = (3/2R_g^2)(5 + 2^{\frac{1}{2}}) = 14.4/R_g^2 \tag{174}$$

$$k^2_{g.b.} = 3k_{s.c.}/R_g \tag{175}$$

when $k_{s.c.}R_g$ is much greater than unity. The detailed dependence is illustrated in figure 8. We shall comment upon it further after analysing the grain boundary lattice.

(*b*) *Grain boundary lattice*

Imagine a lattice with the cell boundaries being the grain boundaries of the structure. Now invoke the Wigner–Seitz approximation. The resulting problem is one of solving the equation

$$\frac{D}{r^2}\frac{\mathrm{d}}{\mathrm{d}r}\left(r^2\frac{\mathrm{d}c}{\mathrm{d}r}\right) - Dk^2_{s.c.}c + K = 0, \tag{176}$$

subject to the conditions that $c(R_g) = 0$ and that $c(0)$ be bounded. The solution within the cell centred on the origin is

$$c = \frac{K}{Dk^2_{s.c.}}\left[1 - \frac{R_g}{r}\frac{\sinh k_{s.c.}r}{\sinh k_{s.c.}R_g}\right]. \tag{177}$$

Using (177), we compute the flux to the grain boundary originating within the cell, and also the volume average of the concentration. From this we obtain the grain boundary sink strength for the lattice model via equation (25)

$$k^2_{g.b.} = \frac{k_{s.c.}R_g \coth k_{s.c.}R_g - 1}{R_g^2[\frac{1}{3} + 1/k^2_{s.c.}R_g^2 - \coth k_{s.c.}R_g/k_{s.c.}R_g]}. \tag{178}$$

This spans the range from $k^2_{g.b.} = 15/R_g^2$ to $3k_{s.c.}/R_g$ as $k_{s.c.}R_g$ increases from zero to large values†. The details are again illustrated in figure 8.

It is evident, first of all, that the two different models presented here give virtually the same sink strength. Secondly, one can see that in most practical situations the zero-order result (i.e. that found in the limit $k_{s.c.}R_g \to 0$) is grossly incorrect. For with typical values of the parameters involved ($k_{s.c.} \approx 2 \times 10^7$ m^{-1} and $R_g \approx 10^{-6}$ m) $k_{s.c.}R_g$ is of the order of 20. The approximation (Brailsford & Bullough 1973)

$$k^2_{g.b.} \approx 3k_{s.c.}/R_g \tag{179}$$

is likely to cover most real situations.

7. Further review of past work

In §§2–6 we have analysed the problems encountered in determining the rate theory sink strengths of four different sink types. Here we wish to give some overall perspective of what has been done. The précis constitutes subsection (*a*). The second aim is to cover those details of previous work that had no natural order within the previous discussion. These are considered in subsection (*b*).

(*a*) *Perspectives*

Two general lines of attack have been formulated, the periodic sink array and the effective medium approaches. In both we have shown that, as a matter of principle, all sink types must be considered. With only one sink, the infinitely long and straight dislocation, have we found the influence of other sinks to be negligible in any real sense.

With periodic arrays, we have seen that the Bullough–Perrin procedure of replacing the discrete 'other sinks' by a continuum is an acceptable simple approximation. Any problem

† A useful power-series expansion, for $k_{s.c.}R_g \ll 1$, is $k^2_gR_g^2 \approx 3k_{s.c.}R_g[1 + 2/k_{s.c.}R_g + 3/(k_{s.c.}R_g)^2]$.

then evolves into the determination of the concentration field within a finite volume. When the sink(s) has stress-fields associated with it, lattice sums ought to be performed to map out the stress within one cell. In no case that we are aware of has this been done.

There is no *a priori* reason why the resulting sink strength so calculated should agree with that for a random array. The end result in the two cases, whether they agree or differ, will ultimately boil down to the question of how sensitive the concentration field is to boundary conditions for the particular sink type of central interest. Straight dislocations provide a case in point.

In the effective medium approach, it is ultimately immaterial whether one specifically includes point defect generation or not, provided, that is, the medium extends all the way inward to the sink boundary. One can equally well exclude defect generation and simply prescribe some arbitrary c_∞ at large distances. This quantity cancels out in the end. The key element here is that the sample volume is large, in the sense specified in §2.

If a stress field is associated with the sink, the evaluation within the effective medium approach evolves into solving an enhanced diffusion problem in the infinite domain, with a continuum-type loss term incorporated. For the straight dislocation, the approximate solution has been given. In other cases it is not available.

The 'last-jump' model (Brailsford & Bullough 1972*a*) offers a semi-quantitative method of estimating what effect internal stresses might have. It is certainly no substitute for solving the problem exactly, but at the least it contains an essence of the physics. Our suspicion is that it is more accurate for estimating the ratio of the strengths of a particular sink for the two point defect types than it is for calculating each quantity separately. It will be of interest to check the conjecture further, should detailed solutions become available for other than the straight dislocation.

For all sinks that are localized in three dimensions, the higher-order sink corrections (for steady state analysis) are important. Nevertheless, we shall here neglect them to make one final point related to the electrostatic analogue discussed in §5. We showed there that one is led via the steps enumerated above, namely (i) extension of the medium to the core, and (ii) the assumption $kr \ll 1$, where r is the largest sink dimension, to the solution of Poisson's equation. Further, if stress effects are subsumed into the last jump, the boundary condition is of the type of equation (160). This we can generalize trivially to incorporate thermal emission, for illustration:

$$\partial c/\partial n = (v_n/D)(c_s - \bar{c}_L), \tag{180}$$

where c_s is the concentration at the L-type sink surface. The remainder of the reasoning after equation (160) is then quite general. By it one obtains the following relation, from equation (25), for the lowest-order sink strength, k^2_{L0}:

$$k^2_{L0} = \frac{1}{Dc_\infty}\left[\frac{N_L}{V_M}\frac{4\pi\mathscr{C}_L(c_\infty - \bar{c}_L)v_n}{(v_n/D + 4\pi C_L/A_L)} + K_L\right], \tag{181}$$

with the appropriate subscripts for parameters pertinent to each point defect, $\mathscr{C}_L$ denoting the capacitance of the sink, and A_L its surface area. One sees from equation (181), therefore, that

$$k^2_{L0} = 4\pi C_L\mathscr{C}_L\frac{v_n/D}{(v_n/D + 4\pi\mathscr{C}_L/A_L)}, \tag{182}$$

and

$$K_L = Dk^2_{L0}\bar{c}_L, \tag{183}$$

where C_L is the sink number density as before.

Equations (182) and (183) subsume some lowest-order forms given earlier, with appropriate interpretation. For the void ($\mathscr{C}_L \to r_c$), the sink strength (182) becomes equal to equation (38) in the limit $kr_c \to 0$, while for two concentric cylinders, one of radius r_c and the other of radius R ($R \gg r_c$), when $\mathscr{C}_L \to \mathscr{L}'(2\ln(R/r_c))^{-1}$, with $\mathscr{L}'$ the dislocation length, the equality is with† equation (123).

The purpose behind this digression, however, is not so much to confirm our previous analysis as it is to enable us to say something about previous sink strength calculations that have used the hybrid model. These involve a boundary condition $c = c_\infty$ at some *finite* outer radius R. We can see now that they will be correct in lowest order (but that only) if the capacitance of the equivalent object formed from the boundary is in fact only slightly different from that where the outer electrode becomes increasingly distant. Clearly, the void is the simplest example. The capacitance of two concentric spheres of inner and outer radii r_c and R is $Rr_c/(R - r_c)$. This is thus the same as $\mathscr{C}_c = r_c$ if and only if terms of order r_c/R are discarded. We see then that the hybrid model should not be trusted for any other than the sink strength to lowest order. It is therefore superfluous to consider adding other sinks to it, because its foundations are shaky even without them! It is, further, important to check that numerical analyses of stress-enhanced diffusion to any sink, made in a finite domain with a fixed concentration at the outer boundary, pay adequate attention to this fact. Various outer radii must be chosen and the limit of large outer radius determined. Only by this limiting process can it be established that the lowest-order sink strength has indeed been obtained.

(*b*) *Other past work*

Many of the investigations not specifically mentioned in the text have, in fact, used the hybrid model. Generally they are open to question for the reason given in §7(*a*). In any particular case of interest, we suggest the reader should see if the previous procedures have been followed or not, and then decide matters for himself.

The one remaining topic we will discuss at any length concerns a very early analysis of void swelling by Bullough *et al.* (1970). The approach developed there has long been superceded by rate theory. Nevertheless it has gained renewed prominence of late because of a fallacious criticism by Nichols (1978*b*). Actually, the total scheme *is* incorrect, but not for the reason given in Nichols (1978*b*). Our intent here is to point out where the error actually resides and thus, we hope, put the matter finally to rest.

The central problem solved by Bullough *et al.* (1970) is that of the concentration of interstitials and vacancies within one Wigner–Seitz cell of the dislocation lattice. The angular dependence of the point defect–dislocation interaction and the presence of voids were ignored. However, in contrast to any other analysis of this paper, intrinsic recombination was included. The two defect equations considered were

$$\frac{D_v}{r}\left(\frac{\mathrm{d}}{\mathrm{d}r}r\right)\frac{\mathrm{d}c_v}{\mathrm{d}r} + K - \alpha c_i c_v = 0, \tag{184}$$

and

$$\frac{D_i}{r}\left(\frac{\mathrm{d}}{\mathrm{d}r}\left(r\frac{\mathrm{d}c_i}{\mathrm{d}r}\right) + \frac{L}{r}\frac{\mathrm{d}c_i}{\mathrm{d}r} - \frac{L}{r^2}c_i\right) + K - \alpha c_i c_v = 0. \tag{185}$$

The elastic size effect interaction with vacancies was neglected.

† The result follows if (i) R_i is set equal to the capture radius r_a, (ii) μ_d is set at $(\pi R^2)^{-1}$, and (iii) $Z^{a,m,c}$ is taken equal to $\pi\delta$.

The above equations were solved numerically subject to ideal boundary conditions at the core (i.e. $c_i = c_v = 0$ at $r = r_0$) and zero flux conditions at the cell radius, $r = R$:

$$\frac{\mathrm{d}c_v}{\mathrm{d}r} = 0, \quad \frac{\mathrm{d}c_i}{\mathrm{d}r} + \frac{Lc_i}{r^2} = 0, \quad \text{at} \quad r = R. \tag{186}$$

It is the contention of Nichols (1978*b*) that, because there must be an equal flux of interstitials and vacancies to the dislocation, $D_i c_i - D_v c_v \equiv 0$ for all values of r within the cylinder. The reason given is that there are no other sinks in the system, and it is enclosed by a reflecting boundary. The implication is that there must be an error in the numerical analysis.

The immediate way to show the fallacy of the first assertion is to take the difference between equations (185) and (184):

$$\frac{\mathrm{d}}{\mathrm{d}r} r \frac{\mathrm{d}}{\mathrm{d}r} (D_i c_i - D_v c_v) + D_i L \frac{\mathrm{d}}{\mathrm{d}r} \left(\frac{c_i}{r}\right) = 0. \tag{187}$$

Clearly $D_i c_i - D_v c_v$ cannot be zero, because this would imply $c_i \propto r$. But c_i must also be non-zero, and therefore the second of equations (186) cannot be satisfied. Thus the assertion is false. What *does* follow from (187) is of some interest. Suppose we integrate it between r_0 and r. We obtain

$$r \frac{\mathrm{d}}{\mathrm{d}r} (D_i c_i - D_v c_v) + D_i L \frac{r}{r} = 0, \tag{188}$$

because the interstitial and vacancy fluxes at the core boundary must be equal†. Now multiply equation (188) by r and integrate from r_0 to R

$$[r^2 (D_i c_i - D_v c_v)]_{r_0}^{R} - 2 \int_{r_0}^{R} r (D_i c_i - D_v c_v) \mathrm{d}r + D_i L \int_{r_0}^{R} c_i \mathrm{d}r = 0. \tag{189}$$

In the first term, only the concentrations at the outer boundary are non-zero. In the second term, the integrals appearing are proportional to the volume averages of the concentration. Introducing these averages explicitly, we have therefore

$$D_v \langle c_v \rangle - D_i \langle c_i \rangle = D_v c_v(R) - D_i c_i(R) - \frac{D_i L}{R^2} \int_{r_0}^{R} c_i \mathrm{d}r. \tag{190}$$

Now we refer to the general rate equations (14) and (15). These represent manipulations of the same two starting equations, but done in a different way so as to introduce sink strengths. Here we have steady state, only one type of sink, and no thermal emission. Therefore, it follows that

$$\left.\begin{aligned} D_v k_{dv}^2 \langle c_v \rangle - K + \alpha \langle c_i \rangle \langle c_v \rangle &= 0, \\ D_i k_{di}^2 \langle c_i \rangle - K + \alpha \langle c_i \rangle \langle c_v \rangle &= 0, \end{aligned}\right\} \tag{191}$$

or

$$\langle c_v \rangle = (D_i k_{di}^2 / D_v k_{dv}^2) \langle c_i \rangle, \tag{192}$$

$$\langle c_i \rangle = (K / D_i k_{di}^2) F(\eta), \tag{193}$$

where

$$F(\eta) = [-1 + (1 + 4\eta)^{\frac{1}{2}}]/2\eta, \tag{194}$$

with

$$\eta = \alpha K / D_i D_v k_{di}^2 k_{dv}^2. \tag{195}$$

† This is the *only* fact that follows from there being no other sinks in the cell and from steady state being achieved.

We insert the expressions for $\langle c_i \rangle$ and $\langle c_v \rangle$ in equation (190), and through the identities $k_d^2 = Z\rho_d$, for each defect, we re-express this relation in terms of the bias parameters:

$$\frac{1}{Z_v} - \frac{1}{Z_i} = \frac{\rho_d}{KF(\eta)} \left[D_v c_v(R) - D_i c_i(R) - \frac{D_i L}{R^2} \int_{r_0}^{R} c_i \mathrm{d}r \right]. \tag{196}$$

Of course, by following this procedure, we have not solved anything. Yet it does serve to highlight a few points. First, it is clear that the difference $Z_i - Z_v$ vanishes as L tends to zero, but only then. In that limit the starting equations and boundary conditions for $D_i c_i$ and $D_v c_v$ are identical†. The sink is then neutral, just as a void is in the models of §3. Secondly, it is possible to perceive why recombination *might* not be too important, for while it reduces the concentrations, it decreases the F factor at the same time.

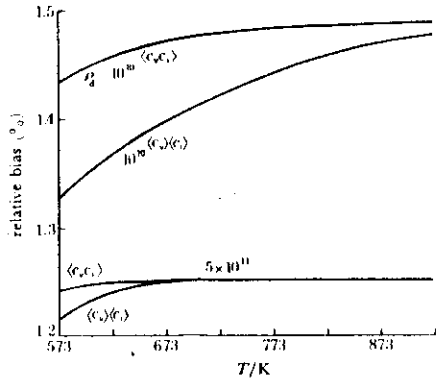

FIGURE 9. The variation of relative bias with temperature for two dislocation densities obtained by using the model and parameter set of Bullough *et al.* (1970). The error involved in neglecting I in equation (10) is also indicated.

We wish now to make some of the above more quantitative by using the results and numerical procedure‡ given by Bullough *et al.* (1970) to yield the required volume averages of the concentrations $\langle c_i \rangle$ and $\langle c_v \rangle$. In terms of these averages the relative bias (196) can be conveniently written

$$\frac{1}{Z_v} - \frac{1}{Z_i} = \frac{\rho_d [D_v \langle c_v \rangle - D_i \langle c_i \rangle]}{K - \alpha \langle c_i \rangle \langle c_v \rangle}. \tag{197}$$

Since we have the spatial variation of the vacancy and interstitial concentration over the cell we can also test the error involved in neglecting the quantity I in equation (10) by evaluating the relative bias

$$\left(\frac{1}{Z_v} - \frac{1}{Z_i}\right)_I = \frac{\rho_d [D_v \langle c_v \rangle - D_i \langle c_i \rangle]}{K - \alpha \langle c_i c_v \rangle}, \tag{198}$$

where the subscript I indicates that the average of the product of the concentrations, rather than the product of the averages, has been used for the recombination loss in the cell.

† It is in this limit only that climb (growth) rates become 'proportional to $D_i c_i - D_v c_v$ (*sic*) as Nichols states. Even then, the 'c_i' and 'c_v' are volume average quantities, i.e. our $\langle c_i \rangle$ and $\langle c_v \rangle$, not local values. All this can be verified from the rate equations. When k_{di}^2 and k_{dv}^2 are unequal, one can only assert that $D_i k_{di}^2 \langle c_i \rangle = D_v k_{dv}^2 \langle c_v \rangle$.

‡ We are most grateful to Dr R. C. Perrin for reprogramming the original numerical technique used by Bullough *et al.* (1970) to solve the simultaneous nonlinear differential equations (184) and (185).

Both these relative biases have been computed as a function of temperature by using the parameter set of Bullough *et al.* (1970). The results are shown in figure 9. The curves labelled $\langle c_v\rangle\langle c_i\rangle$ refer to equation (197) and those labelled $\langle c_i c_v\rangle$ refer to equation (198). We see clearly, as expected, that the error incurred in neglecting I is a maximum for low dislocation density and low temperature. The errors in the relative bias due to neglecting I will be further reduced when the presence of a second sink type is included in the cell since point defect loss at such sinks must reduce the effectiveness of bulk recombination as a loss process.

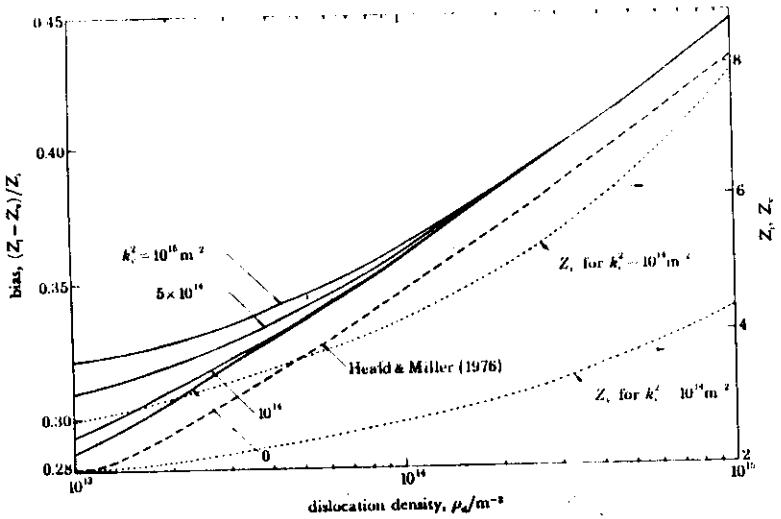

FIGURE 10. The variation of Z_i, Z_v and relative bias, for various internal sink strengths k_c^2, with dislocation density. This is an extension of the work of Heald & Miller (1976) with the use of their parameter set.

Far from it deserving to be discarded, therefore, we see that the Bullough *et al.* (1970) treatment constitutes the most sophisticated currently available for computing the bias factors for straight dislocations in a lattice. Where Bullough *et al.* (1970) err does not reside in the bias factors, but in their subsequent application of this model to the void growth problem. The matter is contained in their equation (1), which gives the growth law in terms of 'average' concentrations $\bar{c}_i$ and $\bar{c}_v$. In fact, they should be *local* concentrations at the void surface. These can be linked to the 'far-field' concentrations $\langle c_i\rangle$ and $\langle c_v\rangle$ by the methods of §3. Thus, if the $c_i(R)$ and $c_v(R)$ calculated by Bullough *et al.* (1970) are to be linked with anything, it should be with these quantities. The net effect of this realization is that the growth rate given by equation (1) of Bullough *et al.* (1970) should be multiplied by a factor $O(b/r_c)$. The absence of this factor accounts for the incorrect growth laws they obtained. It is now recognized that rate theory provides the more reliable method of tackling the void swelling problem.

The Bullough *et al.* (1970) calculation uses a purely radial non-periodic potential and thus the potential must be included explicitly in the zero flow boundary condition equation (186)

on the interstitials. This situation, though probably inevitable when the full angular form of the potential is included, can be avoided in the radial case as was first suggested by Bullough & Newman (1962) by modifying the potential directly to have zero derivative at the cell boundary. Such a single-sink cellular procedure (with bulk recombination neglected) was explored by Heald & Miller (1976) who obtained an analytic expression for the dislocation sink strength. We have used this model to illustrate the dependence of the bias on the presence of the second sink type within the cell (Bullough & Quigley 1981*a*). The results shown in figure 10, have been obtained numerically and by using the physical parameters adopted by Heald & Miller. The small discrepancy between the Heald & Miller results (where $k_i^2 = 0$) and our curve for $k_c^2 = 0$ arises because they defined the dislocation sink strength by using the concentration at the cell boundary rather than the mean concentration over the cell volume. To facilitate comparison with Heald & Miller we define the relative bias in this figure as $(Z_i - Z_v)/Z_i$ rather than $(Z_i - Z_v)/Z_i Z_v$ as in figure 9. The sensitivity of Z_i, Z_v and the relative bias to the presence of the second sink is clearly apparent and serves to confirm the discussion of the analytic results associated with figure 6.

8. Summary

In this paper we have presented a rigorous derivation of rate theory and so defined the problem of determining sink strengths for various point defect sinks. Both periodic sink arrays and random configurations have been treated. It has been shown that the details of the sink strength calculation are different in the two cases.

Only non-saturable sinks have been considered because the field is complicated enough even without them. Saturable sinks, by definition, entail the introduction of an additional degree of freedom to describe their degree of occupancy. This implies that one additional rate equation enters.

We have considered time dependence in the void problem to illustrate the limit of the range of validity of steady state analyses. This mainly influences the higher-order sink corrections, as we have shown.

It has been emphasized that one of the greatest deficiencies of much earlier work has been the entire neglect of sinks other than the one under consideration, apart, that is, from the simplistic introduction of cell boundaries in lattice models. Several new analyses have been presented that focus upon this point. It is hoped that at least one of these will be adopted by other workers in the future. Physically, it is sheer nonsense to disregard the matter entirely without some justification being proffered.

In our judgement, the effective medium approach constitutes the best practical method for solving annealing or radiation damage problems associated with real materials. Doubtless it could be improved upon, academically, but the issue for us has to be of what ultimate utility would such improvements be? It is in this direction, we suggest, that future effort should be directed.

Appendix A

In this section we derive the normalized eigenfunctions and eigenvalues of the equation

$$\frac{1}{r^2}\frac{\mathrm{d}}{\mathrm{d}r}\left(r^2\frac{\mathrm{d}\psi_n}{\mathrm{d}r}\right) - (k_n^2 - \lambda_n^2)\,\psi_n = 0, \tag{A 1}$$

when the boundary conditions on ψ_n are

$$\psi_n(r_c) = 0, \quad (d\psi_n/dr)_R = 0, \tag{A 2}$$

with $R > r_c$.

The solution of (A 1) satisfying the first of (A 2) is

$$\psi_n = A_n \sin[(r-r_c)(\lambda_n^2 - k_0^2)^{\frac{1}{2}}]/r \tag{A 3}$$

if $\lambda_n^2 > k_0^2$, or

$$\psi_n = B_n \sinh[(r-r_c)(k_0^2 - \lambda_n^2)^{\frac{1}{2}}]/r \tag{A 4}$$

if $\lambda_n^2 < k_0^2$. Here A_n and B_n are constants. Now impose the second of equations (A 2). Then either

$$\tan[(R-r_c)(\lambda_n^2 - k_0^2)^{\frac{1}{2}}] = R(\lambda_n^2 - k_0^2)^{\frac{1}{2}}, \tag{A 5}$$

or

$$\tanh[(R-r_c)(k_0^2 - \lambda_n^2)^{\frac{1}{2}}] = R(k_0^2 - \lambda_n^2)^{\frac{1}{2}}. \tag{A 6}$$

But the left hand side of (A 6) is less than $\tanh\{R(k_0^2 - \lambda_n^2)^{\frac{1}{2}}\}$, and this in turn is less than the right-hand side of (A 6). Therefore there are no real eigenvalues less than k_0^2. *All* eigenfunctions are of the form of equation (A 3) and *all* eigenvalues are given by equation (A 5).

The coefficients A_n are determined by the normalization of ψ_n to unity over the cell volume:

$$4\pi \int_{r_c}^{R} r^2 \psi_n^2 \, dr = 1. \tag{A 7}$$

This integral is readily evaluated. The result contains a 'double-angle' sine function which can be simplified by the use of the eigenvalue equation. The final form obtained yields

$$A_n^2 = \frac{1 + R^2(\lambda_n^2 - k_0^2)}{2\pi\{(\lambda_n^2 - k_0^2)R^2 - r_c[1 + R^2(\lambda_n^2 - k_0^2)]\}}. \tag{A 8}$$

The remaining quantity is needed

$$I_n = 4\pi A_n \int_{r_c}^{R} r^2 \psi_n \, dr. \tag{A 9}$$

This integral is also easy to evaluate. After further use of the eigenvalue equation it is found to be

$$I_n = 4\pi r_c A_n / (\lambda_n^2 - k_0^2)^{\frac{1}{2}}. \tag{A 10}$$

Approximations to λ_n^2, A_n and I_n have been given in §3 (*b* ii). The genesis of the approximations resides in the assumption that $r_c \ll R$. To give an idea of the quality of the approximations used, the lowest eigenvalues are plotted in figure 11 for two different values of r_c/R. Except for the lowest mode, the straight line $R(\lambda_n^2 - k_0^2)^{\frac{1}{2}} = (n + \frac{1}{2})\pi$ represents the analytical form used in §3.

For completeness, a sample of normalized eigenfunctions is illustrated in figure 12. These pertain to $r_c = \frac{1}{10}R$.

Appendix B

The following analysis details the manner in which a sink-free region may be assigned to each dislocation.

For the dislocation aspects to be reduced to a two-dimensional problem, the void distribution along the axis must be uniform. Our first step is to imagine the random distribution along this axis being replaced by a regular one. We collect all voids into a sequence of planes spaced a_z apart. The area density of voids in each such plane is then $N_A = C_v a_z$. We pick a_z to be the mean separation between two voids in a random distribution.

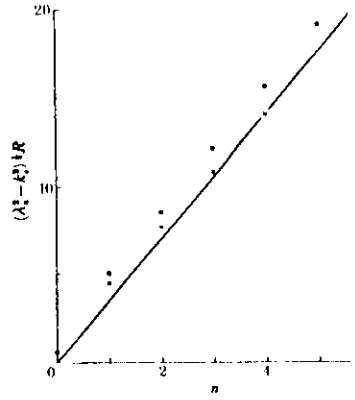

Figure 11. The lowest eigenvalues for $r_c/R = 0.1$ and $r_c/R = 0.001$, indicated as the solid dots and crosses, respectively. In the latter case the lowest mode lies virtually at the origin. It has been omitted.

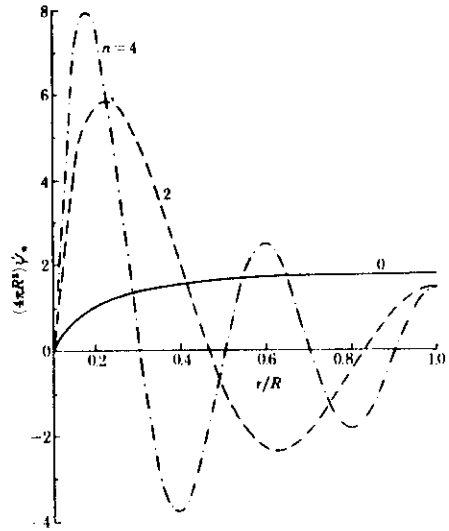

Figure 12. Normalized eigenfunctions for the lowest even modes, when $r_c = 0.1R$.

Imagine next that, in any one void plane, one starts on the dislocation axis and moves radially outward. Within each plane the void distribution is still random. We shall pick R_f to be the mean distance one must travel before encountering one void.

To compute this distance, suppose $P(r)$ is the probability of not encountering a void up to the radius r. Then, considering the consequence of moving out a further distance dr leads to

$$P(r+\mathrm{d}r) = P(r)(1-2\pi r N_A \mathrm{d}r), \tag{B 1}$$

because $2\pi r N_A \mathrm{d}r$ is the *a priori* probability of a void-encounter during the step. Therefore,

$$P(r) = A\mathrm{e}^{-\pi N_A r^2}. \tag{B 2}$$

The constant A is determined by the probability of eventually meeting at least one void being unity: $A\int_0^\infty \mathrm{e}^{-\pi N_A r^2} 2\pi N_A r \mathrm{d}r = 1$. Thus the mean distance traversed before a void encounter is $\bar{r}$, where

$$\bar{r} = \int_0^\infty r^2 \mathrm{e}^{-\pi N_A r^2}\mathrm{d}r \Big/ \int_0^\infty r\mathrm{e}^{-\pi N_A r^2}\mathrm{d}r = \frac{1}{2N_A^{\frac{1}{2}}}. \tag{B 3}$$

This we take equal to R_f, the radius of the sink-free region around the dislocation. To evaluate it we now need the mean linear spacing between voids, a_v. This we find by similar reasoning to the above. In a random array of (small) voids, let $Q(r)$ be the probability of not encountering another void after moving a distance r from the central one, picked arbitrarily. Then we have

$$Q(r+\mathrm{d}r) = Q(r)(1-4\pi r^2 C_v \mathrm{d}r), \tag{B 4}$$

or

$$Q(r) = B\mathrm{e}^{-\frac{4}{3}\pi r^3 C_v}. \tag{B 5}$$

Therefore the mean linear spacing between voids is

$$\left.\begin{aligned} a_v &= \int_0^\infty r^3 \mathrm{e}^{-\frac{4}{3}\pi r^3 C_v}\mathrm{d}r \Big/ \int_0^\infty r^2 \mathrm{e}^{-\frac{4}{3}\pi r^3 C_v}\mathrm{d}r \\ &= \left(\frac{3}{4\pi C_v}\right)^{\frac{1}{3}} \Gamma(\tfrac{4}{3}). \end{aligned}\right\} \tag{B 6}$$

When (B 6) is inserted into the definition of N_A, and equation (B 3) is evaluated, equation (124) results.

References

Brailsford, A. D. 1976 *J. nucl. Mater.* **60**, 257.
Brailsford, A. D. 1979 *J. nucl. Mater.* **84**, 245.
Brailsford, A. D. & Bullough, R. 1972*a* *J. nucl. Mater.* **44**, 121.
Brailsford, A. D. & Bullough, R. 1972*b* A.E.R.E. Harwell Report R 7433.
Brailsford, A. D. & Bullough, R. 1973 *Physical metallurgy of reactor fuel elements*, p. 148. London: Metals Society.
Brailsford, A. D. & Bullough, R. 1976 *Vacancies '76*, p. 108. London: Metals Society.
Brailsford, A. D. & Bullough, R. 1978 *J. nucl. Mater.* **69/70**, 434.
Brailsford, A. D., Bullough, R. & Hayns, M. R. 1976 *J. nucl. Mater.* **60**, 246.
Brailsford, A. D., Matthews, J. R. & Bullough, R. 1979 *J. nucl. Mater.* **79**, 1.
Bullough, R., Eyre, B. L. & Krishnan, K. 1975 *Proc. R. Soc. Lond.* A **346**, 81.
Bullough, R., Eyre, B. L. & Perrin, R. C. 1970 *Nucl. Appl. Technol.* **9**, 348.
Bullough, R. & Hayns, M. R. 1975 *J. nucl. Mater.* **57**, 348.
Bullough, R., Hayns, M. R. & Woo, C. H. 1979 *J. nucl. Mater.* **84**, 93.
Bullough, R., Hayns, M. R. & Wood, M. H. 1980 *J. nucl. Mater.* **90**, 44.
Bullough, R. & Newman, R. G. 1962 *Proc. R. Soc. Lond.* A **266**, 833.
Bullough, R. & Perrin, R. C. 1971 *Voids formed by irradiation of reactor materials* (ed. S. F. Pugh *et al.*), p. 79. London: British Nuclear Energy Society.

Bullough, R. & Quigley, T. M. 1981*a* In *Proc. 2nd Topical Meeting on Fusion Reactor Materials, Seattle, Washington, U.S.A.* (9–12 August, 1981) (ed. J. J. Holmes). Hinsdale, Illinois: American Nuclear Society. (To be published.)
Bullough, R., Wells, D. W., Willis, J. R. & Wood, M. H. 1981*b* *Acta metall.* (To be published.)
Bullough, R. & Willis, J. R. 1975 *Phil. Mag.* **31**, 855.
Cottrell, A. H. & Bilby, B. A. 1949 *Proc. Phys. Soc. Lond.* **62**, 49.
Damask, A. C. & Dienes, G. J. 1971 *Point defects in metals*, ch. 2. New York: Gordon and Breach.
Dienes, G. J. & Vineyard, G. H. 1957 *Radiation effects in solids*, ch. 5. New York: Interscience.
Flynn, C. P. 1972 *Point defects and diffusion*, p. 484. Oxford: Clarendon Press.
Goldberger, M. L. & Seitz, F. 1947 *Phys. Rev.* **71**, 294.
Gosele, U. 1978 *J. nucl. Mater.* **78**, 83.
Gradshteyn, I. S. & Ryzhik, I. M. 1975 *Tables of integrals, series and products*, p. 36. New York: Academic Press.
Ham, F. S. 1958 *J. Phys. Chem. Solids* **6**, 335.
Ham, F. S. 1959 *J. appl. Phys.* **30**, 915.
Harkness, S. D. & Li, C. Y. 1971 *Metall. Trans.* **2**, 1457.
Hayns, M. R. 1979 *J. nucl. Mater.* **79**, 323.
Heald, P. T. & Speight, M. V. 1974 *Phil. Mag.* **29**, 1075.
Heald, P. T. & Speight, M. V. 1975 *Acta metall.* **23**, 1389.
Heald, P. T. & Miller, K. M. 1976 C.E.G.B. Research Rep. RD/B/N3798.
Hudson, J. A., Mazey, D. J. & Nelson, R. S. 1971 *Voids formed by irradiation of reactor materials* (ed. S. F. Pugh *et al.*), p. 21. London: British Nuclear Energy Society.
Jahnke, E., Emde, F. & Losch, F. 1960 *Tables of higher functions*, p. 4. New York: McGraw Hill Book Co.
Mansur, L. K. 1979 *Phil. Mag.* A **39**, 497.
Mansur, L. K., Coghlan, W. A. & Brailsford, A. D. 1979 *J. nucl. Mater.* **85/86**, 591.
Morse, P. M. & Feshbach, H. 1953 *Methods of theoretical physics*, pp. 620, 1323. New York: McGraw Hill Book Co.
Nichols, F. A. 1978*a* *J. nucl. Mater.* **75**, 32.
Nichols, F. A. 1978*b* *Radiation effects* **39**, 169.
Talbot, D. R. S. & Willis, J. R. 1980 *Proc. R. Soc. Lond.* A **370**, 351.
Wiedersich, H. 1970 *Proc. Second Int. Conf. on the Strength of Metals and Alloys*, vol. 2, p. 142. Cleveland, Ohio: American Society for Metals.
Wolfer, W. G. & Ashkin, M. 1975 *J. appl. Phys.* **46**, 547.
Wolfer, W. G. & Mansur, L. K. 1978 *J. nucl. Mater.* **69/70**, 825.
Zener, C. 1949 *J. appl. Phys.* **20**, 1950.

ROYAL SOCIETY MATHEMATICAL TABLES

	U.K. addresses	Overseas
1. The Farey Series of Order 1025	£10.00	£10.30
2. Rectangular-Polar Conversion Tables	£4.00	£4.15
3. Table of Binomial Coefficients	£5.00	£5.15
4. Tables of Partitions	£6.00	£6.20
5. Representations of Primes by Quadratic Forms	£4.75	£4.90
6. Tables of the Riemann Zeta Function	£4.00	£4.15
7. Bessel Functions, Part III: Zeros and Associated Values	£5.50	£5.70
8. Tables of Natural and Common Logarithms to 110 Decimals	£3.25	£3.40
9. Indices and Primitive Roots	£8.00	£8.25
10. Bessel Functions, Part IV: Kelvin Functions	£4.50	£4.65
11. Coulomb Wave Functions	£6.00	£6.20

ROYAL SOCIETY SHORTER MATHEMATICAL TABLES

1. A Short Table for the Bessel Functions $I_{n+\frac{1}{2}}(x), \frac{2}{\pi}K_{n+\frac{1}{2}}(x)$	£0.80	£0.85
2. Bessel Functions and Formulae	£0.50	£0.55
3. A Short Table for Bessel Functions of Integer Orders and Large Arguments	£1.00	£1.05

BRITISH ASSOCIATION MATHEMATICAL TABLES

I. Circular and Hyperbolic Functions. (3rd Edition)	£3.00	£3.10
IV. Cycles of Reduced Ideals in Quadratic Fields	£3.00	£3.10
V. Factor Table	£5.25	£5.45
VII. The Probability Integral	£2.40	£2.50
VIII. Number-Divisor Tables	£3.75	£3.90
IX. Table of Powers giving Integral Powers of Integers	£3.00	£3.10
X. Bessel Functions, Part II: Functions of Positive Integer Order	£7.50	£7.75
Part-Volume A. Legendre Polynomials	£1.30	£1.40
Part-Volume B. The Airy Integral	£1.70	£1.80

Publications Sales Department, The Royal Society
6 Carlton House Terrace, London SW1Y 5AG

QUANTITIES, UNITS, AND SYMBOLS

Second edition 1975

54 pages 250 x 176 mm. Paper cover only

ISBN 0 85403 071 9

	U.K.	Overseas	
Price	£1.00	£1.05	†

This handbook contains in a convenient form a very great deal of information on SI (the International System of Units), symbols for physical quantities, recommended forms for many aspects of scientific writing including mathematical presentation, labelling of graphs and tables, preferred placements and type founts for subscripts and superscripts, favoured abbreviations, etc. It also includes recommended values of physical constants. While SI and other internationally recommended practices are emphasized, values of conversion factors are given for use with imperial units and other units outside SI. References to original international authority are quoted.

Its compact size makes *Quantities, Units, and Symbols* an invaluable aid for scientific writing for all authors who wish to follow modern practice especially in physics and chemistry. Equally it should be an immediately available guide for teachers in higher education many of whom will wish their students to own a copy. It is also invaluable for the reader who has found some unfamiliar notation or terminology, not least when he has strayed from his own narrow specialism.

The contents include:

To encourage the widespread availability and use of Q.U.S. (as it is commonly known) the following special prices are offered for orders for multiple copies:

	U.K.	Overseas
5 copies	£4.00	£4.15
10 copies	£6.50	£6.70
20 copies	£11.00	£11.35
50 copies	£22.50	£23.20

The Royal Society,
6 Carlton House Terrace, London SW1Y 5AG

Printed in Great Britain
for the Royal Society at the University Press, Cambridge